

Antarctic surface melting dynamics using radar scatterometer data

Egli Michailidou

Technische Universiteit Delft



Antarctic surface melting dynamics using radar scatterometer data

by

Egli Michailidou

in partial fulfillment of the requirements for the degree of

Master of Science

in Civil Engineering

at the department of Geoscience and Remote Sensing of the Delft University of Technology,

to be defended publicly on Tuesday March 13, 2018 at 15:00.

Supervisor:	Dr. S. L. M. Lhermitte,	TU Delft
Thesis committee:	Prof. dr. ir. R. F. Hanssen,	TU Delft
	Prof. dr. ir. W. G. M. Bastiaanssen,	TU Delft
	Dr. M. Belmonte Rivas,	KNMI
	Dr. J. T. M. Lenaerts	University of Colorado

An electronic version of this thesis is available at <http://repository.tudelft.nl/>.

Sometimes you have to go up really high to understand how small you really are.

Felix Baumgartner

Abstract

Recent studies have shown that processes like the thinning of the ice shelves, the acceleration of the outlet glaciers and the collapses of the ice shelves are connected to surface melting. Several ice shelves at the Antarctic Peninsula, a region that has experienced an atmospheric warming much larger than the global average, have retreated and disappeared. In order to assess the stability of the ice shelves, snowmelt amount can be used. Microwave remote sensing instruments are used in studying surface melting. The presence of liquid water causes a decrease in volumetric scattering that is dominant over absorption in dry snow, and increases absorption due to the increase of the imaginary part of snow permittivity. Thus, active microwave scatterometers can detect melt because of the decrease in backscatter. In this study, data from QuikSCAT (2000-2009) and ASCAT (2010-2016) are used for the investigation of the Antarctic surface melting dynamics for the period 2000-2016. The methodologies of Trusel et al. (2012) and Bothale et al. (2015) and two other threshold-based melt detection methodologies are applied and evaluated using in-situ meteorological records and are compared to passive microwave threshold-based melt duration results from AMSR-E and AMSR2. In addition, an attempt for a retrieval of a consistent melt time series is performed. The results support the use of a dynamic threshold-based melt detection approach for scatterometer data, but it is not possible to achieve consistency in melt duration results from the two scatterometers mainly due to their differences overpass timing. Overall, a high interannual variation in melt extent and melt index is found and results show that the extent of the areas that experience morning and afternoon melt consistently remains constant through the years. However, morning measurements underestimate melt and thus midday observations are important for melt detection studies, as melting varies throughout the day. In addition, although most of the large scale melting phenomena are captured by AMSR-E, the higher sensitivity of QuikSCAT to melt and its finer resolution result in differences in the derived melt metrics.

Preface

The present Master's thesis marks the end of my MSc studies at the track of Geoscience and Remote Sensing. Working on this thesis has been a challenge and a pleasure at the same time, and thus I would like to express my gratitude to the people that contributed to this journey.

First, I would like to thank my daily supervisor Dr. Stef Lhermitte, who provided me the opportunity to work on this topic, for his support, motivation and immense knowledge. His guidance, comments and feedback helped me during the time of research and writing of this report.

I would also like to thank Prof. Ramon Hanssen, Prof. Wim Bastiaanssen and Dr. Jan Lenaerts for reading my thesis and for their comments. My sincere thanks also goes to Dr. Maria Belmonte Rivas for her insightful comments and suggestions during this period.

My warm thanks to my friends in Delft who supported me during my studies and made this trip unforgettable. Thanks too to my friends in Cyprus for being there for me and encouraging me despite the distance.

Last but not least, I would like to thank my parents Christos and Evi, for their encouragement, love, faith and support especially in the difficult moments. A big thank to my brother Royiros and Antonia for their love, support and the happy moments.

Egli Michailidou

Contents

Abstract	i
Preface	iii
1 Introduction	1
1.1 Introduction to Antarctic Surface Melting	1
1.1.1 Ice Shelves and Climate	1
1.1.2 Surface Melting	2
1.1.3 Melt Detection Methods	3
1.2 Problem Statement and Objectives	3
1.3 Research Question	3
1.4 Thesis Outline	4
2 Background	7
2.1 Antarctic Ice Sheet	7
2.1.1 Ice Shelves and Glaciers	7
2.1.2 Climate	9
2.1.3 Surface Mass balance	10
2.2 Melt Detection	10
2.2.1 Remote Sensing techniques	11
3 Methodology	17
3.1 Data Overview	17
3.1.1 Satellite Data	17
3.1.2 In-Situ Data	20
3.2 Analysis	22
3.2.1 Sensitivity test	22
3.2.2 Melt detection	23
3.2.3 Melt Metrics	28
3.2.4 Diurnal Variability of Melt	28
4 Results and Discussion	31
4.1 Sensitivity Test	31
4.2 Melt Detection	32
4.2.1 Evaluation of Existing Methodologies	34
4.2.2 QuikSCAT	35
4.2.3 ASCAT	37
4.2.4 Consistent dataset	39
4.2.5 Passive Microwave Record	41
4.3 Comparison	41

4.3.1 Continental Scale	42
4.3.2 Regional Scale	45
4.4 Climate	48
5 Conclusions	55
Bibliography	59
List of Figures	65
List of Tables	71
A Appendix	73
A.1 Additional Figures	73
A.1.1 Backscatter Time Series	73
A.1.2 Melt Detection Validation	75
A.1.3 Melt duration maps	80
A.1.4 Comparison QuikSCAT - AMSR-E	95
A.1.5 Comparison Morning and Afternoon Melt	100
A.1.6 Melt Duration Anomaly Maps	102
A.1.7 Melt Intensity Anomaly Maps	108

1

Introduction

Ice sheets are one of the constituents of the Cryosphere, together with snow cover, sea ice, freshwater ice, glaciers, and permafrost. The cryosphere is an important component of the Earth's climate system, because of the high reflectivity of snow and ice and the impact on the distribution and flow of water. The largest ice masses on Earth are the Greenland and Antarctic ice sheets. An introduction to surface melting over Antarctica, its impact and the methods for detecting it follows. In addition, the problem statement, the research objectives and the research question are introduced in this chapter.

1.1 Introduction to Antarctic Surface Melting

Antarctica has a major impact on global climate circulation and Earth's energy balance, but its extent of 14.4 km² and the harsh climatic conditions make the collection of ground data difficult (Tedesco, 2009). The climate in Antarctica is unique, as it is the coldest, windiest and on average the highest continent on Earth, with long polar nights in winter, which impose extra challenges in the field observations (Liu et al., 2006). Thus, the use of data collected by space-borne instruments for its observation is inevitable. Especially microwave sensors provide the opportunity to observe the complete coverage of Antarctica through clouds, day and night on a daily basis because of the large swath and the weak influence of clouds and atmosphere. Besides these advantages, microwave data are also important for the surface and sub-surface melt detection (Tedesco, 2009).

1.1.1 Ice Shelves and Climate

Over the last half century, the Antarctic Peninsula has experienced an atmospheric warming much larger than the global average (Kuipers Munneke et al., 2012b). As a result, a significant number of ice shelves (e.g. Larsen A, Larsen B, parts of Wilkins Ice Shelf) around it has been entirely lost or retreated significantly with the rates of retreat varying from slow retreat to abrupt collapse (Cook and Vaughan, 2010). Ice shelves are thick floating extensions of glaciers, draining grounded ice to the ocean and are sensitive to changes in their surroundings (van den Broeke, 2005). In addition to this, recent studies document that many processes, such as ice shelves thinning (Holland et al., 2011), acceleration of outlet glaciers (Pritchard and Vaughan, 2007) and ice shelf collapses (Scambos et al., 2000) are connected to surface melting. As Scambos et al. (2000) have concluded, snowmelt amount can be used to assess the stability of ice shelves. In particular, they found that prior a collapse event, large lakes were formed on the ice shelf surface. The accumulated

meltwater on ice shelves can fill any surface crevasses and impose an outward and downward pressure, which forces the crevasses to propagate through the full ice thickness. Therefore, in order to evaluate the stability of the Antarctic ice shelves, surface melt should be monitored.

Although an ice shelf collapse has little effect on sea level, because ice shelves are already floating, it causes an acceleration of land-based glaciers, which also get thinner and contribute to sea level rise (Trusel et al., 2012). Moreover, even though surface melting is so impactful in Antarctic Peninsula, the runoff of meltwater is not a major component in the surface mass balance (SMB) of Antarctic ice sheet (Lenaerts et al., 2012) and most of it refreezes locally (Kuipers Munneke et al., 2012b). Furthermore, melting alters snow albedo and reflectivity, leading to an increase in solar radiation absorption which causes additional melting (Lenaerts et al., 2017). Thus, as surface melting is important for the surface energy balance and the snowpack energy budget, density and morphology, the understanding of this process is of great importance in terms of climatology and glaciology.

1.1.2 Surface Melting

Surface melting over Antarctica has been examined using several methods, such as ice core stratigraphy and in situ surface energy balance (Trusel et al., 2013). Moreover, Antarctic surface melting has also been studied using active and passive microwave sensors. Volumetric scattering is dominant over absorption in dry snow (Tedesco, 2014). However, the presence of liquid water causes a decrease in volumetric scattering and an increase in absorption. This is due to the increase of the imaginary part of snow permittivity (Tedesco, 2014). According to these, melt can be detected using passive microwave radiometers, due to the sudden increase in brightness temperature (T_b) and using active microwave scatterometers, due to the decrease in backscatter (σ^0). Several studies (e.g. Ohmura, 2001; Hock, 2005) have indicated a strong correlation between melt events and near surface air temperature, leading to the conclusion that melt detection and the understanding of its dynamics across space and time can also serve as an indicator of regional temperature scale.

Specifically, several researchers (e.g. Torinesi et al., 2003; Liu et al., 2006; Tedesco et al., 2007; Tedesco, 2009) have used passive microwave radiometers such as the Scanning Multichannel Microwave Radiometer (SMMR) and the Special Sensor Microwave Imager (SSM/I) for Antarctic surface melting studying from 1978 to present. Active microwave scatterometers have also been used in studies over Antarctica (Kunz and Long, 2006; Nghiem et al., 2007; Trusel et al., 2012; Barrand et al., 2013; Bothale et al., 2015) and for several other studies, such as monitoring melting over Greenland (Wismann, 2000; Nghiem et al., 2005; Wang et al., 2007), over glaciers and ice caps in the Arctic (Wang et al., 2005), over USA and Canada (Hillard et al., 2003), over low latitude alpine regions (Panday et al., 2011) and other applications regarding sea ice (Frey et al., 2003; Haarpaintner et al., 2004; Lindell and Long, 2016). Scatterometers offer surface melt studying at a higher spatial resolution than radiometers and they are more sensitive to melt (Ashcraft and Long, 2006). In addition, it is reported that correlation exists between summed backscatter reductions and integrated positive air temperatures during melt seasons (Wismann, 2000). Therefore, by taking into account that positive degree days (PDD) (days with positive air temperatures) are correlated to meltwater production (Hock, 2005), scatterometers can provide estimations for melting. Moreover, information for relative melt intensity can be retrieved from scatterometers based on the integrated backscatter reductions as proposed by Wismann (2000), in contrast to radiometers that can only provide information indicating the presence or absence of melt, because the T_b saturates at small fractions of liquid water (Trusel et al., 2012). However, there is still discussion whether a backscatter saturation point exists and melting does not cause further backscatter reductions after that (Smith et al., 2003; Trusel et al., 2012). The shorter length of scatterometer time series relative to passive microwave radiometers is its major disadvantage.

1.1.3 Melt Detection Methods

Recent studies employed different methodologies for melt detection using scatterometer data. One of them is a threshold-based melt detection approach (Ashcraft and Long, 2006; Trusel et al., 2012; Barrand et al., 2013; Bothale et al., 2015), where every day is defined as a melting day for each pixel if its daily backscatter value is lower than a certain threshold. In order to analyse the spatial and temporal melting characteristics, total areal melt extent (in km²), melt index (in km² days) and total annual melt intensity are used. Melt index or cumulative melting surface is a useful climatic indicator as it gives information about both the temporal and spatial dimensions of melting. To date, enhanced resolution data from the SeaWinds radar scatterometer onboard the QuikSCAT satellite [1999-2009] (hereafter QuikSCAT) have been widely used for documenting the Antarctic surface melting dynamics until 2009 (Kunz and Long, 2006; Nghiem et al., 2007; Trusel et al., 2012; Barrand et al., 2013). The Oceansat Scatterometer (OSCAT) [2009-2014] is viewed to be a continuity mission for QuikSCAT, due to their similar characteristics and Bothale et al. (2015) used data from the two aforementioned sensors to investigate melting over Antarctic ice sheet. The Advanced Scatterometer (ASCAT)[2007 - present] has different characteristics from the other two scatterometers in terms of frequency and scattering geometry, but ASCAT data can provide information for melt until the present, even though combining the datasets for a consistent melt time series from 2000 to today remains a challenge. The results of the previous studies show that active microwave scatterometers can provide reliable high-resolution spatially melt climatology, encouraging the continuation of the scatterometer time series to the present. However, the results and the melt metrics produced by the different methods show some deviations that suggest further research to fully assess the limitations and capabilities of these approaches.

1.2 Problem Statement and Objectives

Surface melting is not a major component of the Antarctic ice sheet surface mass balance, but there is an important link between meltwater production and ice shelf stability, as meltwater exerts potentially extra hydrostatic pressure that can drive existing fractures through the full thickness of the ice shelves. In addition, liquid water reduces albedo that causes increased solar radiation absorption and additional melting and it modifies the snowpack density, morphology and isotopic signature. Hence, surface melting is important to be monitored. Among various methods for melt monitoring, active microwave scatterometers can provide information for examining melting processes over various regions.

To date, different methods have been applied for the study of surface melting dynamics across Antarctica using radar backscatter data from QuikSCAT and OSCAT (Trusel et al., 2012; Bothale et al., 2015). However, divergences among the metrics produced by the different methodologies exist. Therefore, current research is mainly focused on assessing the capabilities and limitations of threshold-based melt detection methodologies using scatterometers (QuikSCAT, OSCAT and ASCAT) to detect and study Antarctic surface melting and expanding the melt time series to the present. The time series are important for better understanding the melt processes and the way they may affect ice shelf stability.

In light of the problem discussed above, the main objective of this study is to evaluate the existing active microwave algorithms for melt detection over Antarctic Ice Sheet based on the studies of Trusel et al. (2012) and Bothale et al. (2015) using radar backscatter data from QuikSCAT, OSCAT and ASCAT and produce a consistent melt time series for the period 2000-2016, in order to estimate the temporal and spatial trends of Antarctic surface melt dynamics.

1.3 Research Question

Based on the problem statement and the objectives of the study, the main research question that will be answered is the following:

What is the temporal and spatial evolution of the Antarctic surface melting dynamics in the period 2000 – 2016 using scatterometer data?

The research question is further divided into these sub-questions:

1 How does the backscatter coefficient react to different satellites and snowpacks?

Backscatter coefficient (σ^0) depends on the frequency, polarization and incidence angle of the emitted electromagnetic wave and the roughness, geometric shape and dielectric properties of the target. Thus, it is important to understand the way that these parameters influence backscattering. This can be achieved by using a backscatter model for active microwave remote sensing of snow, such as the Microwave Emission Model of Layered Snowpacks (MEMLS), and testing the backscatter change for different satellites and snowpacks.

2 What threshold should be used for the melt detection method for QuikSCAT data?

A threshold-based melt detection method will be used in this study. For this reason, a suitable threshold should be selected, in order to detect the true melt events. As previous studies have used different thresholds depending on the study region and the application, an evaluation of two of the existing methodologies (Trusel et al., 2012; Bothale et al., 2015) will be performed firstly. In addition, air temperature can be used as a reliable proxy for melt presence and hence, meteorological data from weather stations can be used for the validation of the methodologies.

3 How to modify the melt detection method for OSCAT and ASCAT data and produce a consistent melt time series?

OSCAT has similarities with QuikSCAT and it is viewed as a continuity mission for QuikSCAT. On the other hand, the characteristics of ASCAT and QuikSCAT differ in terms of frequency and scattering geometry. Therefore, it should be examined whether data from OSCAT and ASCAT can be used in this study successfully and modify the melt detection method according to these differences, in order to achieve consistency in the final results. A consistent melt time series is important, so as to be able to observe the temporal and spatial evolution of surface melting dynamics. The passive microwave remote sensing record can be used for the validation and assessment of consistency and for a comparison between the results of scatterometers and radiometers.

4 What is the observed temporal and spatial trend of melt dynamics?

Melt metrics (melt duration, melt index, melt extent and melt intensity) can be used for the analysis of the spatial and temporal characteristics. Important information can be retrieved based on these metrics in an attempt to understand the diverse drivers of the Antarctic surface melting and its impact.

1.4 Thesis Outline

This thesis consists of five chapters and an appendix. In the current chapter, an introduction to the study is given. Moreover, the problem statement is presented and the research question is formulated.

Chapter 2 contains the scientific and technical background relevant of this study. It starts with information about the Antarctic Ice Sheet and continues with the remote sensing techniques for melt detection.

In Chapter 3 the methodology is described. Firstly, there is an overview of the in-situ and satellite data used, followed by the description of the melt detection methods that are implemented and the fractional melt detection method that is applied in order to produce a consistent time series.

In Chapter 4 the results of the study are presented and discussed. The chapter starts with the results of the sensitivity test, followed by the results from the evaluation of the existing methodologies and continues with the results of the consistent melt time series. It ends with a discussion about the spatial and temporal evolution of melt dynamics in continental and regional scale.

The study is concluded with Chapter 5, in which the answers to the research question and its sub-questions can be found. Finally, additional figures are included in the appendix.

2

Background

In this chapter the technical and scientific background relevant for this study is discussed. Information about the Antarctic ice sheet and ice shelves is given, followed by a description of remote sensing techniques for melt detection.

2.1 Antarctic Ice Sheet

The Antarctic continent is surrounded by the Southern Ocean and it is the windiest, highest and coldest place on Earth. Sea ice forms in the surroundings of the continent with an average area ranging from two million square kilometres in austral summer (January/ February) to thirteen million square kilometres in austral winter (September/ October) (Luis, 2013). The average thickness of the Antarctic ice sheet, which covers the 98% of the continent (Cook and Storey, 2015), is around 1800 m (Masson-Delmotte, 2013) and its maximum ice depth is more than 4770 m, found in a subglacial trench in Terre Adelie (Oerlemans and Van Der Veen, 1984). The continent is divided into two parts, the East and West Antarctica by the Transantarctic Mountains, which extend from the tip of Antarctic Peninsula to Cape Adare (Luis, 2013). The West Antarctic Ice Sheet is called a marine ice sheet, since a large part of the ice sheet lies below sea level and it is surrounded by ice shelves. On the contrary, the East Antarctic Ice Sheet stands above sea level (Oerlemans and Van Der Veen, 1984) and it is colder than West Antarctica (Luis, 2013). Therefore, the 90% of the equivalent sea level of Antarctic Ice Sheet, 57 m, is due to the East Antarctic Ice Sheet (Masson-Delmotte, 2013).

2.1.1 Ice Shelves and Glaciers

Ice shelves are attached to almost half of the Antarctic coastline (45%) (Sinclair, 2015). They are thick platforms of ice connected to the coast and float onto the ocean surface (Fig. 2.2). Due to the fact that they are in contact with the ocean, the friction at their base is little, and thus they reach velocities of several kilometres a year at the edge (Sinclair, 2015). The largest ice shelves are the Ronne-Filchner, the Amery and the Ross, with thickness ranging from 100 to 1000 m (Masson-Delmotte, 2013). The largest thickness is found at the grounding line, which is the boundary between the grounded ice and the floating ice shelf. The calving of icebergs is the main process which leads to a mass loss from the ice shelves.

The location of the grounding line is directly linked with the change in environmental conditions. In particular, the grounding line moves further into the ocean when the ice sheet expands in colder climate, and the opposite happens when the ice sheet retreats in warmer climate. The warm ocean waters and surface

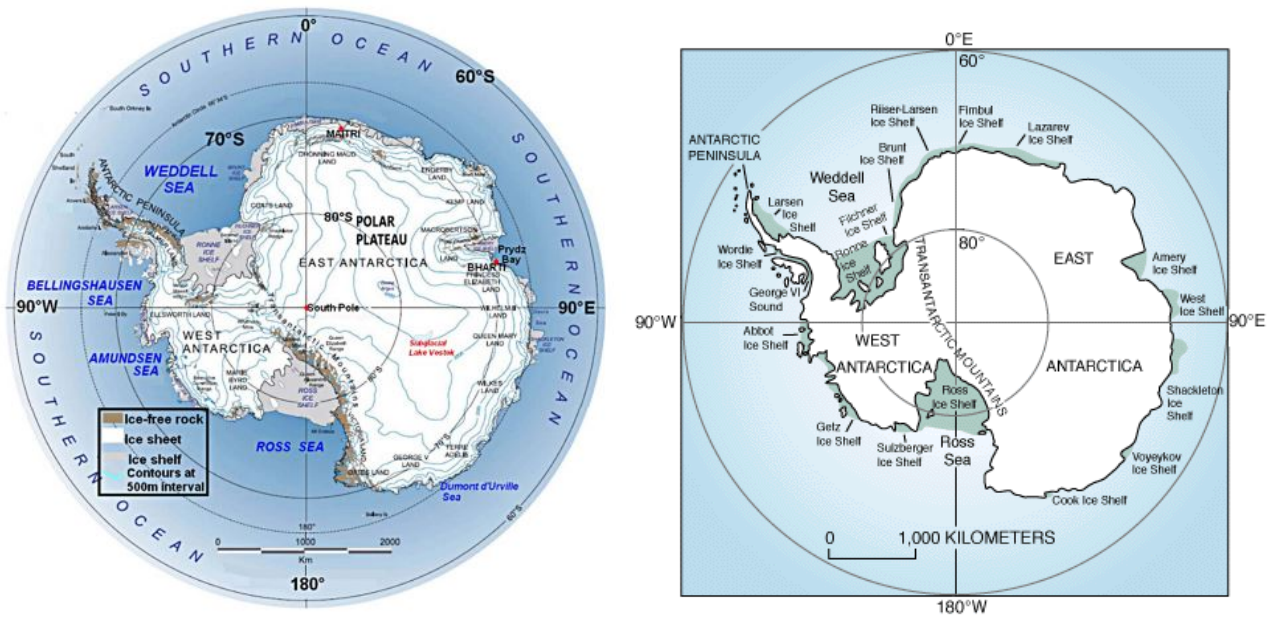


Figure 2.1: (a) Map of Antarctica from (Luis, 2013) and (b) Antarctic ice shelves.

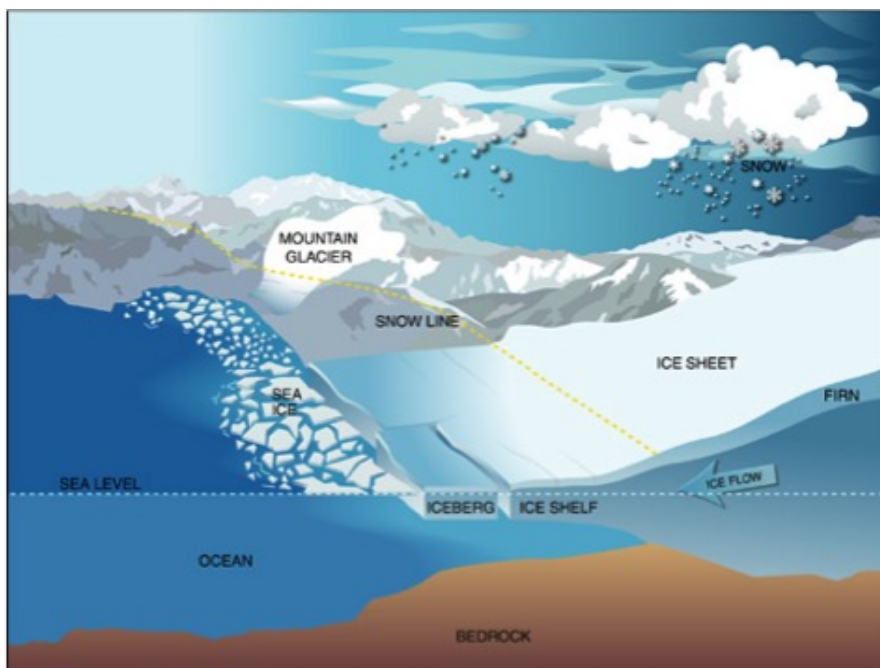


Figure 2.2: Illustration of the cycle through which glacial ice and water ends up in the oceans (Goddard Space Flight Center NASA).

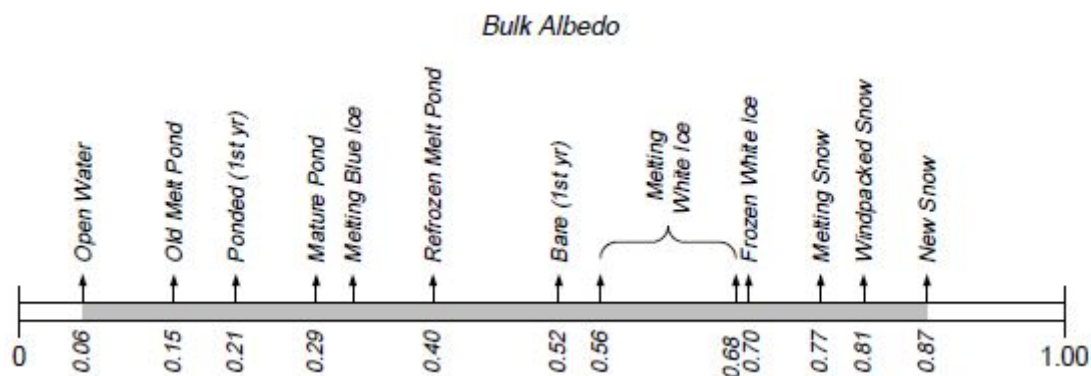


Figure 2.3: Range of albedo of different surfaces (Perovich, 1996).

melt has already caused the collapse of several ice shelves around the Antarctic Peninsula. As the ice shelves prevent warmer marine water to reach the glaciers, such a collapse can cause an acceleration of the glaciers (Luis, 2013). Rignot et al. (2004) have already found that the collapses of Larsen B and Larsen A have caused the acceleration of the glaciers in the Peninsula.

Ice streams are responsible for the drainage of the West Antarctic Ice Sheet and they feed the ice shelves. They are separated by regions with slowly moving ice and in these fractured zones the ice stream flows 10 - 1000 times faster than the surrounding ice (Sinclair, 2015). The ice thickness in the ice streams is less than the surroundings and the basal conditions beneath them are responsible for the amount of ice that is drained out from the interior of the continent. The change of ice streams is a rapid response to changing ice thickness, pressure and temperature beneath the ice. It is worth mentioning that the mass loss of some of the largest glaciers is a response to ice thinning and acceleration of the ice streams (Sinclair, 2015).

Ice streams together with outlet glaciers are responsible for 40% of the ice lost from the continents (Sinclair, 2015). Even though outlet glaciers behave like ice streams, they flow through mountain range and especially through the Transantarctic Mountains. Another type of glaciers, dry-based glaciers, is found in Antarctica. These glaciers are frozen to the rock and sediment beneath them and they have no subglacial water (Sinclair, 2015). In addition, alpine glaciers are found on the Antarctic Peninsula.

2.1.2 Climate

Antarctica receives solar radiation continuously six months of the year and no solar radiation for the following six months, causing a large seasonal temperature range. In general, ice sheets affect the global energy budget due to their high albedo as well as the dynamics of the atmosphere, due to their high topography and cooling effects, and ocean through meltwater fluxes. In particular, the Antarctic continent reflects most of the incoming solar radiation back to space since 98% of its surface is covered by ice. The fraction of solar energy that is reflected from surface back to space is defined as the albedo and it is different for each surface (Fig. 2.3). This net radiation deficit is the reason for the cold temperatures. In addition, the high elevation of the ice sheet makes the Antarctic colder than the Arctic.

Winds are another characteristic of the Antarctic climate, due to the steeply sloping terrain at the edge of the continent. The horizontal temperature contrast over these regions is responsible for a density contrast. Thus, the dense colder air that floats out from the polar plateau will sink, accelerating down the surface of the ice sheet due to gravity, producing katabatic winds (Cassano, 2013). Antarctica can be considered as a dry region, since the coastal and the inner regions of the continent receive an average precipitation of 203 mm and 51 mm per year in the form of snow respectively (Luis, 2013). Even though the actual amount of water vapour in the atmosphere is small, the relative humidity over the Antarctic continent is high (90%)

(Cassano, 2013). Relative humidity is a measure of the amount of water vapour in the atmosphere compared to the maximum amount of water vapour that the atmosphere can contain at a specific temperature. In particular, the air over Antarctica can contain less water vapour than other places because of the low temperatures. In addition, Antarctica plays a significant role in global atmospheric and oceanic circulations. Therefore, changes over the Antarctic ice sheet, such as ice loss, can affect the energy balance over it. West Antarctica and the Antarctic Peninsula have the largest warming trend of the continent in the past decades due to the global climate change. The enhancement of the circumpolar westerlies over the Southern Ocean is thought to be the reason of the austral summer warming over the eastern Peninsula (Luis, 2013).

2.1.3 Surface Mass balance

In general, the processes that contribute to the mass balance of ice sheets are snowfall and deposition, which increase mass, and sublimation, surface melt, meltwater runoff, basal melt due to geothermal heating, iceberg calving and basal melt of ice shelves that lead to mass loss (Vizcaíno et al., 2014). The surface mass balance (SMB) (Eq. 2.1.1) is defined as the annual difference of mass accumulation, through snowfall and rain, and ablation, through sublimation and runoff, whereas runoff (Eq. 2.1.2) can be further interpreted as the available liquid water (ALW) from melting (ME) and rain that is not refrozen (RF). Melting is the sum of surface turbulent, radiative and subsurface heat fluxes (Eq. 3.1.1).

$$SMB = SNOW + RAIN - RU - SU \quad (2.1.1)$$

$$RU = ALW - RF = ME + RAIN - RF \quad (2.1.2)$$

Antarctic ice sheet is fed by snowfall, which varies between the years and the largest ablation term is sublimation of drifting snow (Lenaerts et al., 2012). Most of the meltwater in Antarctica refreezes locally causing the runoff to be negligible. In addition, drifting snow erosion is important locally (Lenaerts et al., 2012). Models project for the future an increase in snowfall that is connected with atmospheric warming due to the increased moisture holding capacity of warmer air (Church et al., 2013).

2.2 Melt Detection

Snow is a mixture of air, ice crystals, liquid water and amounts of chemical impurities (Rees, 2005). As snow deposits onto the ground, an endless process of metamorphism begins. Changes in temperature, humidity and pressure cause a physical change of snow grains within the snowpack. Melting reduces the snow albedo and the reflectivity leading to an increase in absorbed solar radiation, which then provides energy for the production of additional melting (Kuipers Munneke et al., 2011). In addition, meltwater at the surface can percolate downward and partly refreeze, a procedure that forms ice layers in the snowpack and modifies its energy budget and morphology (Cuffey and Paterson, 2010).

Several methods for examining Antarctic surface melting have been used the past years. These include the assessment of melt using ice core stratigraphy and in situ surface energy balance (Trusel et al., 2013). The first method helps in the understanding of melt history for long timescales and in combination with available climate and glaciological records, the changing climate conditions can be observed (Das and Alley, 2008). Regarding the second method, the use of both data collected by weather stations and models that compute the surface energy balance can lead to an analysis of surface melt presence and evolution (Kuipers Munneke et al., 2012b). Near surface air temperature is used as a proxy for melt detection, as it is assumed that melting occurs when the air temperature exceeds 0°C, which is the melting point (Tedesco,

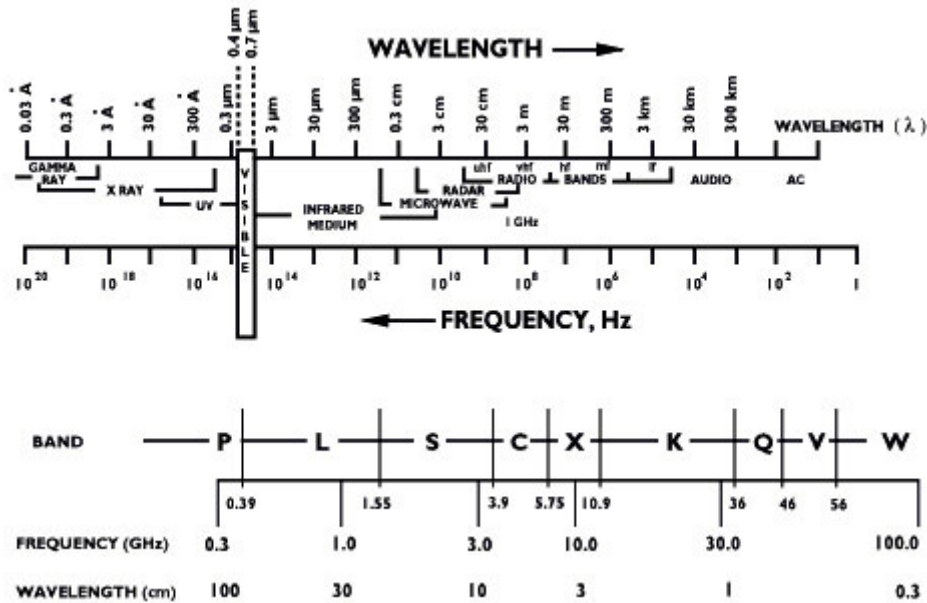


Figure 2.4: Range of electromagnetic radiation and radar frequency bands (From <https://earth.esa.int>).

2014). However, radiative forcing can cause melting even when near surface temperatures are below 0°C . Ice core stratigraphy has the advantage of the long record, which serves in capturing the interannual variations in melt events, and provide robust melt records. However, the major drawback of both methods is the limitation of spatial coverage.

2.2.1 Remote Sensing techniques

Remote sensing offers the opportunity to monitor surface melting at large spatial scales with high temporal resolution and at places where ground observations are difficult to be taken. Remote sensing is defined as the collection of information about an object or feature by an instrument without direct physical contact. Optical and thermal sensors, can provide information about land surface temperature and ice surface temperature that can replace air temperature measurements from in-situ observations. For example, a near surface moisture index (NSMI) for snow was used for the modelling of snow surface moisture (Lampkin and Yool, 2004). However, microwave remote sensors have cloud penetrating capabilities as they operate in the microwave region of electromagnetic spectrum (Fig. 2.4) and they do not require solar illumination, providing the opportunity of a higher temporal resolution compared to optical/thermal sensors that their temporal resolution depends on the presence of clouds. Furthermore, microwave sensors can detect sub-surface melt even when the surface is frozen, since the emitted or backscattered radiation can originate from below the surface (Tedesco, 2014). Moreover, these sensors provide direct measurements of the changes in the electromagnetic properties of the surface from dry to wet conditions. The aforementioned advantages and the greater Ground Instantaneous Field of View (GIFOV) compared to optical data make the microwave sensors suitable for use in climatological studies over ice sheets (Tedesco, 2014).

Electromagnetic Properties of Snow In The Microwave Region

The electrical properties of a material influence the microwave emission and return (Hall and Martinec, 1985). The complex dielectric constant determines the response of a material when forming an electrical field on it and it is a function of frequency and temperature (Hall and Martinec, 1985). The real (ϵ') and the imaginary part (ϵ'') compose the complex dielectric constant (ϵ) of a material (Eq. 2.2.1).

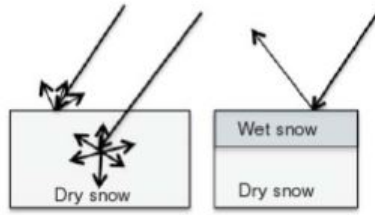


Figure 2.5: Wet snow (right) causes a decrease in backscattered signal because of the surface scattering and increased absorption (Tedesco, 2014).

$$\epsilon = \epsilon' - j\epsilon'' \quad (2.2.1)$$

The real part of the dielectric constant of pure ice is independent of frequency between 100 MHz and 900 GHz and has a weak dependence on temperature (Tedesco, 2014). On the contrary, the imaginary part of the dielectric constant for ice depends on temperature and frequency. The presence of impurities affect ice permittivity and change the values of both real and imaginary part. Stogryn (1986) and Matzler and Wegmuller (1987) have developed models for the real and imaginary part of the dielectric constant of ice.

A snow layer is an homogeneous medium with ice particles that are randomly oriented and have different shapes and sizes (Fung, 1994). The presence of liquid water classifies the snow layer as dry or wet snow and changes its properties. Dry snow is a mixture of ice and air, with air the host medium and ice particles the scatterers. On the other hand, water droplets reside between the ice particles instead of air in wet snow, making water to be considered as a part of the host medium that contributes to absorption. According to these, the real part of dry snow is considered constant with frequency and temperature. On the contrary, the imaginary part is very small, determines the extent of absorption and has a weak dependence on temperature. Due to the low values of absorption coefficient, volumetric scattering of the microwave radiation dominates in the dry snowpack (Fig. 2.5).

Active microwave remote sensing

Active microwave sensors observe the normalized radar backscatter of the Earth's surface (Kunz and Long, 2006). The small dielectric contrast between snow and air for dry snowpack leads to negligible surface backscattering making the microwave backscatter in winter to be a function of volume scattering (Wismann, 2000). According to Fung (1994), the reflectivity of the wet snow is lower than that of the dry snow, thus there is a reduction in volume scattering and an increase in microwave absorption (Fig. 2.5). This is caused by the large increase in the imaginary part of the dielectric constant of water from ice to liquid (Trusel et al., 2012) and it is the main principle in melt detection using scatterometers. Therefore, the presence of liquid water in the snow cover causes the decrease in radar backscatter.

A scatterometer as an active radar device transmits a pulse of electromagnetic energy to a target and measures the back-scattered signal. An object scatters an incident wave into all possible directions with varying strength and with a different scattering pattern depending on the incident direction and the portion of the scattered energy that is directed to the radar receiver is referred to as backscatter. The radar cross section σ of an object observed in a given direction is the ratio of the total power scattered by an equivalent isotropic scatterer to the incident power density on the object and it is dependent on direction and polarization. When the radar transmitter and receiver (monostatic radar) are in the same medium the radar cross section of the object is given by Eq. (2.2.2) (Fung, 1994):

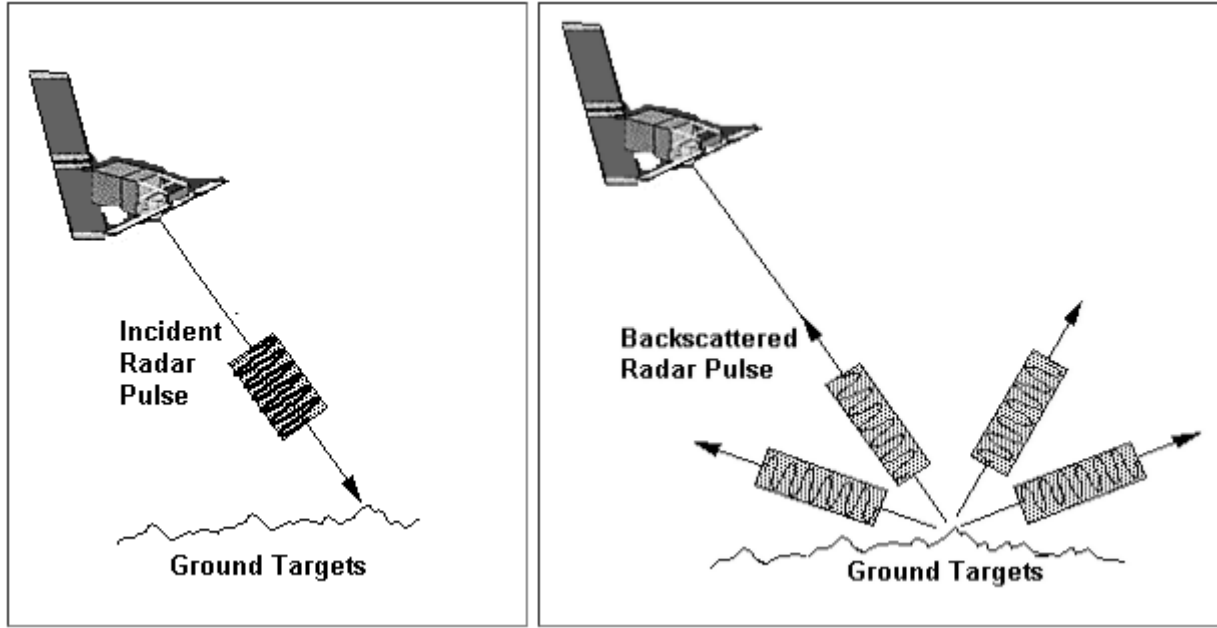


Figure 2.6: A radar pulse is transmitted from the antenna to the ground and is scattered back to the antenna by ground targets (From <https://crisp.nus.edu.sg/>).

$$\sigma = \frac{4\pi R^2 |E^s|^2}{|E^i|^2} = 4\pi |S|^2 \quad (2.2.2)$$

Where R is the range between the target and the radar receiver, E^i the incident field, E^s the scattered field and S the scattering amplitude of the object.

The returned power in radar backscattering measurements (bistatic radar) is given by Eq. (2.2.3):

$$P_r = \frac{P_t}{4\pi R_t^2} G_t \sigma \frac{A_r}{4\pi R_r^2} \quad (2.2.3)$$

$$A_r = \lambda^2 G_r / (4\pi)$$

Where P_t is the transmitted power, G_t is the transmitter-antenna power gain, A_r is the receiver-antenna aperture, λ is the radar wavelength and G_r is the receiver - antenna power gain. It is important to be mentioned that the above equation (2.2.3) is not formulated for area extensive targets and does not include polarization. In order to generalize to a bistatic scattering from an area extensive target, the target is supposed to be composed of an infinite collection of statistically identical targets with a statistically averaged cross section of differential size $d\sigma$, which is the product of the averaged radar cross section per unit area σ^0 times the differential area ds occupied by each target.

$$dP_r = \frac{P_t G_t G_r \lambda^2 \sigma^0}{(4\pi)^3 R_r^2 R_t^2} ds \quad (2.2.4)$$

Where σ^0 is the scattering coefficient (normalized radar cross section) and it is dimensionless. Scatterometers obtain measured values of σ^0 from Eq. (2.2.5) and since it can cover many orders of magnitude it is often specified logarithmically in decibels (Eq. 2.2.7).

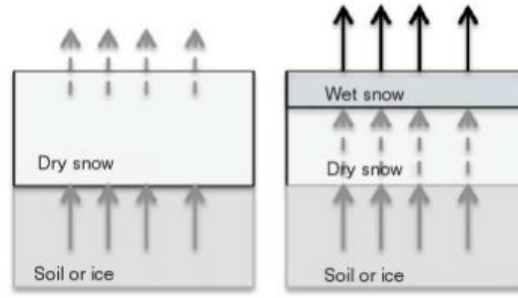


Figure 2.7: The wet snow layer (right) absorbs the radiation from the bottom layers and emits a stronger signal than that of the dry snow (left) (Tedesco, 2014).

$$\sigma^0 = \frac{(4\pi)^3 P_r R_t^2 R_r^2}{P_t \lambda^2 G_t G_r A} \quad (2.2.5)$$

$$\sigma^0 = \frac{\sigma}{A_0} \quad (2.2.6)$$

$$\sigma^0(dB) = 10 \log_{10} \sigma^0 \quad (2.2.7)$$

Backscattering coefficient (σ^0) depends on the frequency, polarization and incidence angle of the emitted electromagnetic wave and the roughness, geometric shape and dielectric properties of the target. The frequency of the emitted radiation affects the penetration depth of the waves that tends to be longer with longer wavelengths. However, other parameters, such as moisture, are related also to the penetration depth. Specifically, the penetration depth decreases with increasing water content. In addition, the relative roughness of the targeted surface is determined by the frequency and the local angle of incidence of the incident wave. If the surface has dimensions comparable to the incident wavelength, then it is considered rough. A smooth surface tends to reflect most of the incident energy away from the radar. Furthermore, the incidence angle, the angle between the perpendicular to the surface and the direction of the incident radiation, influences backscattering coefficient.

Passive microwave remote sensing

Radiometers in passive remote sensing measure the brightness temperature of the target. The basis of radiometer meltwater detection is the sudden increase in microwave brightness temperature (T_b). The presence of liquid water in the snowpack causes the absorption of the radiation emitted from the bottom snow layer and soil by the wet snow layer (Fig. 2.7), and the increase in upwelling T_b . Consequently, T_b approaches the physical temperature of the wet snow layer making it to act as a black body and emit more energy (Tedesco, 2014), hence causing a significant increase in brightness temperature (Liu et al., 2006). Even though other factors, such as a decrease in grain size or an increase in snow temperature, can cause a rise in brightness temperature, the presence of liquid water causes a shorter and significant increase in T_b (Tedesco, 2009). However, radiometers can only provide information indicating the presence or absence of melt, because T_b saturates at small fractions of liquid water (Trusel et al., 2012).

Differences between active and passive microwave record

Some major differences between active and passive measurements exist. Specifically the passive microwave record starts from 1978 to present (SMMR, SSM/I, AMSR-E, AMSR 2) and it is longer than the active microwave record that starts in 1991 (ERS 1 & 2, QuikSCAT, OSCAT, ASCAT). In addition, it is reported that

the scatterometers are more sensitive to liquid water than radiometers (Kunz and Long, 2006). Finally, the spatial resolution of scatterometers is higher (e.g. effective resolution of QuikSCAT is 8-10 km and SSM/I 19-GHz channel is 38-45 km), allowing them to observe surface melt more precisely.

3

Methodology

The goal of this study is the investigation of the Antarctic surface melting dynamics. Thus, radar backscatter data, passive microwave brightness temperatures and in-situ data from weather stations are used for the analysis of surface melting dynamics across Antarctica. Further details regarding the data and the methods used are presented in this chapter.

3.1 Data Overview

Active and passive microwave remote sensors have been used for surface melting studies with very promising results that need to be further investigated. A description of the satellite data and temperature data used for validation follows.

3.1.1 Satellite Data

In this study satellite data from the SeaWinds scatterometer aboard the QuikSCAT satellite, the Oceansat Scatterometer (OSCAT) and the Advanced Scatterometer (ASCAT) are used and downloaded from the Brigham Young University (BYU) NASA Scatterometer Climate Record Pathfinder (SCP) ¹.

QuikSCAT

QuikSCAT operated between June 1999 and November 2009 at Ku-band (13.4 GHz) and measured normalized dual polarization radar cross-section backscatter (σ^0). It is a dual-pencil-beam conically scanning scatterometer (Spencer et al., 2000). The measurements were made at two constant incident angles of 46° and 54°, corresponding to 1400 km and 1800 km for the horizontally polarized inner beam and vertically polarized outer beam, respectively. For the QuikSCAT, the nominal instantaneous antenna footprint is an ellipse and slices are the individual σ^0 measurements obtained for each footprint. Although twelve measurements per footprint are obtained, 4-6 km long and 20 km wide, only the central eight of them are obtained in the L1B data product, which are summed producing the 'egg' measurements. The egg measurements have lower resolution, but they have less noise and are less sensitive to calibration errors (Long, 2010). The QuikSCAT data can be enhanced from their native 25 km spatial resolution to 4.45 km (8-10 km effective

¹<http://www.scp.byu.edu/>

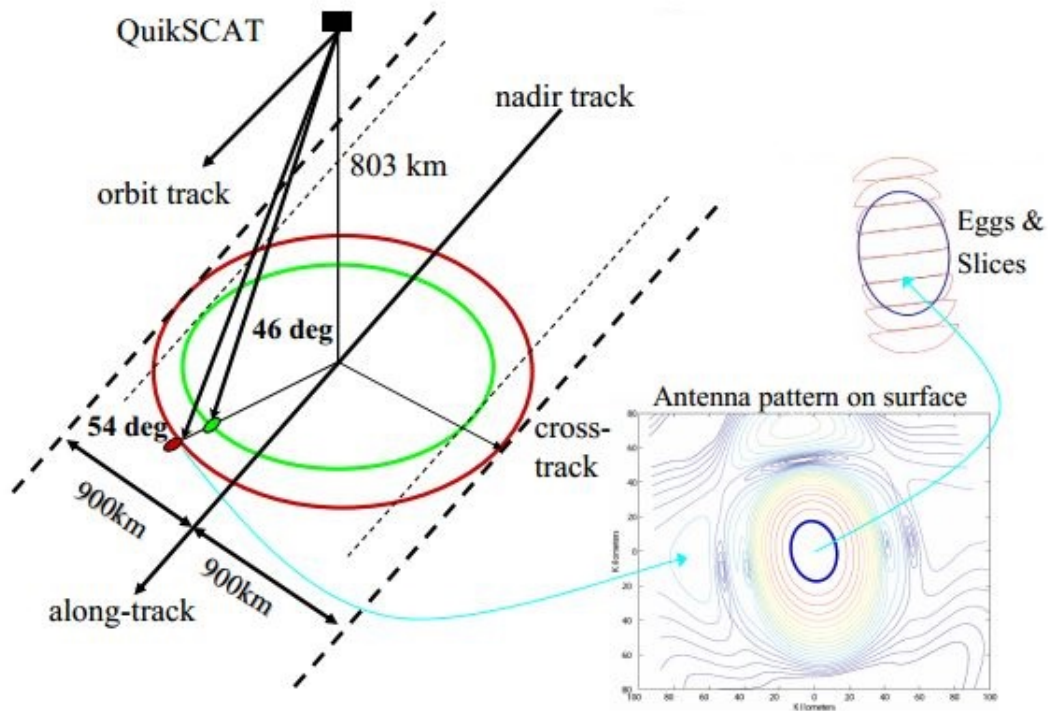


Figure 3.1: QuikSCAT observation geometry (Long, 2010).

resolution) for the egg-based images and to 2.225 km (5 km effective resolution) for the slice-based images. This can be done by using the Scatterometer Image Reconstruction (SIR) algorithm², by utilizing the multiple daily overpasses (Long, 2010) of QuikSCAT over the polar regions due to its orbit geometry (98.6° inclination and 803 km altitude) and wide swath. In order to generate the final image product, SIR extracts information in the side lobes of the measurement response function, and thus it is considered a true reconstruction algorithm (Long, 2010). The SIR images for the polar regions are separated into morning, midday and evening data (4 AM to 12 PM, 12 PM to 8 PM and 8 PM to 4 AM local times for southern hemisphere respectively). Based on QuikSCAT orbit geometry, the available images for Antarctica are morning that contain data from 4 AM to 12 PM and midday that contain data from 12 PM to 8 PM.

OSCAT

The Oceansat-2 Ku-band (13.5 GHz) scatterometer (OSCAT) was launched on September 2009 and operated until February 2014. It has similarities with QuikSCAT, and thus it is viewed as a continuity mission for QuikSCAT. OSCAT is also a dual-pencil-beam conically scanning scatterometer and has similar features with QuikSCAT, including antenna dimensions, frequency, polarization and orbital characteristics (Lindell and Long, 2016). Both scatterometers have a similar sun-synchronous near-polar orbit with similar orbital inclinations of 98.6° and 98.28° and an orbital altitude of 803 km and 720 km for QuikSCAT and OSCAT respectively. There is a difference in the incidence angles between the two instruments, which is 54° and 57° (outer vertically polarized beam) and 46° and 49° (inner horizontally polarized beam) for QuikSCAT and OSCAT respectively. As backscatter is partially dependent on the incidence angle, this difference is relevant to the melt detection algorithm. The same image formation algorithms are used for OSCAT as described above. In addition, there are calibration inconsistencies in OSCAT dataset in contrast to QuikSCAT that a consistent calibration throughout its mission lifetime exists (Lindell and Long, 2016). Based on OSCAT orbit geometry, the available images for Antarctica are morning that contain data from 4 AM to 12 PM and evening that contain data from 8 PM to 4 AM.

ASCAT

²Developed by Brigham Young University (BYU)

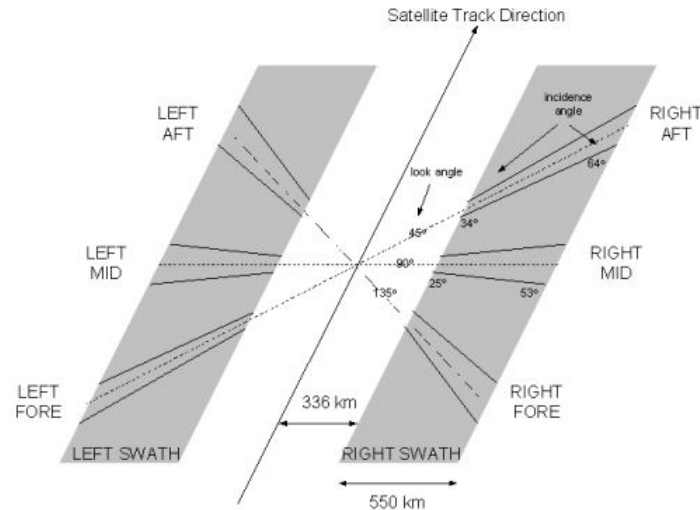


Figure 3.2: ASCAT observation geometry (EUMETSAT, 2015).

ASCAT on board the European Meteorological Satellite Organisation (EUMETSAT) MetOp-A was launched on October 2006. Its characteristics are different from the two aforementioned scatterometers, since it operates in C-band (5.225 GHz) and it consists of 50 km-resolution cells. It is a dual-fan-beam scatterometer with vertically polarized fixed three beam antennas looking 45° (fore-beam), 90° (mid-beam) and 135° (aft-beam) of the satellite track, which together sweep out two 500 km swaths on both sides of the ground track separated by a nadir gap (Bentamy et al., 2012). The incidence angle varies in the range 34° - 64° for the outermost beams and 25° - 53° for the mid-beam. The data used for this study were reconstructed using the SIR algorithm with 4.45 km/pixel resolution and σ^0 values in dB are normalized to the 40° reference incidence angle (Lindsley and Long, 2010). Based on ASCAT orbit geometry, the available images for Antarctica are morning that contain data from 4 AM to 12 PM and evening that contain data from 8 PM to 4 AM. It is mentioned that data from 2007 - 2009 are not currently available at the NASA Scatterometer Climate Record Pathfinder (SCP).

The data of resolution 4.45 km/pixel from morning (QuikSCAT, OSCAT, ASCAT) and midday (QuikSCAT) passes with vertical (QuikSCAT, OSCAT, ASCAT) and horizontal (QuikSCAT, OSCAT) polarization are used in the study. Regarding the use of vertically or horizontally polarized data, Kunz and Long (2006) have reported that even though the QuikSCAT dual polarization backscatter measurements are correlated, they show different sensitivities to the presence of liquid water. Particularly, the horizontally polarized backscatter has a greater sensitivity to liquid water in the snow cover than the vertically polarized backscatter (Fig 4.1), and especially for QuikSCAT the horizontally polarized backscatter is stronger because of the lower incident angle at horizontal polarization (46°) compared to that of vertical polarization (54°) (Ulaby and Stiles, 1981). While Trusel et al. (2012) used vertically polarized data, others (Kunz and Long, 2006; Wang et al., 2007, 2008; Barrand et al., 2013; Bothale et al., 2015) have used horizontally polarized QuikSCAT data.

AMSR

In addition to the data from scatterometers, data from radiometers are also used. Specifically in this study, data from the Advanced Microwave Scanning Radiometer - Earth Observing System (AMSR-E) on NASA's Aqua satellite and the Advanced Microwave Scanning Radiometer 2 (AMSR2) on JAXA's GCOM-W1 spacecraft are used for the comparison of the results.

AMSR-E was developed based on the AMSR design and it is a twelve channel, six frequency, passive microwave radiometer system. It was launched on May 2002 and ceased operations on December 2011. Vertically and horizontally polarized brightness temperatures are measured at 6.9, 10.7, 18.7, 23.8, 36.5, 98.0 GHz at spatial resolution that varies from 5.4 km at 89 GHz to 56 km at 6.9 GHz at an altitude of 705 km over an angular $\pm 61^\circ$ about the sub-satellite track, which results in a swath width of 1445 km. It is a conically

Table 3.1: Characteristics of the sensors used in the study

	QuikSCAT	OSCAT	ASCAT	AMSR-E	AMSR2
Frequency (GHz)	13.4	13.5	5.225	6.9, 10.7, 18.7, 23.8, 36.5, 98.0	6.9, 7.3, 10.7, 18.7, 23.8, 36.5, 98.0
Incidence angle	46° & 54°	49° & 57°	25° - 64°	55°	55°
Polarization	HH & VV	HH & VV	VV	HH & VV	HH & VV
Swath Width (km)	1400 & 1800	1400 & 1836	500	1445	1450
Orbit Altitude (km)	803	720	800	705	700
Orbit inclination (deg)	98.6	98.28	98.6	98.2	98.2
Resolution of data	4.45 km/pixel	4.45 km/pixel	4.45 km/pixel	12.5 km/pixel	10 km/pixel
Time of day	Morning & Midday	Morning & Evening	Morning & Evening	Midday & Evening	Midday & Evening
Time period	1999 - 2009	2009 - 2014	2007 - present	2002 - 2011	2012 - present

scanning radiometer which rotates continuously about an axis parallel to the Aqua satellite at 40 revolutions per minute (rpm). AMSR2 is similar to AMSR-E with some important improvements. One of them is the addition of 7.3 GHz channels. It was launched on May 2012 and is currently operating. AMSR2 measures weak microwave emission of the surface and temperature from about 700 km altitude over a 1450 km swath.

3.1.2 In-Situ Data

Meltwater production can be determined using energy balance observations [Eq. (3.1.1) where M is the melt energy, SW_d and LW_d are the downward directed fluxes of shortwave and longwave radiation, α is the surface albedo, $\epsilon = 0.97$ is the surface emissivity for longwave radiation, σ is the Stephan-Boltzmann constant, LHF and SHF are the turbulent fluxes for latent and sensible heat and G_s is the subsurface heat flux toward the surface]. Since there is lack of this kind of observations over most of Antarctica, near surface air temperature is used as a reliable proxy for melt presence. According to Ohmura (2001) this approximation is sufficiently accurate, as air temperature is correlated with longwave atmospheric radiation, which is the dominant heat source, and with shortwave radiation and sensible heat fluxes. Hence, although there is no direct relationship between surface meltwater and air temperature, the positive degree day (PDD) approach is found to be correlated with meltwater production (Hock, 2005).

$$\begin{aligned}
 M &= SW_{net} + LW_{net} + LHF + SHF + G_s \\
 &= SW_d(1 - \alpha) + LW_d - \epsilon\sigma T_s^4 + LHF + SHF + G_s
 \end{aligned}
 \tag{3.1.1}$$

For this reason, air temperature data from the National Climate Data Center (NCDC) Global Surface Summary of the Day (GSOD) database are used for the calibration and validation of the melt detection method. The GSOD is derived from the Integrated Surface Hourly (ISH) dataset and provides single daily measurements. The raw data are collected from the weather stations at temporal resolutions ranging from 10 minutes to 3 hours intervals. Ten weather stations were selected in this study as it is shown in Figure 3.3.

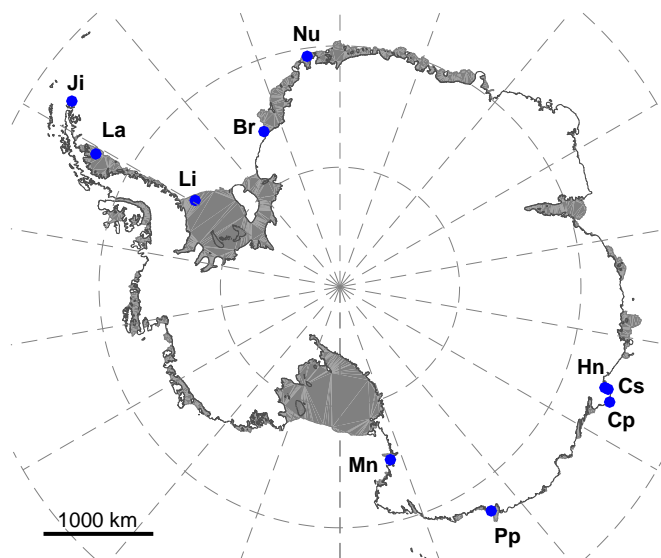


Figure 3.3: Map of Antarctica showing the location of the weather stations used in this study as blue dots (Ji: Joinville Island, La: Larsen C, Li: Limbert, Br: Brunt, Nu: Neumayer, Hn: Haupt Nunatak, Cs: Casey Skiway, Cp: Cape Poinsett, Pp: Penguin Point, Mn: Manuela).

Table 3.2: List of dataset from the National Climatic Data Center (NCDC) Global Surface Summary of the Day (GSOD)

Station Name	Short Name	Latitude [°]	Longitude [°]	Elevation [m]	Begin Date	End Date
Joinville Island	Ji	-63.183	-55.4	75	04/2007	07/2013
Larsen C	La	-67.017	-61.467	45	05/1990	02/2016
Limbart	Li	-75.867	-59.15	40	03/1998	05/2014
Brunt	Br	-75.58	-26.17	10	07/2006	02/2012
Neumayer	Nu	-70.667	-8.25	50	11/1981	-
Haupt Nunatak	Hn	-66.583	110.7	63	04/2004	-
Casey Skiway	Cs	-66.283	110.8	390	08/2001	04/2008
Cape Poinsett	Cp	-65.85	113.067	90	06/2004	-
Penguin Point	Pp	-67.617	146.183	30	01/1997	02/2009
Manuela	Mn	-74.95	163.683	80	05/1990	09/2013

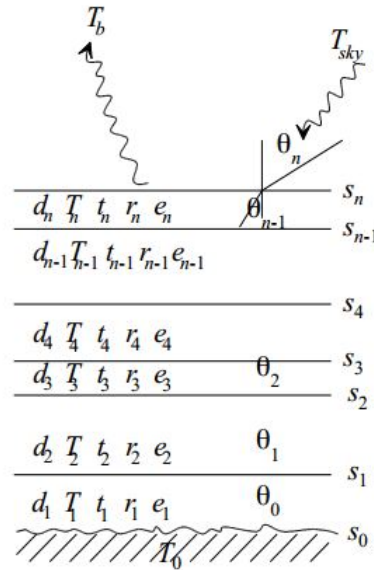


Figure 3.4: Geometry of the n -layered snowpack with an electromagnetic wave incident from above at an incidence angle θ_n . Snow-ground reflectivity s_0 , ground temperature T_0 , layer thickness d_j , temperature T_j , transmissivity t_j , volume reflectivity r_j , emissivity e_j , interface reflectivity s_j , refracted angle θ_{j-1} for layer number j from 1 (bottom) to n (top) (Mätzler and Wiesmann, 2014).

3.2 Analysis

In order to study surface melting over Antarctica using scatterometer data, it is important to understand the backscatter response of different snowpacks and how backscatter changes for different sensor characteristics. Thus, the first step is the investigation of the change in backscatter to changes in snowpack for different frequencies and incident angles using the Microwave Emission Model of Layered Snowpacks (MEMLS). The next step is to evaluate some of the existing threshold-based melt detection approaches and apply some other methodologies with different thresholds for comparison of the melt duration results. Lastly, a methodology for achieving consistency in the final results is described.

3.2.1 Sensitivity test

The first aim of this study is to investigate the backscatter change for different satellites and different snowpacks. For this reason, the Microwave Emission Model of Layered Snowpacks (MEMLS)³ was used. This model was initially developed in 1990s (Mätzler, 1996; Wiesmann and Mätzler, 1999) for microwave emissions of snowpacks in the frequency range 5 - 100 GHz and in order to describe the radiative transfer in snow including multiple volume scattering and absorption, it used the six-flux theory⁴. Recently, an extension of the model including a backscatter model for active microwave remote sensing of snow was introduced (Proksch et al., 2015). The snowpack is considered as a stack of horizontal layers, each one of them characterized by snow parameters, such as temperature, liquid water content, salinity, density, layer thickness and correlation length (Fig. 3.4). In order to take into account the internal scattering and the reflections at the interface, a sandwich model is used.

As the scattering coefficient depends on frequency and snow properties, parameters that are required as an input in the model include information about the microwave sensor, such as viewing angle and frequency,

³The model is written in Matlab and it is publicly available through the website <http://www.iapmw.unibe.ch/research/projects/snowtools/memls.html>

⁴A detailed description of MEMLS is included in the technical documentation of the model Mätzler and Wiesmann (2012, 2014)

Table 3.3: Simulation parameters

Layer No	Temperature (K)	Density (kg/m ³)	Thickness (cm)	Exponential Correlation Length (mm)	Salinity (ppt)	Snow - ground reflectivity	Mean Slope of Surface Undulations
						0	0.07
1 (Bottom)	240	917	10000	0.6	0		
2	250	750	500	0.5	0		
3	250	550	500	0.5	0		
4 - 21	260 - 270	300 - 500	5 - 30	0.1 - 0.4	0		
22 (Top)	270	250	5	0.1	0		

and about the snowpack such as density, temperature and roughness. In this way, testing of different satellites and snowpacks is possible, in order to investigate the different sensitivities of each sensor to changes in the snowpack.

In particular, the main snowpack used for the experiments has 22 layers as it is specified in Table 3.3, consisting of a thick ice layer at the bottom and thinner and less dense layers on the top. Several other snowpacks with a lower number of layers or with the presence of ice layers within the snowpack were used for the experiments but the results are not shown. The influence on the different snowpack parameters on backscatter response is examined, by changing the parameters of the main snowpack (density, temperature, layer thickness and exponential correlation length). The angular response of the backscatter to dry and wet snowpacks at different frequencies for both vertical and horizontal polarization is also examined. In addition, a comparison in backscatter change and brightness temperature change with increasing liquid water content only to the top 5 cm snow layer between QuikSCAT, ASCAT and AMSR follows.

3.2.2 Melt detection

Microwave melt detection was used in various studies for different regions, as it is already mentioned in section 1.1, and the basis for this concept is the influence of the presence of liquid water on the snow electrical properties at microwave frequencies (Barrand et al., 2013). The high dielectric constant of liquid water causes a reduction in volume scattering and an increase in microwave absorption (Trusel et al., 2012). Thus, as the amount of liquid water in the snow cover increases, the radar backscatter decreases (Kunz and Long, 2006).

The threshold-based melt detection method is the standard method used by recent studies and it will be followed in this study using different thresholds. According to this approach, a day for each pixel is characterized as a melting day (*MD*) if its backscatter value (σ_i^0 in dB) is lower than the austral mean winter backscatter ($\overline{\sigma_w^0}$ in dB) by a certain threshold (b in db) (Eq. 3.2.1). In general, the basis of this method lies on the characteristic backscatter pattern of the majority of melt events: large and abrupt reductions in backscatter during melting, followed by large and abrupt increases during freeze-up leading to generally stable winter backscatter. However, this pattern varies depending on the location (e.g. ablation area, percolation zone) and the climatic conditions (amount of snow accumulation and rate of melting) that contribute to the firn formation. Specifically, ice layers that contain big scatterers that dominate radar backscatter can be formed due to refreezing after a melt event. Snow accumulation in the following winter buries the ice layers and tends to attenuate microwave signal, causing a slow temporal reduction in backscatter during

winter. In addition, heavy snow accumulation during summer modifies backscatter even in places experiencing surface melting. It is worth mentioning that backscatter variability is also caused by SIR imaging artifacts introduced by surface conditions (megadunes, sastrugi) sensitive to satellite observations at multiple azimuth angles (Long, 2010), even though instrument noise is in general minimal for the QuikSCAT backscatter signal (Bartsch et al., 2007). All these procedures should be taken into account when implementing a threshold-based melt detection method and in the threshold selection, as they can lead in false melt event detection.

This approach is widely used for melt detection algorithms, with different thresholds depending on the application and the sensor used. A threshold of 2 dB was used by Trusel et al. (2012) for Antarctica, which is close to constants used by other QuikSCAT studies: 3 dB by Barrand et al. (2013) for Antarctic Peninsula, 2 and 3 dB by Wang et al. (2007) for Greenland, 1.7 dB by Wang et al. (2008) for Arctic snowmelt and 1.65 dB by Rotschky et al. (2011) over Svalbard. On the contrary, Bothale et al. (2015) have used an adaptive threshold based classification methodology, in order to capture the backscatter characteristics of an individual grid due to its location. The modeled Ku-band response to wetness by Ashcraft and Long (2006) showed that 1% liquid water content in a 3.8 cm snow layer causes a 3 dB reduction in backscatter. Furthermore, Stiles and Ulaby (1980) found that 1.3% liquid water content in a 48 cm snow layer causes a reduction ranging from 3.5 dB at 8.6 GHz to 8 dB at 17 GHz.

$$\begin{aligned} MD &= 1, \text{ if } \sigma_i^0 < (\overline{\sigma_w^0} - b) \\ MD &= 0, \text{ if } \sigma_i^0 \geq (\overline{\sigma_w^0} - b) \end{aligned} \tag{3.2.1}$$

The Antarctic melt years are determined as the day 201 of first year ($year_i$) to day 200 of the second year ($year_{i+1}$), in order to avoid a split of austral summer. Therefore, winter mean backscatter is calculated from days 201 to 273 (July to September). This value is calculated for every pixel with elevation less than 1000 m (for computational reasons and most of melt occurs below 1000 m) for every melt year. Melt duration for a pixel is defined as the sum of the days that melting occurred at that pixel.

It is important to be mentioned though, that as data from different sensors are used in this study a different threshold should be used. More specifically, the lower frequency of ASCAT compared to QuikSCAT and OSCAT results in less absorption by a layer of wet snow with the same depth and moisture content. Thus, another threshold should be used for melt detection using ASCAT data. However, a relatively small threshold can create false indication of melt events due to other processes which affect the backscatter (Ashcraft and Long, 2006).

A) Evaluation of existing methodologies

Firstly, existing methodologies are applied and evaluated. These methodologies are from Trusel et al. (2012) and Bothale et al. (2015) and a description of them follows. Vertically and horizontally polarized morning data from QuikSCAT and OSCAT and midday data from QuikSCAT are used for the evaluation.

Trusel et al. (2012)

Trusel et al. (2012) used a decision tree method to determine the melting days (Fig. 3.5). According to this method, varying thresholds are used in four detection algorithms and their output is compared in order to select the right threshold for each pixel for each year. Using this tree, false melt detection is eliminated in regions where long melt duration was discovered using a fixed threshold. However, as it is stated 94% of all melting was detected using a fixed 2 dB threshold below the winter mean (Case A). Case B was necessary for the areas, where true surface melting existed but heavy snow accumulation during austral summer caused backscatter reduction. On the other hand, Case C and D were necessary for the cases where snow accumulation in autumn, winter or spring caused a backscatter reduction greater than 2 dB from the winter mean and a larger threshold was used in order to prevent false melt detection after the true melting event. Post melt conditions were calculated as the mean of days 122 - 152 (May) of each year. The first value of

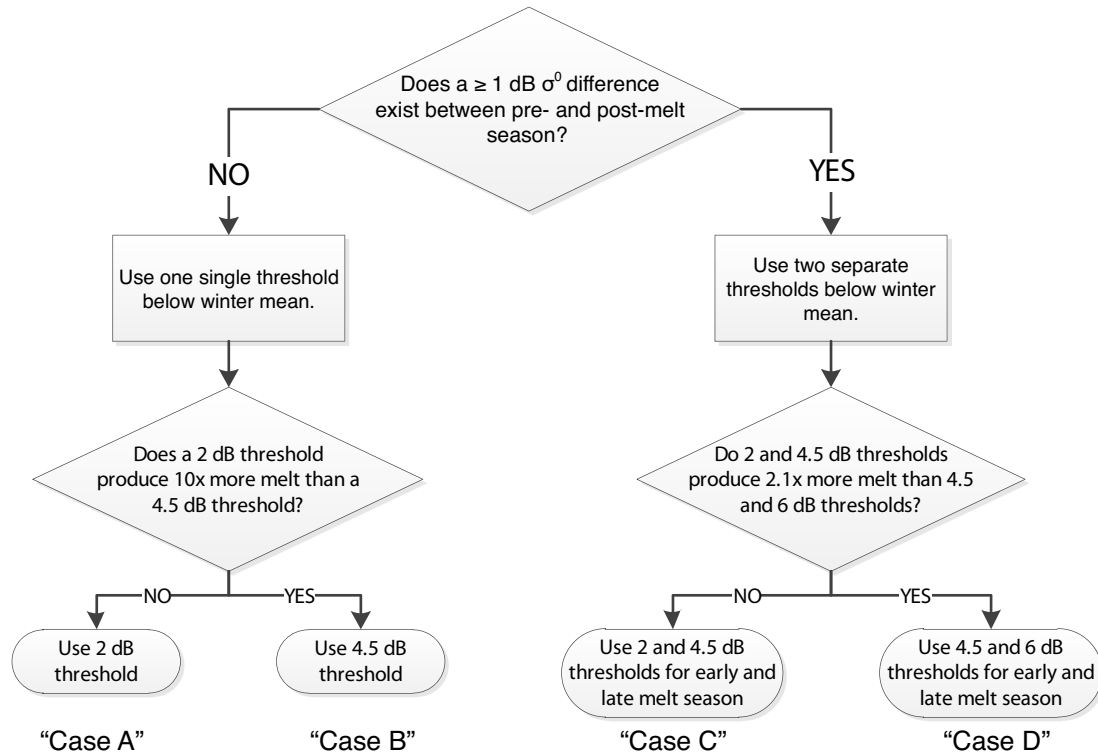


Figure 3.5: Decision tree process for surface melting classification (Trusel et al., 2012).

threshold is effective from day 201 of year one to day 90 of year two and the second from day 91 to day 200 of year two. The data used in the study are vertically polarized QuikSCAT data for the years 1999 - 2009 with spatial resolution 4.45 km from the midday passes (1200 - 2000 h) of the satellite.

Bothale et al. (2015)

Bothale et al. (2015) used horizontally polarized QuikSCAT and OSCAT data (2001 - 2014) with spatial resolution 2.25 km. As it is stated, their adaptive threshold-based classification can capture the different characteristics of every grid. A pixel is defined as melting, when the daily backscatter is below the austral winter mean backscatter by two times the maximum standard deviation of austral winter backscatter in the period 2001-2014. It is mentioned that for the year 2009-10, the winter mean value was calculated by QuikSCAT and the melt detection was performed on OSCAT and thus, an additional offset of 0.5 dB was deducted from the adaptive threshold. According to a cross-calibration performed over various calibration sites, the difference between the backscatter coefficients of QuikSCAT and OSCAT is around 0.25 dB (Bhowmick et al., 2014).

For the Bothale et al. (2015) methodology two different experiments are done, (i) using only the QuikSCAT dataset (1999-2009) to compute the maximum winter backscatter standard deviation and (ii) using both the QuikSCAT and OSCAT dataset (1999-2014) for the computation of the maximum winter backscatter standard deviation.

B) Other methods

In order to understand the importance of the threshold selection and further investigate the capabilities of the threshold-based melt detection approach, a sensitivity analysis is performed by implementing two other methods that combine the approach of Trusel et al. (2012) and Bothale et al. (2015). Specifically, one method uses a single threshold for all the days of an austral melt year that it is a function of the different surface conditions (pixel dependent). The second method uses two thresholds for early and late melt season as it is

described below in the case that σ^0 decreases substantially during winter due to snow accumulation.

QuikSCAT

In the first additional method, called M1, the threshold b is set proportional to two times the winter standard deviation ($2std$) of the signal, in order to take into account the spatial variability, but if $2std$ is less than 3 dB, then b is set to 3 dB. The sensitivity test (Fig. 4.2) showed that a 3 dB threshold can still detect small values of liquid water content. The logic behind M1 is that a small standard deviation can result to a small threshold that will lead to false melt events.

The second method, called M2, follows the Trusel et al. (2012) and Wang et al. (2007) proposition, by using two different thresholds for early and late melt season if the difference in pre- and post- melt conditions exceeds 1 dB. Thus, the threshold b for the days from day 201 of year one to day 90 of year two is the same as above ($2std$ or 3 dB) and for the days from day 91 to day 200 of year two is 4.5 dB as in Trusel et al. (2012).

ASCAT

In the SCP archive, the difference between ASCAT and QuikSCAT images is that, in order to be able to have two-day local time-of-day images for Antarctica, four consecutive days of ASCAT data are used for the production of the final product and they overlap by two days (e.g. days of year 111-114, 113-116 are produced) (Lindsley and Long, 2010). For this reason, the ASCAT dataset does not have daily resolution as the QuikSCAT dataset does. This difference makes the two time series of melt duration obtained by the different datasets inconsistent. In addition, as melting varies throughout the day, it is less probable to detect melting during morning and evening than midday. The underestimation of melting days by ASCAT due to morning measurements instead of midday enhances the inconsistency. A way to overcome the problems discussed above is to multiply the melt duration results obtained by implementing the melt detection methodology as for QuikSCAT dataset, by a fraction as it is discussed later.

As Lindsley and Long (2016) mention, the azimuth modulation magnitude is larger for ASCAT data than for QuikSCAT data, due to the geophysical structures (like megadunes and sastrugi) that are more significant at C-band than at Ku-Band. In general, the measurements of scatterometers are taken over a range of incidence angles and azimuth angles. Even though in more regions σ^0 does not depend on azimuth, there are regions in East Antarctica with physical structures that cause a strong azimuth dependence (Long and Drinkwater, 2000). However, the SIR algorithm does not take into account the azimuth angle information (Lindsley and Long, 2010) and this results in some noise in the data (Fig. 4.9 locations: Cs, Mn, Pp).

The Trusel et al. (2012) methodology is applied again using the same thresholds as for QuikSCAT. As the sensitivity of ASCAT in liquid water content is less than QuikSCAT, a lower threshold can be also used for the detection of small liquid water amounts. The two other methodologies followed for melt detection are the same as those discussed above for QuikSCAT with an alternative threshold of 2 dB instead of 3 dB for the method called M3 and 4 dB instead of 4.5 dB for the method called M4.

Consistent Dataset

In order to obtain consistency between the melt duration results from QuikSCAT and ASCAT, a fractional melt detection method is tested. In this method, the annual melting days calculated from ASCAT are multiplied by two fractions. The first fraction represents a temporal fraction, i.e. the difference of a dataset with daily resolution (available images for all days of year) and a dataset with data for the number of days as ASCAT dataset (Full year / half year). The second fraction represents a diurnal fraction, i.e. the missing melting days when using the morning instead of the midday measurements (Midday / Morning). Both of the fractions are computed using the QuikSCAT melt duration results for a dataset with half days (morning), the full morning dataset and the full midday dataset respectively. In particular, the fractions are computed for each pixel each year and the mean value is used for the final multiplication with the ASCAT melting days. The uncertainty is computed using the error propagation law on the equation (3.2.2) by assuming no error in the first term ($ASCAT_{morning}$) and using the standard deviation computed for the two last terms

Table 3.4: Overview of threshold based melt detection methods

Method	Threshold Early Melt Season (dB) [day 201 year _i to day 90 year _{i+1}]	Threshold Late Melt Season (dB) [day 91 to day 200 year _{i+1}]
Trusel et al. (2012) [QuikSCAT / ASCAT]	2 (case A & C) / 4.5 case(B & D)	2 (case A) / 4.5 (case B & C) / 6 (case D)
Bothale et al. (2015) [QuikSCAT]	$2 * \sigma_{max(std)}^0$	$2 * \sigma_{max(std)}^0$
M1 [QuikSCAT]	$\max(2 * \sigma_{std}^0, 3)$	$\max(2 * \sigma_{std}^0, 3)$
M2 [QuikSCAT]	$\max(2 * \sigma_{std}^0, 3)$	4.5
M3 [ASCAT]	$\max(2 * \sigma_{std}^0, 2)$	$\max(2 * \sigma_{std}^0, 2)$
M4 [ASCAT]	$\max(2 * \sigma_{std}^0, 2)$	4

($F_{temporal}$, $F_{diurnal}$). The different sensor and threshold sensitivities to melt are not taken into account in this method because of the lack of overlapping QuikSCAT and ASCAT data in 2007-2009, that would assist in the comparison of melt duration results in the same years and climatic conditions.

$$ASCAT_{afternoon} = ASCAT_{morning} * F_{temporal} * F_{diurnal} \quad (3.2.2)$$

Passive Microwave Record

Passive microwave radiometers were used in several studies for melt detection over Antarctica. Even though the resolution of these sensors is coarser than scatterometers, the melt detection results from radiometers can be useful in this study for extracting information for the interannual variations of melting in the different regions. Previous work done using the Scanning Multichannel Microwave Radiometer (SMMR) and the Special Sensor Microwave Imager (SMM/I) reported that the 19 and 37 GHz frequencies are suitable for snowmelt detection, in contrast to 22 GHz frequency that is used for water vapor and the 85 GHz frequency that is influenced by water vapor and clouds (Abdalati and Steffen, 1997; Torinesi et al., 2003). For this reason, the 18.7 GHz frequency for AMSR-E and AMSR2 is used in this study.

The melt detection algorithm followed is adapted from Torinesi et al. (2003) and Tedesco et al. (2007). Specifically, a snow pixel is classified as wet, if the brightness temperature of the pixel on a specific day (T_b) is greater than T_c (Eq. (3.2.3)). Thus, T_c is computed for each pixel and each year as the sum of T_m (mean winter temperature) plus a $\Delta T = 3std$, where std is the standard deviation that is computed by removing the values more than 30 K above the annual mean as described in Torinesi et al. (2003). The filter is used in order to eliminate strong melting signals from the computations. In addition, in the case that $3std$ is less than 30 K, then ΔT is set to 30 K (Tedesco et al., 2007). The data used in the study are daily ascending (midday), in order to correspond with peak insolation and melting with spatial resolution 12.5 km/pixel for AMSR-E and 10 km/pixel for AMSR2. As Torinesi et al. (2003) mention, the increase in brightness temperature is greater at horizontal than at vertical polarization for small amounts of liquid water content for a given frequency. For this reason, as scatterometers are already more sensitive to melt, observations at horizontal polarization are used.

$$\begin{aligned}
 MD &= 1, \text{ if } T_b > T_m + \Delta T \\
 MD &= 0, \text{ if } T_b \leq T_m + \Delta T \\
 T_c &= T_m + \Delta T
 \end{aligned} \quad (3.2.3)$$

Comparison

A comparison of the melt detection results of the active and passive microwave records is performed. As it is not possible to compare the results from scatterometers and radiometers spatially, because of the different resolution, four classes that represent the percentage of the pixel in the coarse resolution of AMSR-E that melts, based on the results at the fine resolution of QuikSCAT are created (1-25%, 26-50%, 51-75%, 76-100%). Thus, the number of melting pixels in the fine resolution that correspond to a pixel in the coarse resolution of AMSRE based on the QuikSCAT data is found, and the pixel in the coarse resolution is classified to one of the four classes according to that number. Hence, the final result are annual melt duration results using QuikSCAT data at the same resolution as AMSR-E data.

3.2.3 Melt Metrics

Three other metrics calculated and analysed temporally and spatially (regional and local scale) by other recent studies (Trusel et al., 2012; Barrand et al., 2013) are the total area melt extent in km², the melt index in km²*days and the total annual melt intensity. Melt extent is calculated by multiplying each pixel in which melting occurred for at least one day with the pixel area (QuikSCAT and ASCAT: 19.8025 km², AMSR-E: 156.25 km², AMSR2: 100 km²). On the other hand, melt index is important and commonly used, as it takes into account both spatial and temporal dimensions of melting and it can be calculated as the product of pixel area and the total annual melt duration in that pixel, summed for all pixels experiencing melt within an area of interest.

A proxy for annual relative melt intensity was proposed by Trusel et al. (2012) to be the summed melting-decibel days for each austral summer melt season. Their results showed that the scatterometer reductions can be used as a proxy for annual relative melt intensity, as there is a strong correlation between the annual positive degree days and the annual melting decibel days. This comes in agreement with previous studies, as Wismann (2000) and Smith et al. (2003) also demonstrated that even though there is no direct relation between the air temperature and the backscatter, the magnitude and duration of the reduction in C-band radar cross section correlates with the positive degree days (PDD). According to these, the seasonally summed melting decibel days (MDD in dB days) are computed for every pixel for every austral summer melt season using the equation (3.2.4).

$$MDD_{year\ n+1} = \sum_{i=day201, year\ n}^{i=day200, year\ n+1} MD(\overline{\sigma_w^0} - \sigma_i^0) \quad (3.2.4)$$

The mask determining the continental and ice shelf margins that was used for calculating the metrics is taken from the MODIS Mosaic of Antarctica (Haran et al., 2005). The mapping toolbox Antarctic Mapping Tools was used for creating Antarctic maps (Greene et al., 2017). As the mask refers to data from period 2003-2004, it does not take into account changes in the margins like the existence of Larsen B ice shelf prior 2002, when it collapsed.

3.2.4 Diurnal Variability of Melt

A comparison of the melt detection results from the morning and midday QuikSCAT data can give information about the extent of the regions that experience morning and afternoon melt or only afternoon melt. Thus, for each year (2000 - 2009) the melting areas in Antarctica are classified into the regions that melt is detected in the morning and in the afternoon (at least for one day of the year), marked with 1, and the regions that experience only afternoon melt, marked as 0. The mean of the ten years is calculated and another classification takes place, with three classes, (*i*) the areas in which morning and afternoon melt almost

always overlap (mean ≥ 0.9), *(ii)* the areas that there is only afternoon melt (mean ≤ 0.1) and *(iii)* the areas that can experience morning and afternoon melt in some years (Fig. A.29).

4

Results and Discussion

In this chapter the results of the sensitivity test and the different melt detection methods are presented and discussed.

4.1 Sensitivity Test

The aim of the sensitivity test is to check how the different sensors react differently to changing snowpack parameters. This is achieved by using an electromagnetic model, the Microwave Emission Model of Layered Snowpacks (MEMLS). According to the results of the experiments, the snow layer temperature does not influence backscattering and the larger dependence of the response is on the presence of liquid water in the snow layer that alters the dielectric constant, on the exponential correlation length of snow, on the density of the layers and their thickness, on the incidence angle and the frequency of the emitted radiation. This is in accordance with literature, as Rees (2005) mentions that the dielectric constant of the surface, its roughness properties and the scattering geometry are affecting scattering radiation from a surface.

Specifically, backscatter decreases as the thickness of snow layer increases at incidence angles over 10° , because the contribution of layers below is less. The total backscatter is dominated by the scattering from large scatterers in the ice layers below snow layer. Increasing values of exponential correlation length and density cause an increase in backscattering. It is worth mentioning that the difference in backscatter response for the different parameters (thickness, density, exponential correlation length) of the top (snow) layer in lower frequencies is less important than in higher frequencies (Fig. 4.1), because the shorter wavelength of the higher frequencies results into smaller penetration in the snowpack and backscatter is more influenced by the top layer. Figure 4.1 shows the angular response of σ^0 for wet and dry snow conditions at different microwave frequencies for both vertical and horizontal polarization. The differences in the backscatter for the other snowpacks response were noticed in the lower frequencies. However, the shape of the curves does not change significantly. According to Rees (2005) the general form of the dependence of the backscattering coefficient of wet snow to incidence angle is typical, as volume and surface backscatter that contribute to the total backscatter tend to dominate at large incidence angles and at incidence angles near zero respectively. From these simulations it is concluded that the sensitivity to liquid water content is larger at higher frequencies, increases slightly with incidence angle and it is slightly higher at horizontal than vertical polarization. As only vertical polarization measurements are acquired by ASCAT, vertical polarization measurements from QuikSCAT will be used in order to have consistency in the data.

Figure 4.2 shows the change in σ^0 with increasing liquid water content for QuikSCAT (frequency 13.4 GHz

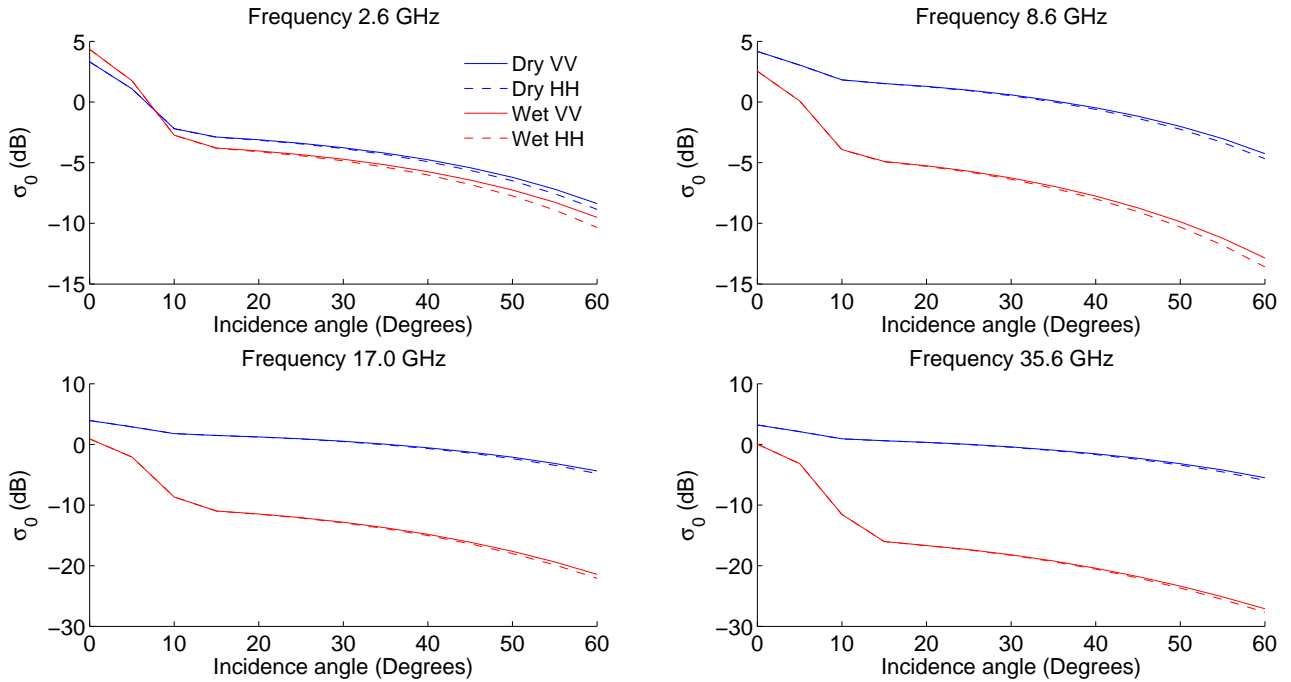


Figure 4.1: Angular response of σ^0 to dry and wet snow at different frequencies for vertical and horizontal polarization. The snowpack used is described in Table 3.3.

and incidence angle 54°) and ASCAT (frequency 5.225 GHz and incidence angle 40°) for vertical polarization and the influence of the snow layer density and exponential correlation length is compared for the two different sensors for the same snowpack as above. It is worth mentioning that the result was insignificantly different for other snowpacks, especially in low values of liquid water content. It is clear that the backscatter decreases at a higher rate for QuikSCAT than for ASCAT (Fig. 4.3) and the sensitivity of QuikSCAT backscatter to liquid water decreases for less rough snow surfaces for values of liquid water content greater than 1%, whereas the sensitivity of ASCAT backscatter remains constant. This is the result of what was already discussed as the QuikSCAT backscatter is more affected by the changes in top snow layer than ASCAT, due to the shorter wavelength. A decrease of approximately 3 dB is a consequence of liquid water values below 0.2% for QuikSCAT and around 1% for ASCAT. From Figures 4.2 and 4.3 the choice of the threshold for the melt detection follows. Specifically, on the one hand a 3 dB threshold for QuikSCAT is enough to detect the presence of very small liquid water content. However, on the other hand the corresponding threshold for ASCAT is much smaller than for QuikSCAT (less than 1 dB) and it can cause false melt events detection due to backscatter variability caused by other processes. Thus a greater threshold should be used, such as 2 dB. Regarding OSCAT, the small difference in the incidence angle (57°) does not cause any significant difference in backscatter decrease due to the presence of liquid water compared to that of QuikSCAT.

4.2 Melt Detection

Firstly, the existing methodologies for melt detection from Trusel et al. (2012) and Bothale et al. (2015) are evaluated and the implementation of other methodologies follows.

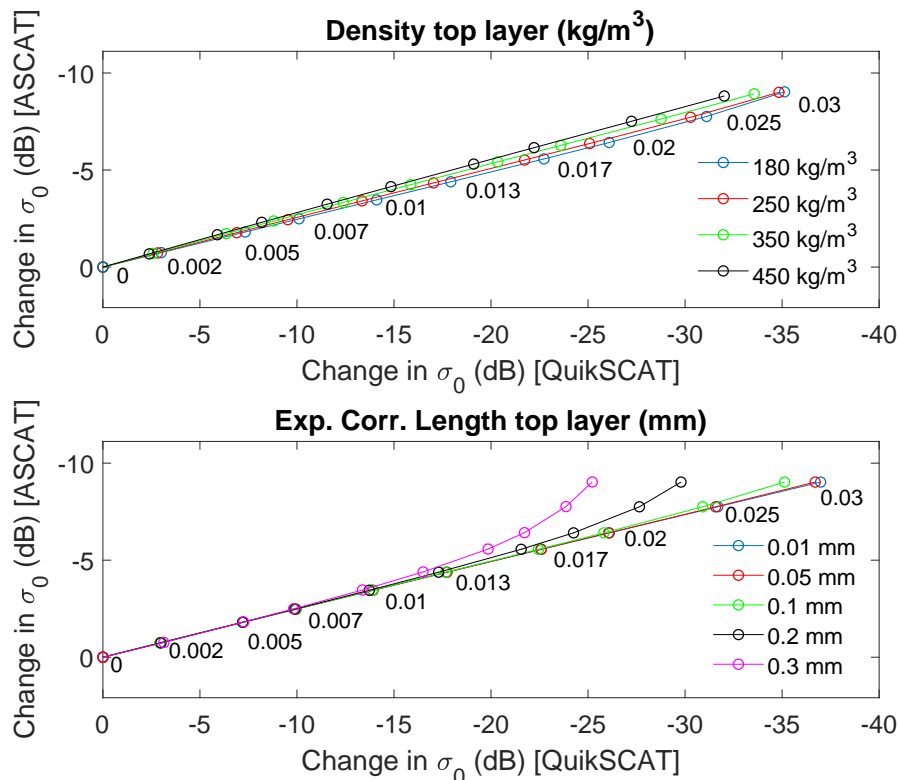


Figure 4.2: Change in σ_{vv}^0 with increasing liquid water content [0.2%, 0.5%, 0.7%, 1%, 1.3%, 1.7%, 2%, 2.5%, 3%] for QuikSCAT (frequency 13.4 GHz, incidence angle 54°) and ASCAT (frequency 5.225 GHz and incidence angle 40°) for different values of density (top) and exponential correlation length (bottom) of the top snow layer.

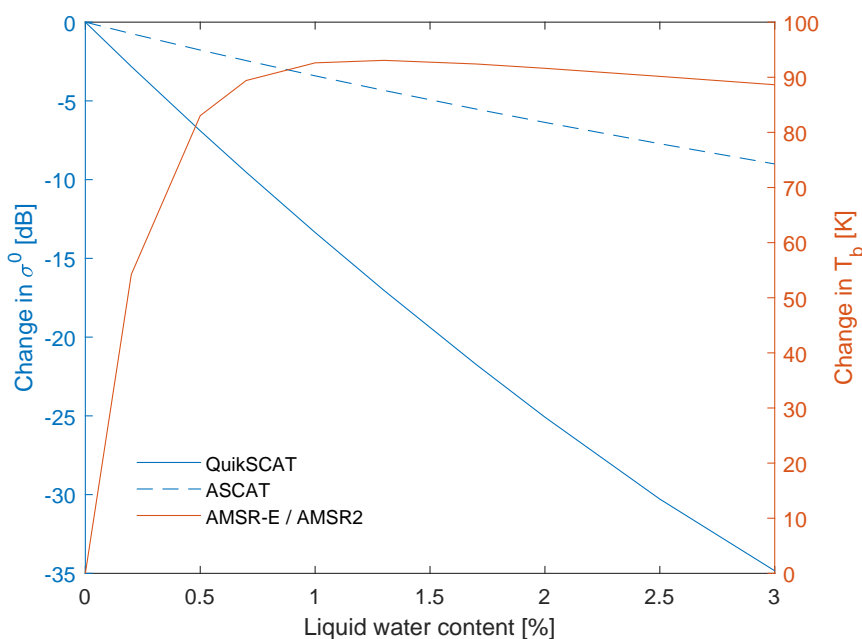


Figure 4.3: Change in σ_{vv}^0 and T_b with increasing liquid water content for QuikSCAT, ASCAT and AMSR-E / AMSR2.

4.2.1 Evaluation of Existing Methodologies

The methodologies of Trusel et al. (2012) and Bothale et al. (2015), which are discussed in section 3.2.2 are applied and compared. Figure 4.4 shows the time series of QuikSCAT vertically polarized morning data for the locations of the ten weather stations and the thresholds calculated from the two aforementioned methods. The thresholds that are calculated using the Trusel et al. (2012) decision tree methodology are indicated with green lines. The differences in thresholds of Bothale et al. (2015) using the different datasets (as described in previous chapter) indicate a higher standard deviation in OSCAT dataset, that is explained by the OSCAT calibration inconsistencies.

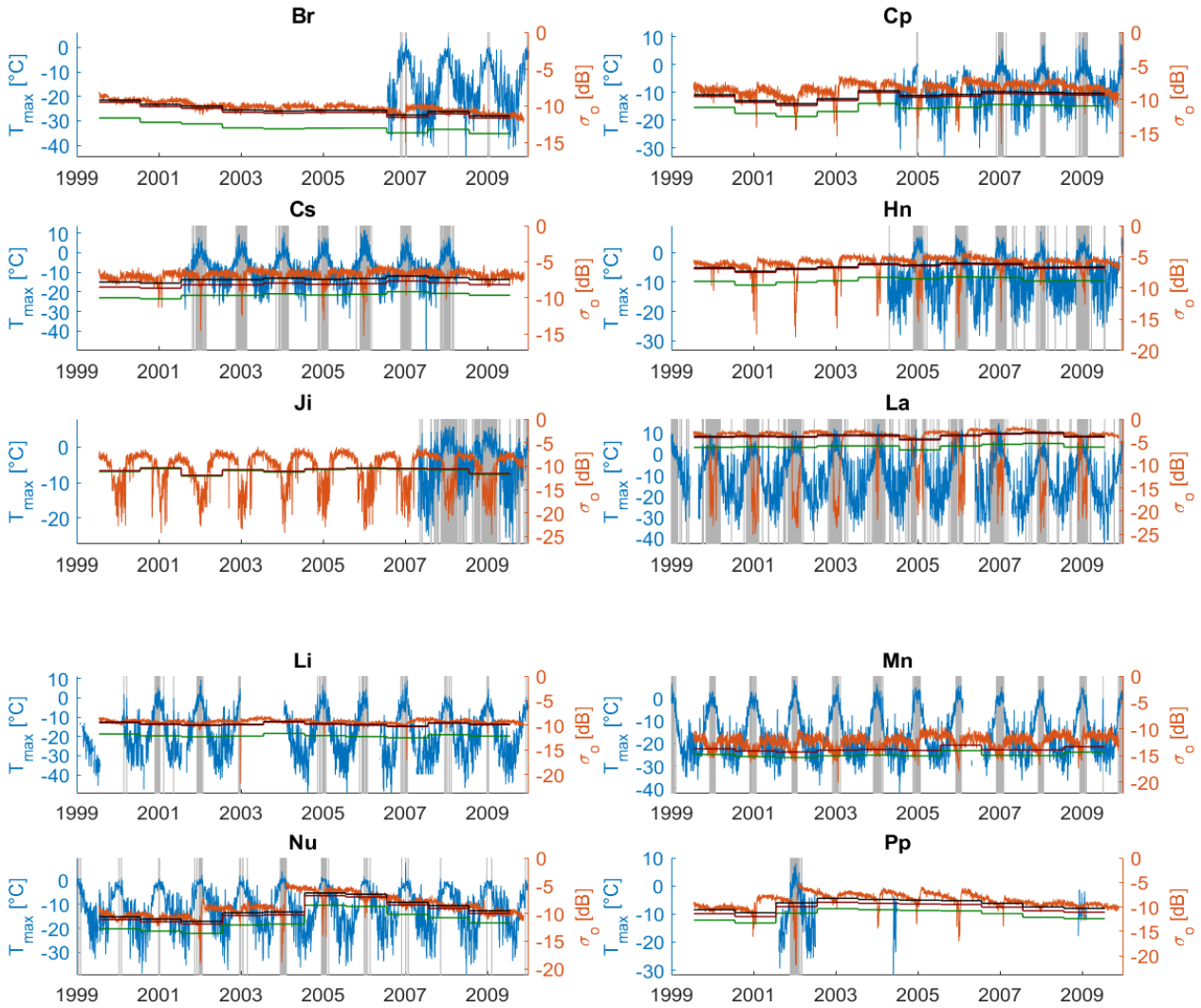


Figure 4.4: Time series of QuikSCAT σ_{vv}^0 from morning data (red line), maximum daily temperature (blue line) at the location of weather stations together with varying thresholds of Trusel et al. (2012) (green line) and Bothale et al. (2015) using maximum standard deviation from QuikSCAT data only (black line) and using the maximum standard deviation from QuikSCAT and OSCAT data (brown line). Vertical gray boxes indicate the days with temperature higher than 0°C .

In addition, there are some differences in vertically (Fig. 4.4) and horizontally (Fig. A.1) polarized backscatter (Table 4.1). Specifically, the backscatter at horizontal polarization is stronger than at vertical polarization as Wang et al. (2007) also stated, due to the lower incidence angle (Fig. 4.1) of the horizontally polarized beam. Furthermore, the winter backscatter standard deviation is greater in horizontal polarization than

Table 4.1: Comparison of the kappa coefficient of the different melt detection methods applied on the different datasets of vertically polarized morning and midday data from QuikSCAT and ASCAT with AWS maximum temperature data

	Trusel				ASCAT	M1				M2				M3	M4
	QuikSCAT		ASCAT			QuikSCAT				QuikSCAT				ASCAT	ASCAT
	Morning		Mid day		Morning	Morning		Mid day		Morning		Mid day		Morning	Morning
	VV	HH	VV	HH	VV	VV	HH	VV	HH	VV	HH	VV	HH	VV	VV
Br	0.22	0.22	0.26	0.12		0.22	0.22	0.14	0.14	0.22	0.22	0.14	0.14		
Cp	0.25	0.16	0.31	0.30	0.21	0.28	0.19	0.31	0.33	0.28	0.19	0.31	0.33	0.21	0.21
Cs	0.24	0.13	0.58	0.58		0.09	0.06	0.55	0.52	0.09	0.06	0.55	0.52		
Hn	0.47	0.43	0.71	0.71	0.35	0.33	0.31	0.68	0.67	0.33	0.31	0.68	0.67	0.35	0.35
Ji	0.62	0.60	0.62	0.62	0.15	0.57	0.55	0.60	0.60	0.57	0.55	0.60	0.60	0.06	0.15
La	0.56	0.55	0.63	0.63	0.31	0.54	0.54	0.63	0.63	0.54	0.54	0.63	0.63	0.31	0.31
Li	0.04	0.03	0.21	0.21		0.02	0.04	0.16	0.14	0.02	0.04	0.16	0.14		
Mn	0.32	0.29	0.42	0.42	0.18	0.28	0.28	0.52	0.53	0.28	0.28	0.52	0.53	0.12	0.17
Nu	0.29	0.28	0.40	0.40	0.25	0.25	0.20	0.41	0.44	0.25	0.20	0.41	0.44	0.25	0.25
Pp	0.62	0.59	0.66	0.65		0.50	0.42	0.67	0.66	0.50	0.42	0.67	0.66		

vertical. However, as it is already mentioned in 4.1 the vertically polarized dataset will be used in order to achieve consistency in the final results, since only vertically polarized measurements are acquired from ASCAT.

Midday and morning observations also show some differences (Table 4.1 and Fig. A.3). Trusel et al. (2012) and Barrand et al. (2013) used the QuikSCAT midday images as the time (12 PM - 8 PM) corresponds with peak insolation and melting. The differences are reflected in the melt duration results and in validation of results using the independent dataset of weather stations and the maximum daily temperature (Section 3.1.2). The positive days (PD) are the sum of the total annual days with maximum daily temperature greater than 0°C. The relationship between the positive days and the total melting days (MD) at the location of the weather stations is calculated and is found to be positive and statistically significant (Fig. 4.5). However, even though a correlation between all the datasets and temperature seems to exist, a much stronger correlation can be observed between PD and MD when using the midday data, as R^2 increases from 0.79 (morning) to 0.83 (midday) for vertical polarization. In addition to that, according to these results the correlation is weaker using the Bothale et al. (2015) method (Fig. A.4 and A.5) compared to the Trusel et al. (2012) method (Fig. 4.5), as R^2 decreases from 0.79 to 0.51 for morning vertically polarized data. It is worth mentioning though, that the correlation depends on the location, as for some areas there is a much stronger correlation than others, like Casey Skiway (Cs) compared to Limbert (Li). Figure 4.6 shows the annual maps of melt duration for QuikSCAT vertically polarized midday data, using the Trusel et al. (2012) method.

4.2.2 QuikSCAT

The results (Table 4.1) of the comparison of the datasets from the different sensors (also in Appendix A.1) show that the QuikSCAT dataset is more complete compared to that of ASCAT and OSCAT. Specifically, midday observations that are available from QuikSCAT are more accurate in melt detection compared to morning and evening observations, since it coincides with peak insolation and melting. In addition, there is a consistent calibration throughout its mission lifetime and a small number of missing files. On the contrary, midday measurements are not acquired neither by OSCAT or ASCAT, leading to an underestimation of melting days, if the morning observations are used. Moreover, there are many missing files that cause significant gaps in the OSCAT dataset that together with the calibration inconsistencies and the small time overlap with QuikSCAT (September - November 2009), lead to the decision of not including it in the further processing and final results.

The implementation of the M1 and M2 methods showed some differences in the melt duration results from the three methods, Trusel et al. (2012), M1 and M2 (e.g. Fig. 4.6, A.8 and A.9). Firstly, the Trusel et al. (2012)

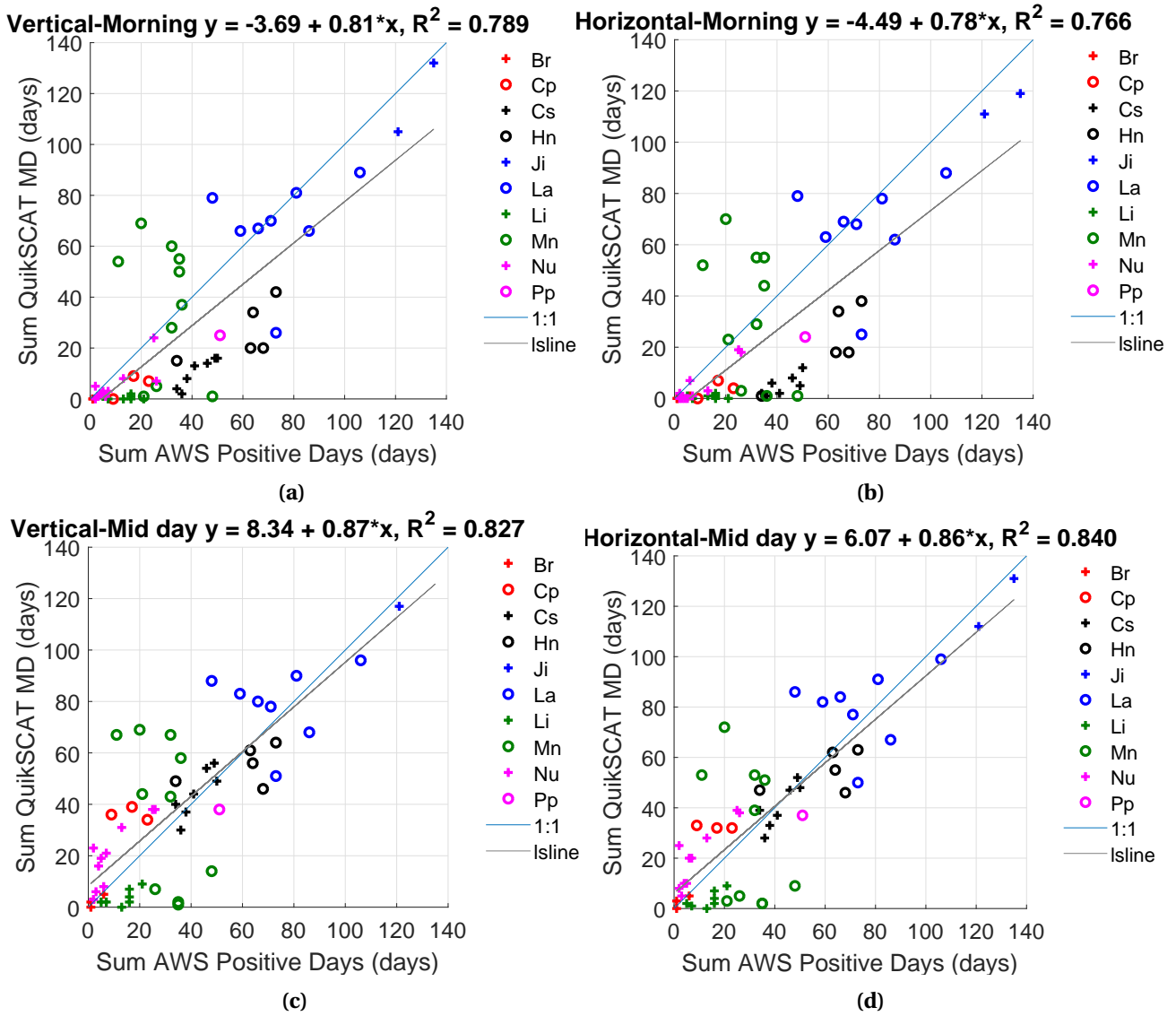


Figure 4.5: Dependence of annual QuikSCAT melting days (MD) as computed using the Trusel et al. (2012) method on annual positive days (PD) for (a) vertically polarized morning data (b) horizontally polarized morning data (c) vertically polarized midday data and (d) horizontally polarized midday data.

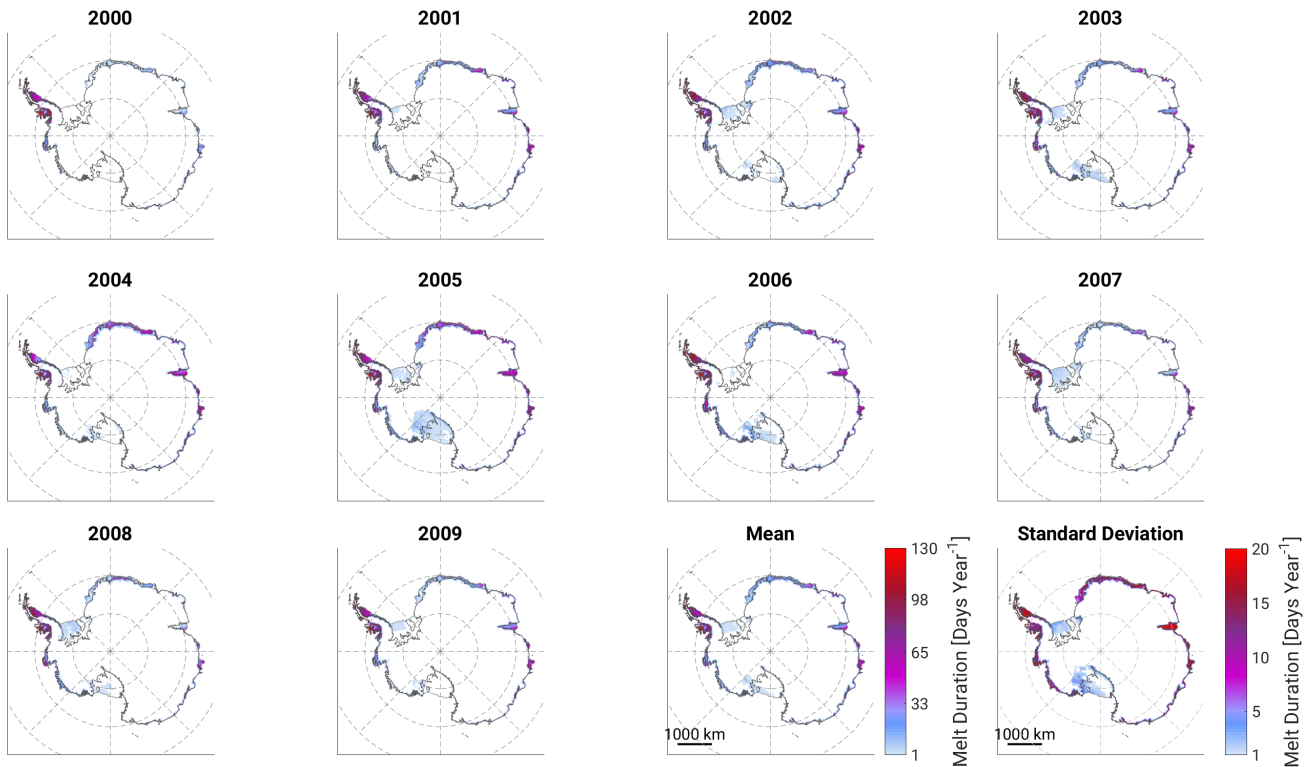


Figure 4.6: Annual maps of melt duration and mean melt duration for the period 2000-2009 as calculated using the Trusel et al. (2012) method for the QuikSCAT vertically polarized midday data.

method detects more melting days in most of Antarctica (Fig. A.10), due to the lower threshold (if case A is true [2 dB]). On the contrary, less melting days are found in West Antarctica (close to Amundsen Sea), when using the Trusel et al. (2012) method. Figure 4.7 shows some spots in which M1 and M2 methods detected high melt duration. In order to understand the cause of this large difference in melting days, a time series of a pixel in the region is examined (Fig. 4.8). According to the time series, there is a high difference in mean early and late melt season σ^0 in some years (e.g. 2000) that causes false melt detection when using one threshold (M1). Usually the upward jumps in backscatter indicate the formation of ice layers that contain large ice scatterers and the accumulation of snow tends to make the contribution of those ice scatterers to backscatter weaker, resulting in a slow decrease in backscatter. However, the difference between M2 and Trusel et al. (2012) (case D in this example) indicates that a greater threshold than M2 for both early (3 dB or $2std$) and late (4.5 dB) melt season is needed as it is for case D (4.5 and 6 dB respectively for early and melt season). In some other cases, Trusel et al. (2012) method detects less melting days because case B (4.5 dB) is used instead of case A (2 dB) and a greater threshold than that of M1 and M2 is used.

4.2.3 ASCAT

Annual melt duration is calculated for the ASCAT dataset using the Trusel et al. (2012), M3 and M4 methods. Three different cases are identified based on a comparison of the results. Firstly, there are areas over which the same threshold is used for the three methods (i.e. 2 dB) and hence the same annual melt duration is calculated. Secondly, there are regions (e.g. location shown in Fig. 4.7) that M3 and M4 detected more melting days than Trusel et al. (2012) method, indicating that a larger threshold than 2 dB (M3 and M4) is necessary. Finally, M3 and M4 detect less false melting events from Trusel et al. (2012) method in regions in the coast of East Antarctica (e.g. near Shackleton Ice Shelf), where the signal is more noisy, due to the presence of snow structures that introduce dependency of radar backscatter on the azimuth direction.

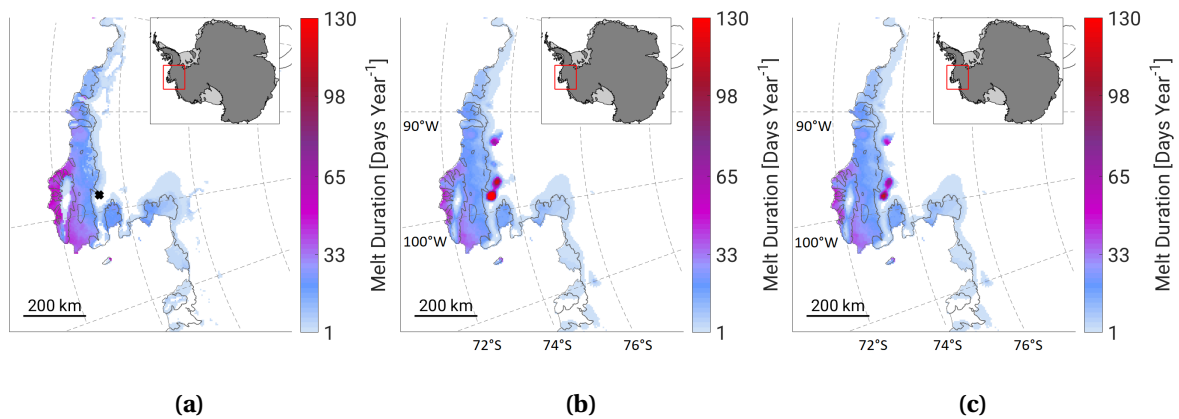


Figure 4.7: Melt duration maps for 2000 [QuikSCAT midday vertically polarized data] at Amundsen Sea Embayment for (a) Trusel et al. (2012) method, (b) M1 method and (c) M2 method. The black dot in the first figure indicates the location that the time series of Figure 4.8 refers to.

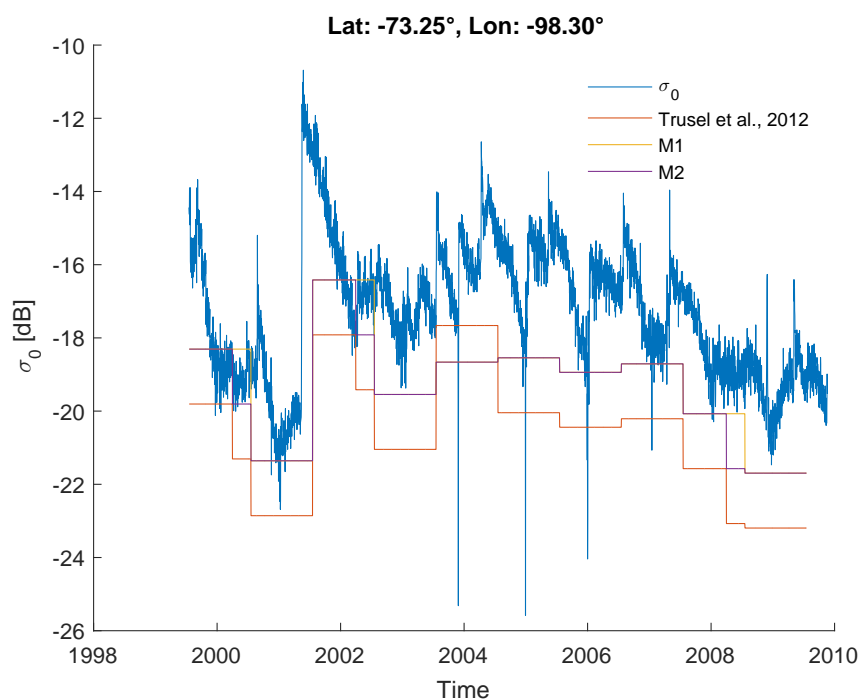


Figure 4.8: Time series of QuikSCAT σ^0 (blue line) at latitude -73.25° and longitude -98.30° in West Antarctica, together with the threshold of Trusel et al. (2012), M1 and M2 methods. The upwards jumps in σ^0 indicate the formation of ice layers with large ice scatterers, whereas the gradual decrease in σ^0 is caused by snow accumulation.

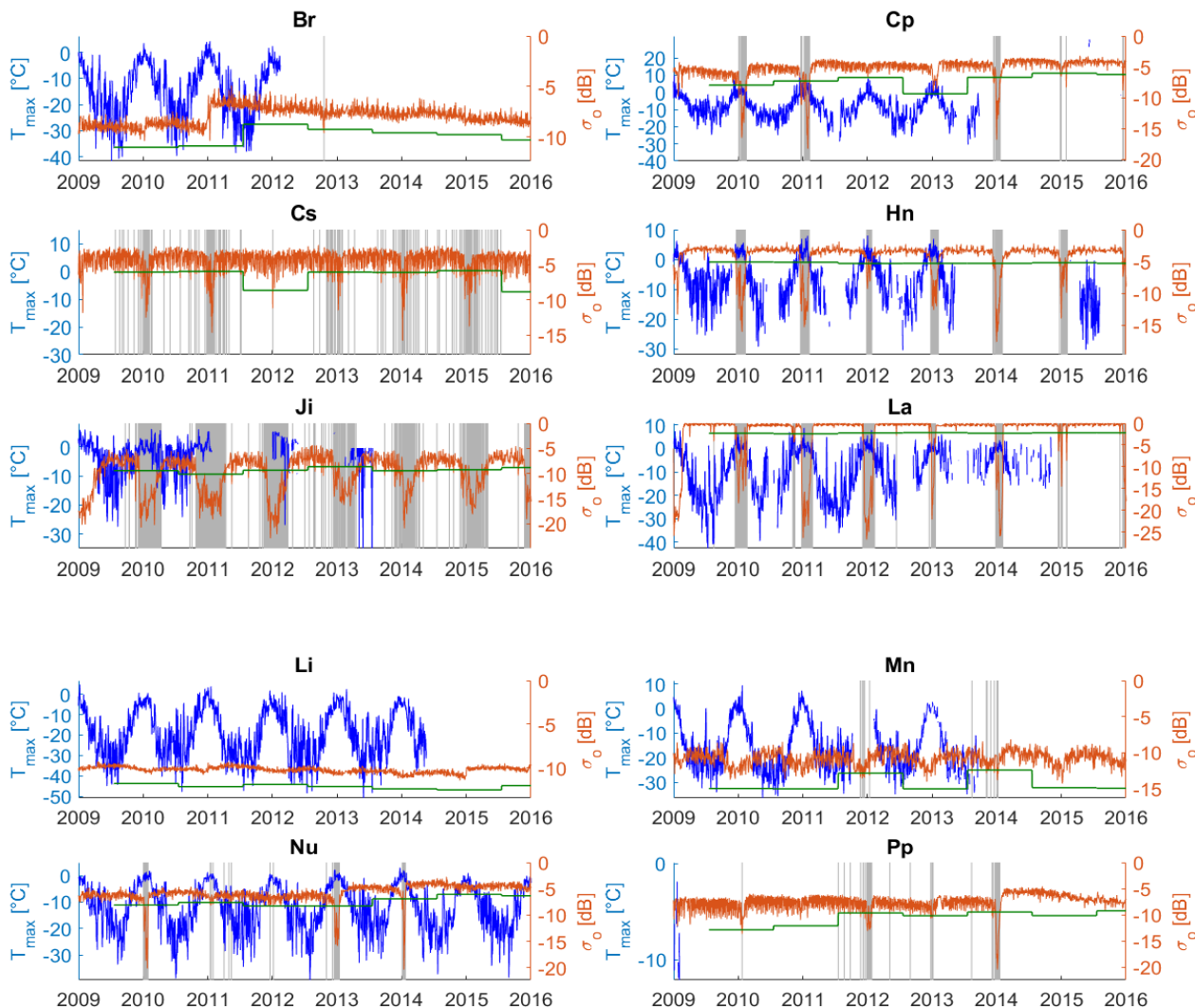


Figure 4.9: Time series of ASCAT σ_{vv}^0 from morning data (red line), maximum daily temperature (blue line) at the location of weather stations together with threshold of Trusel et al. (2012) (green line). Vertical gray boxes indicate the melting days.

4.2.4 Consistent dataset

The results of applying the fractional melt detection method to achieve consistency in the melt time series are presented and discussed (Fig. 4.10). Firstly, fraction values equal to infinity were calculated (when there is no melting in morning dataset or half days dataset), for all the three methodologies Trusel et al. (2012), M1 and M3, M2 and M4 for QuikSCAT and ASCAT respectively. In addition, fraction values lower than zero were found, when using the Trusel et al. (2012) method that are wrong, as melt duration for the full dataset and the midday dataset should be larger than melt duration for the half dataset and the morning dataset respectively. The different datasets (full/half, morning/midday) have different annual σ^0 winter, early and late melt season statistics and the threshold used (based on the cases of the decision tree Fig. 3.5) is not always the same for all the datasets, leading to the error values discussed before. Hence, the fraction values (multi-year mean) are calculated by excluding the infinity and false values. It is noted that it is impossible to retrieve information about midday melting using this method at the areas that do not experience morning melting, as zero morning melt duration will remain zero after the fraction multiplication.

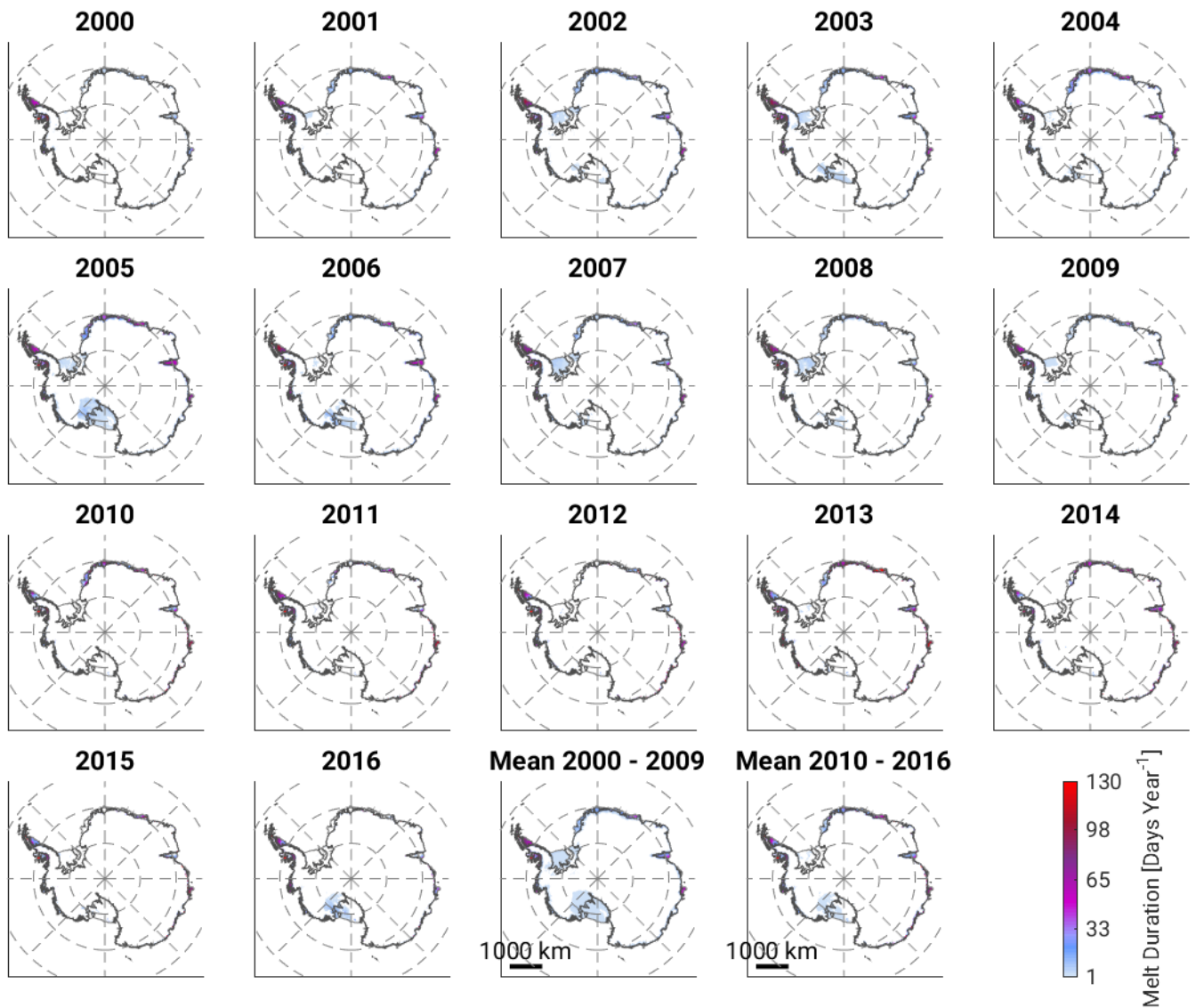


Figure 4.10: Annual maps of melt duration for the period 2000-2016 from QuikSCAT (2000 - 2009) and ASCAT (2010-2016) multiplied by the fractions, as calculated using the Trusel et al. (2012).

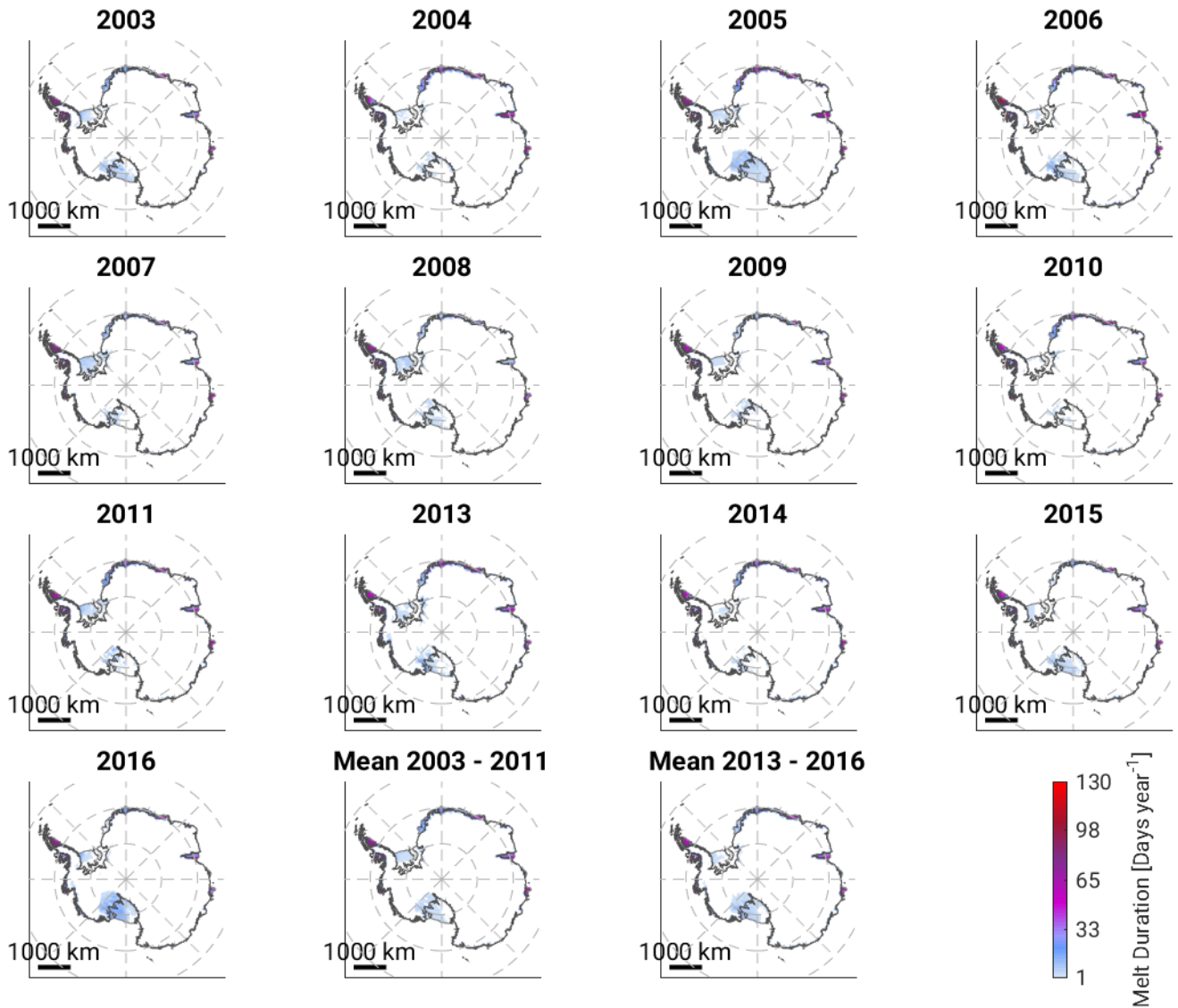


Figure 4.11: Annual maps of melt duration for the period 2003-2016 from AMSR-E (2003 - 2011) and AMSR2 (2013-2016) 18.7 GHz horizontally polarized data.

4.2.5 Passive Microwave Record

The results of the annual melt duration for AMSR-E and AMSR2 are shown in Figure 4.11. It is noted that the spatial patterns of melting detected from AMSR-E for the years 2003-2009 are similar to those of QuikSCAT. However, a more detailed comparison of the results of passive and active sensors follows in section 4.3.

4.3 Comparison

In order to compare the different methodologies, the temporal and spatial melting characteristics are analysed. Total areal melt extent (in km^2) and melt index (in km^2 days) are two basic parameters for the comparison.

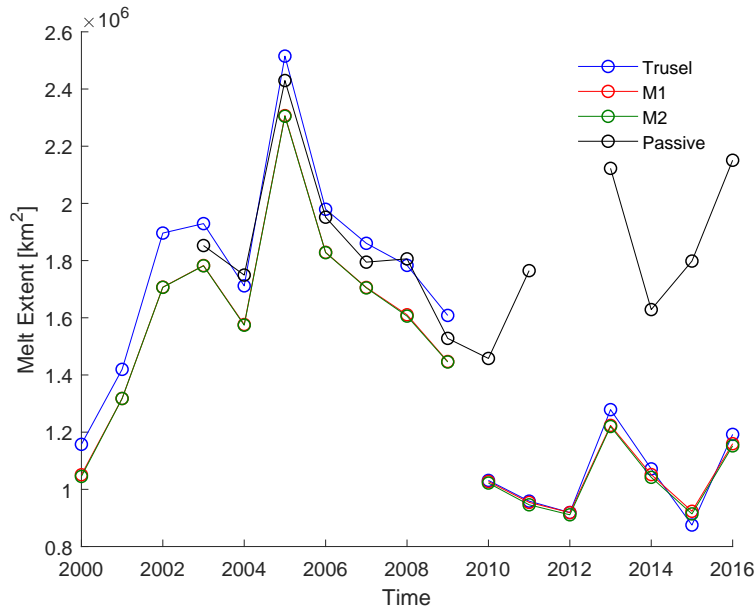


Figure 4.12: Time series of total melt extent for active and passive microwave data over the Antarctic continent. Melt extent is based on the results using QuikSCAT data for the period 2000 - 2009, ASCAT results from the fractional melt detection method for the period 2010 - 2016, AMSR-E data for the period 2003 - 2011 and AMSR2 data for the period 2013 - 2016.

Table 4.2: Correlation coefficient between three methods used for QuikSCAT data and AMSR-E data for melt extent

Method	M1 QSCAT	M2 QSCAT	Trusel et al. (2012) QSCAT	AMSR-E
M1 QSCAT	1.0	1.0 (n = 10)	0.999 (n = 10)	0.985 (n = 7)
M2 QSCAT		1.0	0.998 (n = 10)	0.985 (n = 7)
Trusel et al. (2012) QSCAT			1.0	0.986 (n = 7)
AMSR-E				1.0

4.3.1 Continental Scale

Figures 4.12 and 4.13 show the temporal evolution of melt extent and melt index over the whole Antarctic continent for the three methods.

Time Period 2000 - 2009

Firstly, a strong relationship exists between the results of M1, M2 and Trusel et al. (2012) methods for QuikSCAT and of AMSR-E for both melt extent (Table 4.2) and melt index (Table 4.3). As it is expected, M1 and M2 melt extent and melt index values are very similar. The largest difference between the two methods is in 2008, as M1 detected much more melting days than M2 in the south-west Palmer Land (West Antarctica). In addition, Trusel et al. (2012) detects melt in areas where M1 and M2 methods do not detect (Fig. 4.15), thus melt extent is larger.

On the other hand, differences in melt extent and melt index between AMSR-E and QuikSCAT exist. Figure 4.16 shows the amount of pixels summed for all days for the years 2003-2009 that indicate melt (1) or no melt (0) in AMSR-E results and the corresponding class in which they are classified according to the QuikSCAT results using the Trusel et al. (2012) method. In particular, the majority of the AMSR-E melting pixels cor-

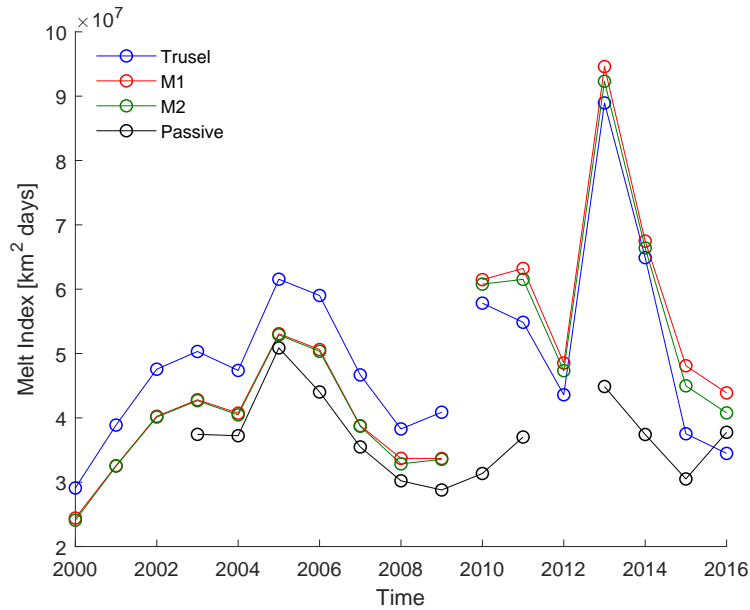


Figure 4.13: Time series of total melt index for active and passive microwave data over the Antarctic continent. Melt index is based on the results using QuikSCAT data for the period 2000 - 2009, ASCAT results from the fractional melt detection method for the period 2010 - 2016, AMSR-E data for the period 2003 - 2011 and AMSR2 data for the period 2013 - 2016.

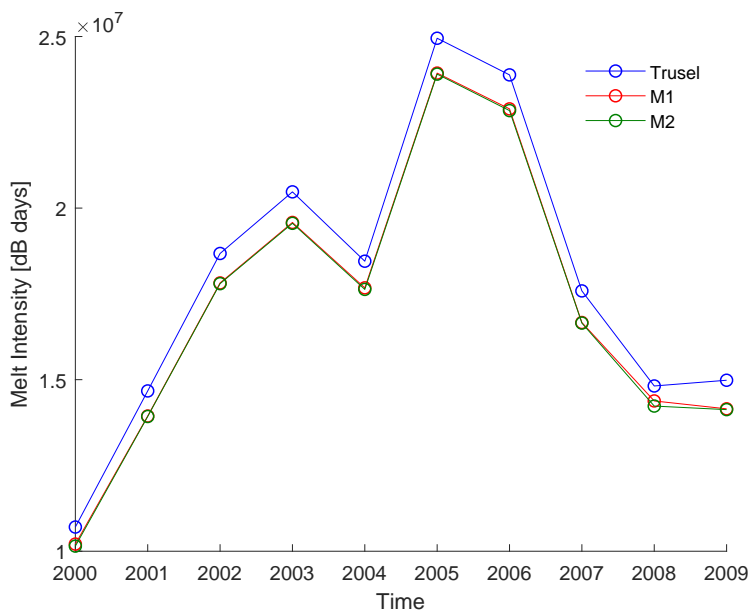


Figure 4.14: Time series of total melt intensity for QuikSCAT data over the Antarctic continent.

Table 4.3: Correlation coefficient between three methods used for QuikSCAT data and AMSR-E data for melt index

Method	M1 QSCAT	M2 QSCAT	Trusel et al. (2012) QSCAT	AMSR-E
M1 QSCAT	1.0	1.0 (n = 10)	0.997 (n = 10)	0.981 (n = 7)
M2 QSCAT		1.0	0.998 (n = 10)	0.979 (n = 7)
Trusel et al. (2012) QSCAT			1.0	0.971 (n = 7)
AMSR-E				1.0

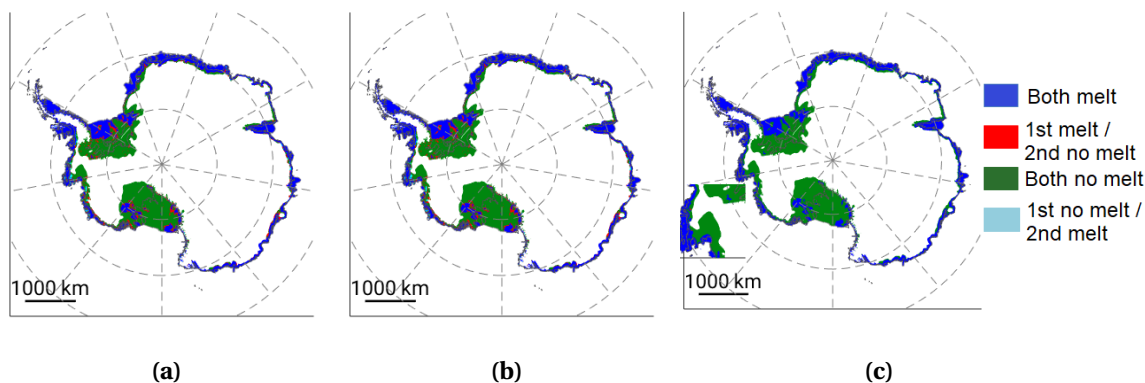


Figure 4.15: Spatial comparison of melt extent results (a) from Trusel et al. (2012) and M1 methods, (b) from Trusel et al. (2012) and M2 methods and (c) from M1 and M2 methods for year 2002. Blue indicates that both methods detected melt for at least one day of the year, red indicates the regions where only first method (in each case) detected melt, green indicates the regions where both methods did not detect melt and cyan indicates the regions where only the second method (in each case) detected melt.

respond to the 76-100% class, indicating that AMSR-E detects large scale melting phenomena. However, there is a number of pixels where AMSR-E detects melt and QuikSCAT not. On the other hand, a significant number of pixels classified as non melting in AMSR-E correspond to either small or large scale melting phenomena captured by QuikSCAT. The differences are attributed to the fine resolution of QuikSCAT that can detect small scale melting phenomena and to the higher sensitivity of QuikSCAT to melting. Spatially the differences in the results of passive and active sensors can be seen in Figure 4.17. Areas in red are the areas that AMSR-E did not detect melt but QuikSCAT (Trusel et al. (2012)) does for the year 2005. These areas are mainly inland areas around the coast of Antarctica. On the contrary, there are areas where only AMSR-E detected melt (cyan) mainly on Ronne-Filchner Ice Shelf and Ross Ice Shelf. These areas vary depending on the method (Trusel et al. (2012), M1 and M2) used for melt detection for QuikSCAT data. The differences between the methods are attributed to the fact that Trusel et al. (2012) is more sensitive to brief melting than M1 method.

Even though the melt extent calculated from AMSR-E, can exceed the melt extent of QuikSCAT depending on the method used, melt index is significantly lower for all the years in the period 2003 - 2009. Figure 4.18 shows the melt duration difference between the results of AMSR-E and QuikSCAT (Trusel et al. (2012)). It is demonstrated that melt duration over Peninsula, Wilkins Ice Shelf and most of the coast of Antarctica in general is higher using QuikSCAT and less over Amery Shelf, Ross Ice Shelf and the ice shelves close to Dronning Maud Land. The differences can be attributed to the different threshold at the melt detection methodology used, even though all the methodologies are sensitive to brief melting, to the different sensitivities of the sensors and to the different time of observation.

Time Period 2010 - 2016

Regarding the melt index and melt extent for the years 2010 - 2016 that were calculated using the results from the fractional melt detection method, it is observed that consistency could not be achieved. Specifically, melt extent is much less for this period and it is more consistent with the results from morning observations. This is in accordance with what was already concluded, that it is not possible to get information for afternoon melt in the places where no morning melt occurs using the proposed method. In addition, melt index is much higher for 2010 - 2016, even though the extent is less. This is explained by the fact that in some regions, like Lazarev Ice Shelf (2013), a substantially large number of melting days is calculated. According to the AMSR2 results, melt duration in 2013 is slightly higher in that area compared to other years. Thus, more morning melting days than usual multiplied by a fraction computed for less melting days (in

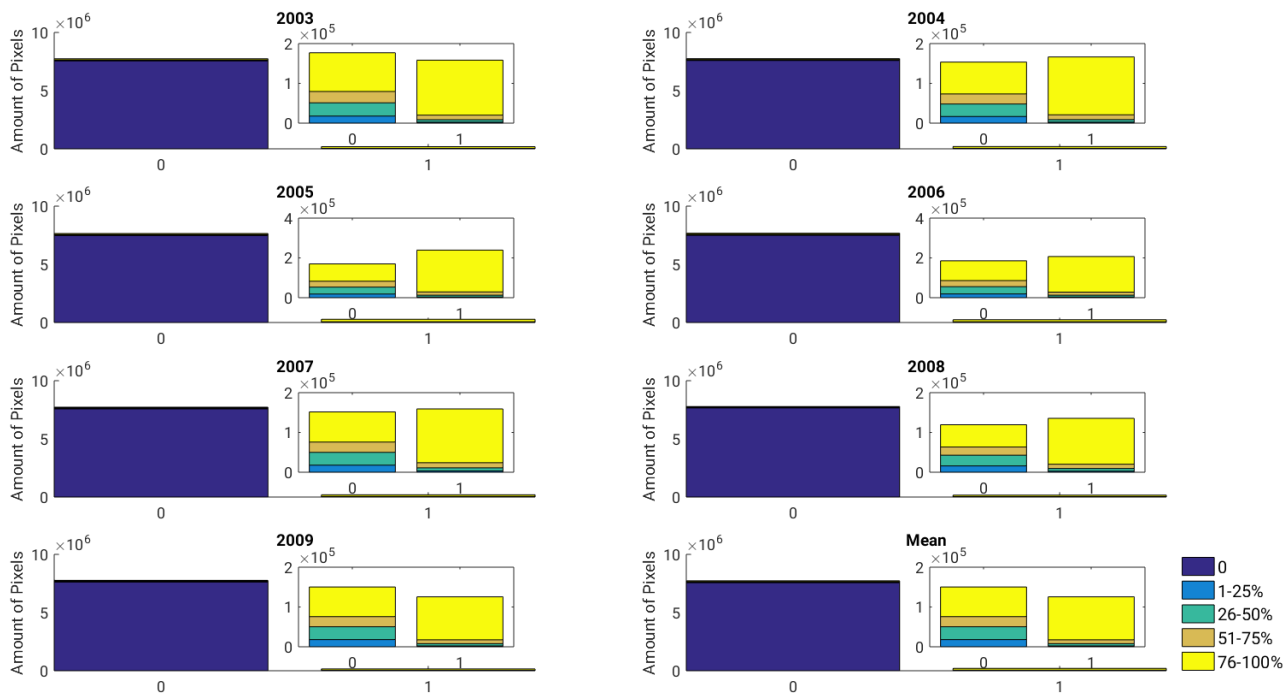


Figure 4.16: The amount of pixels that belong to each QuikSCAT class and are classified for AMSR-E as melting (1) and non-melting (0) pixels [x axis]. The box in each year is a zoom in the plot excluding the pixels classified for both QuikSCAT and AMSR-E as non-melting. Classification was performed based on the Trusel et al. (2012) method results.

the period 2000-2009) can lead to false high melt duration. Consequently, it is less likely to get a reliable estimation of melt duration at areas with high interannual variations in annual melting days.

As it is already mentioned above, the method for consistency is more likely to give results close to the reality for the regions that experience melt throughout the day (morning and afternoon). Based on the analysis for the diurnal variability of melt (Fig. A.29), the ice shelves at Antarctic Peninsula, Abbott Ice Shelf, West Ice shelf and Shackleton Ice Shelf experience both morning and afternoon melt, whereas on the rest ice shelves morning melt occurs in some years. Based on this specific classification, melt extent is calculated separately for the three classes (Fig. 4.19). According to the figure, the extent of the areas that morning and afternoon melt overlaps is greater when the Trusel et al. (2012) method is used compared to M1 and M2. This can be explained by the fact that the first method has a lower threshold and detects morning melt at a larger extent (e.g. part of Amery Ice Shelf) than the latter methods. Moreover, the melt extent of this class remains constant over the years, indicating that the interannual variations in melt are mostly influenced by the regions of the other two classes.

4.3.2 Regional Scale

The three metrics (melt index, extent and intensity) are calculated for seven regions of Antarctica (Fig. 4.20). The interior area is not included in a region because no melt was detected based on the methodologies applied (elevation higher than 1000 m). In general, no trend is observed in the time series but a high interannual variability is apparent. Ronne - Filchner Ice Shelf and Ross Ice Shelf show higher melt extent and melt index for the AMSR-E horizontal polarized data than for QuikSCAT data, as it was already observed from the annual maps of melt duration and melt extent difference between the results from QuikSCAT and AMSR-E. The greatest difference between the metrics from the two sensors is observed at Antarctic Peninsula, where more melting days and over a more extensive area is noticed for QuikSCAT. In addition, the differences in extent at regions Dronning Maud Land, Wilkes Land and Marie Byrd Land are caused by the areas near coast

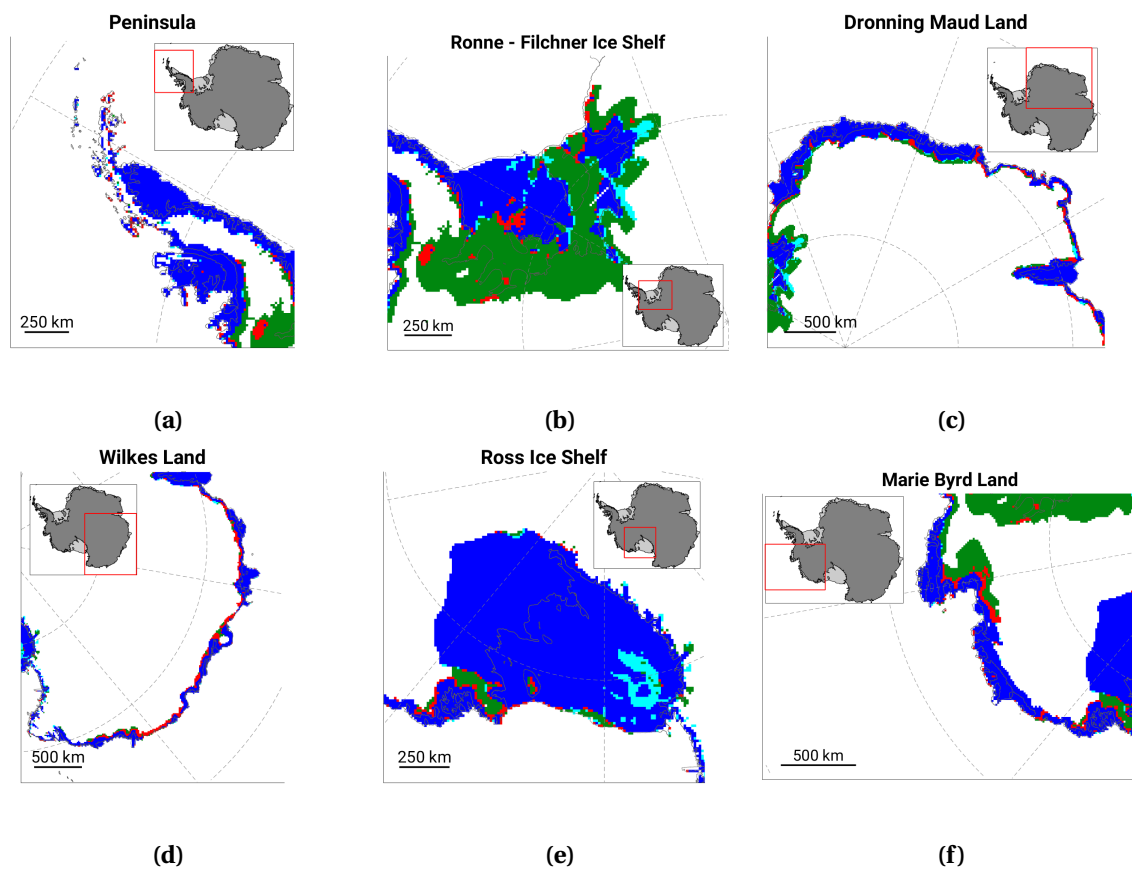


Figure 4.17: Maps showing the regions in which melt occurred for at least 1 day for both AMSR-E and QuikSCAT (Trusel et al., 2012) with blue, only for QuikSCAT in red, only for AMSR-E in cyan and the regions where none of the methods detects melt in green for the year 2005.

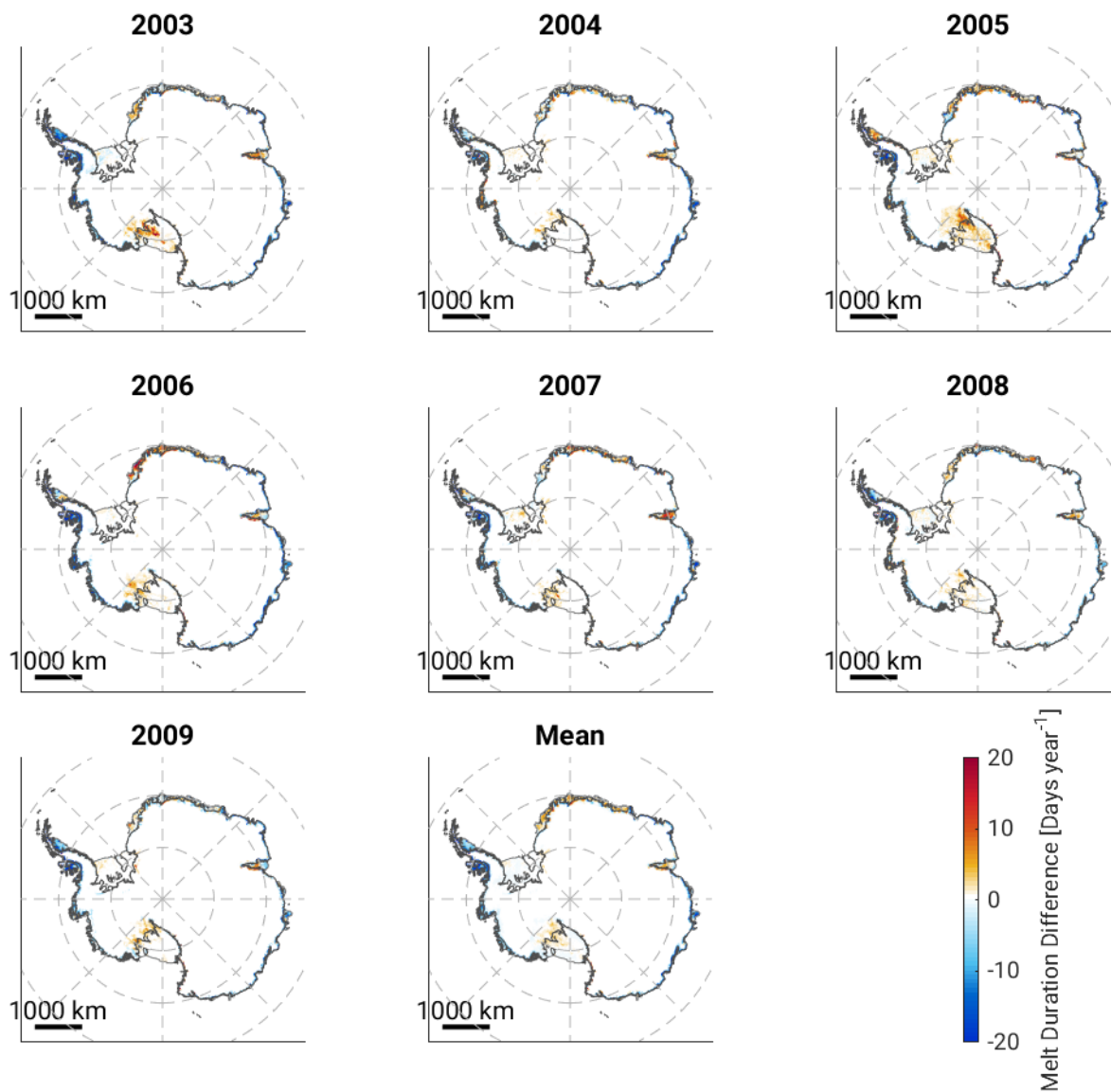


Figure 4.18: Annual maps of melt duration difference between AMSR-E melting days and the QuikSCAT (Trusel et al. (2012) method) coarse resolution melting days.

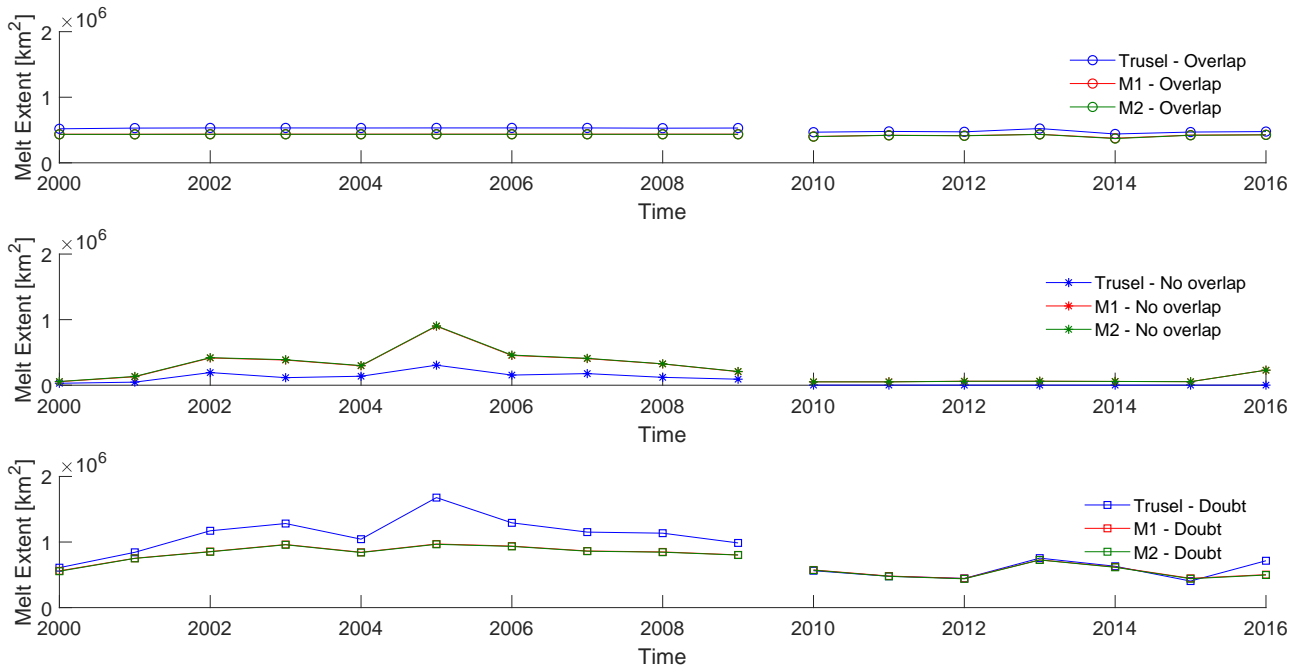


Figure 4.19: Total annual melt extent for (a) regions with always morning and afternoon melt (top), (b) regions with only afternoon melt (middle) and (c) regions with sometimes morning melt (bottom).

over which AMSR-E does not detect melt.

Moreover melt extent for the period 2010-2016 is much less for Ronne - Filchner and Ross Ice Shelf, regions in which morning melt is rare and thus it is difficult to acquire information about afternoon melt duration and extent. On the other hand, the difference in the melt extent in the periods 2000-2009 and 2010-2016 is less for the other regions and that difference varies depending on the year. Specifically, the 2016 melt extent for Marie Byrd Land is the highest for the period 2010-2016, indicating an extensive melt. Regarding the 2010-2016 melt indices, they are substantially higher than the 2000-2009 values for the regions of Wilkes Land, Dronning Maud Land and Amery Ice Shelf. In addition, the 2013 melt index for Dronning Maud Land and Marie Byrd Land, and the 2014 melt index for Wilkes Land and Amery Ice Shelf are significantly higher than any other year. This is a result of the amplification of melt duration caused by the fraction multiplication due to more morning melting days in the specific year.

Although melt index and melt intensity show a similar interannual variability, melt extent differs and important information regarding melting dynamics can be retrieved from this. Specifically, melt metrics at Peninsula are the least correlated, and at the years 2000, 2001, 2007 there is an inverse variation between them. This can be attributed to the fact, that melt extent has a lower interannual variability compared to melt index and melt intensity (Trusel et al., 2012). Finally, the differences in the amplitudes of melt metrics provide information for the years that the increase in meltwater production (intensity) was higher than the increase in melt extent and duration, like the year 2005 for Ross Ice Shelf.

4.4 Climate

Overall, there is not any clear trend in melting, as it is noticed from the melt metrics. High interannual variability that is similar between the metrics is observed. Specifically, there is an increasing trend from the beginning of the period reaching a peak in 2005 and a decrease afterwards. However, a difference in

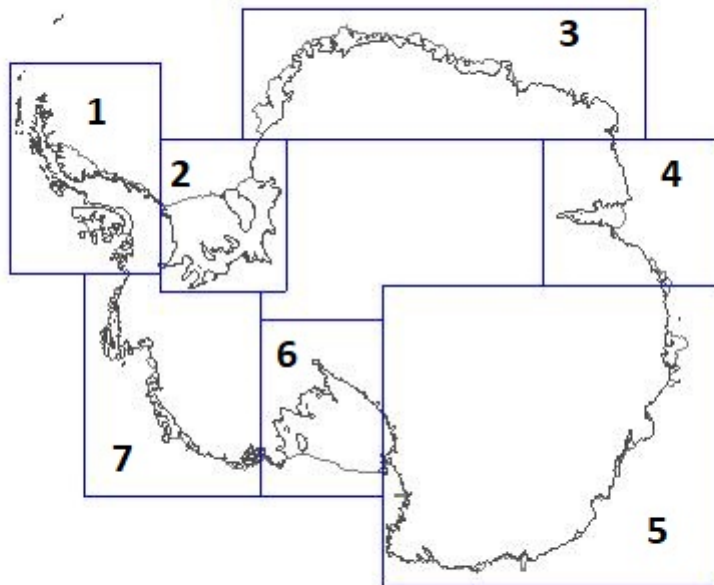


Figure 4.20: Sections in which Antarctic continent is divided for the calculation of melt metrics in regional scale: (1) Antarctic Peninsula, (2) Ronne-Filchner Ice Shelf, (3) Dronning Maud Land, (4) Amery Ice Shelf, (5) Wilkes Land, (6) Ross Ice Shelf and (7) Marie Byrd Land.

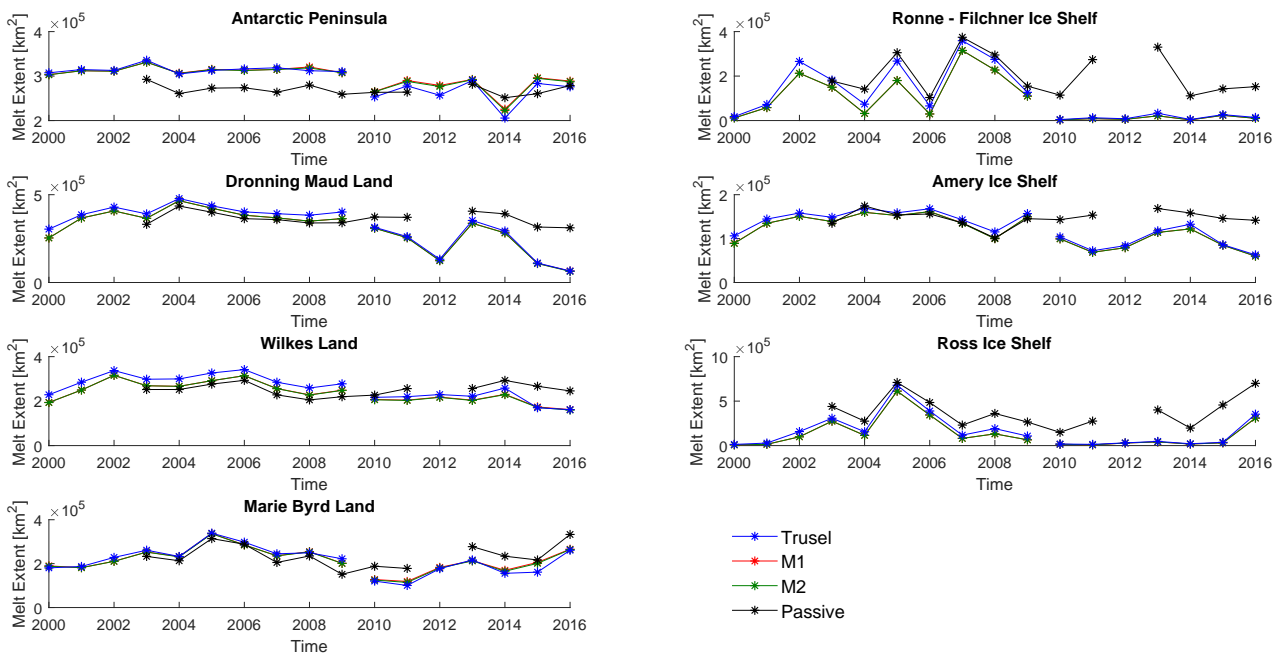


Figure 4.21: Regional variations in melt extent.

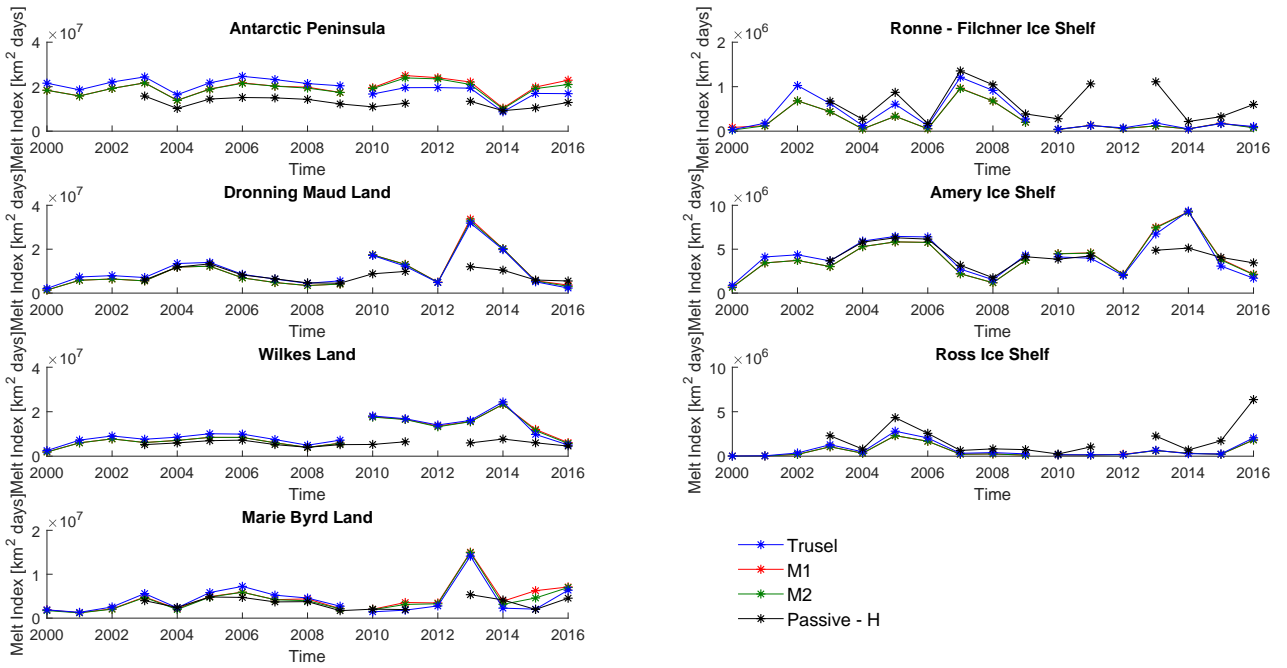


Figure 4.22: Regional variations in melt index.

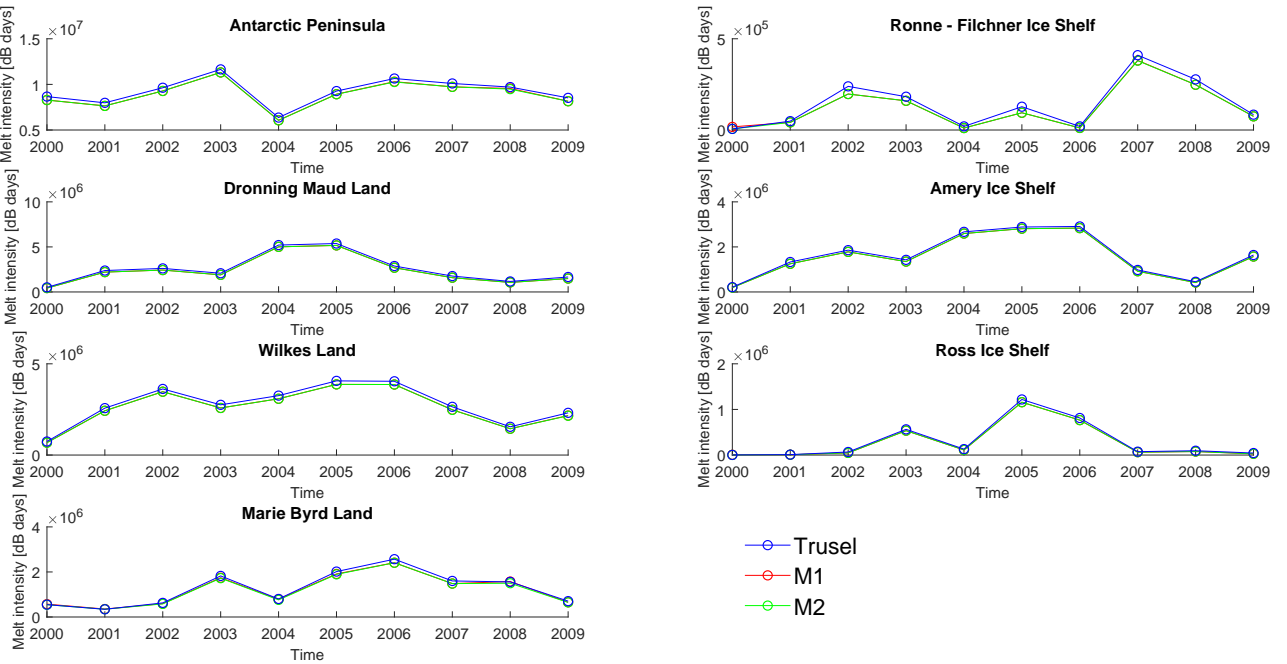


Figure 4.23: Regional variations in melt intensity.

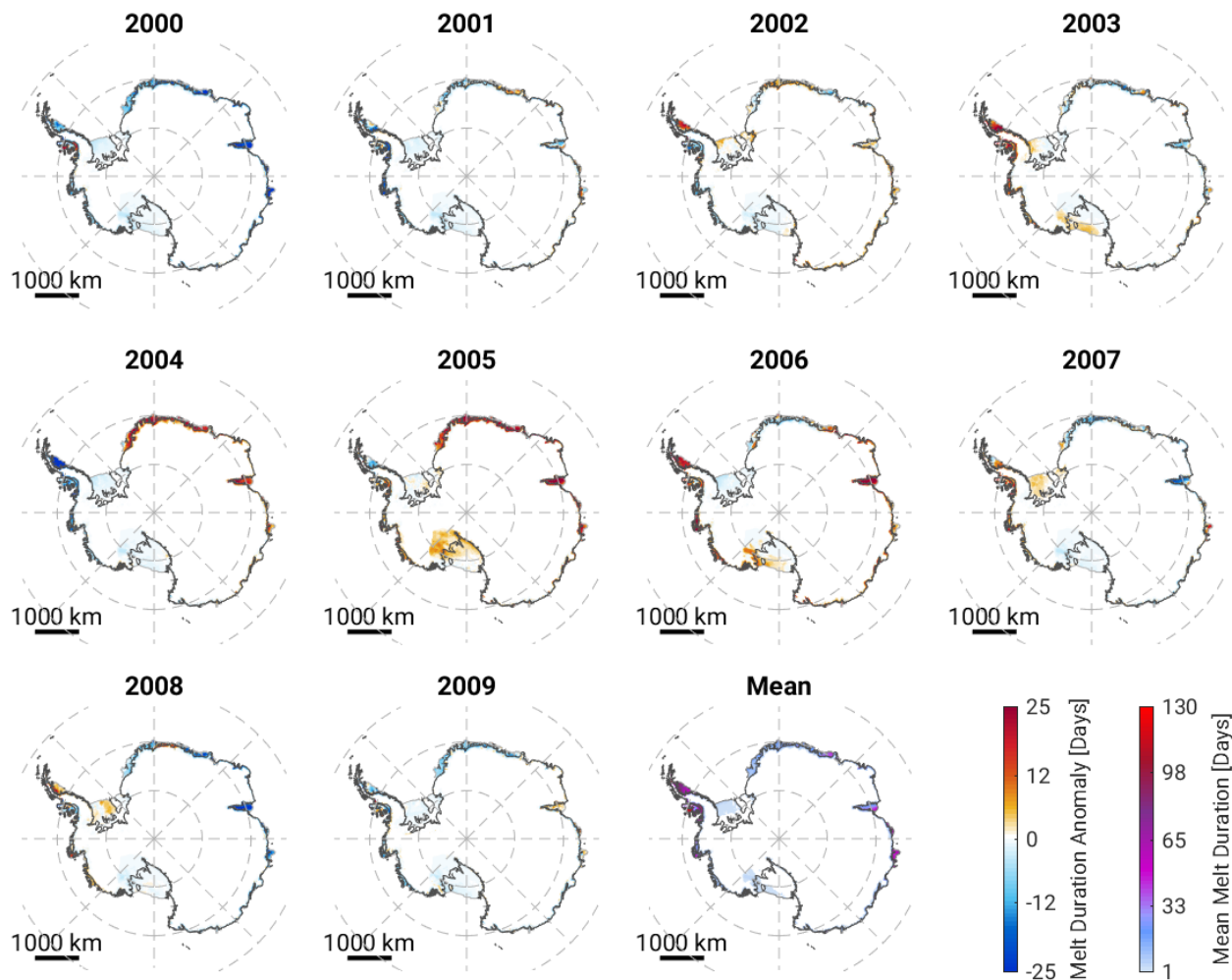


Figure 4.24: Annual maps of melt duration anomalies for the period 2000-2009 using the Trusel et al. (2012) method.

the trend among the metrics is the large decrease in melt extent in 2006 compared to the small decrease in melt index and melt intensity. Therefore, in 2006 a less extensive melt event took place that lasted for more days and at a greater intensity compared to other years. This behaviour applies in both the AMSR-E and QuikSCAT results, although the melt index decrease in 2006 is sharper for AMSR-E.

Figure 4.24 shows the annual maps of melt duration anomalies that are calculated by subtracting the annual melt duration from the mean over the period 2000-2009 for the Trusel et al. (2012) method. The year with less melting, 2000, according to melt extent and melt index, shows melt below the mean for all the regions experiencing melting, except for the ice shelves of Wilkins and George VI on the Antarctic Peninsula. On the contrary, the majority of ice shelves, except for Larsen C, experiences melt above average at the year of 2005, that coincides with the peak of the metrics. According to the results, the longest melt seasons are observed over Peninsula, and even if its average melt extent of the period 2000-2009 (around $3.1 \times 10^5 \text{ km}^2$) is 18-19% (depending on the method) of the total melt extent, its mean melt index nearly equals that of the rest continent (47-48% of total melt index).

A westerly circumpolar vortex dominates the mean atmospheric circulation of the mid-high latitudes at the Southern Hemisphere. The strength of the vortex reaches its maximum during winter and it varies from month to month and from year to year (Thompson and Solomon, 2002). The Southern Annular Mode (SAM) is the hemispheric pattern of climate variability that encircles South Pole. In its positive phase pres-

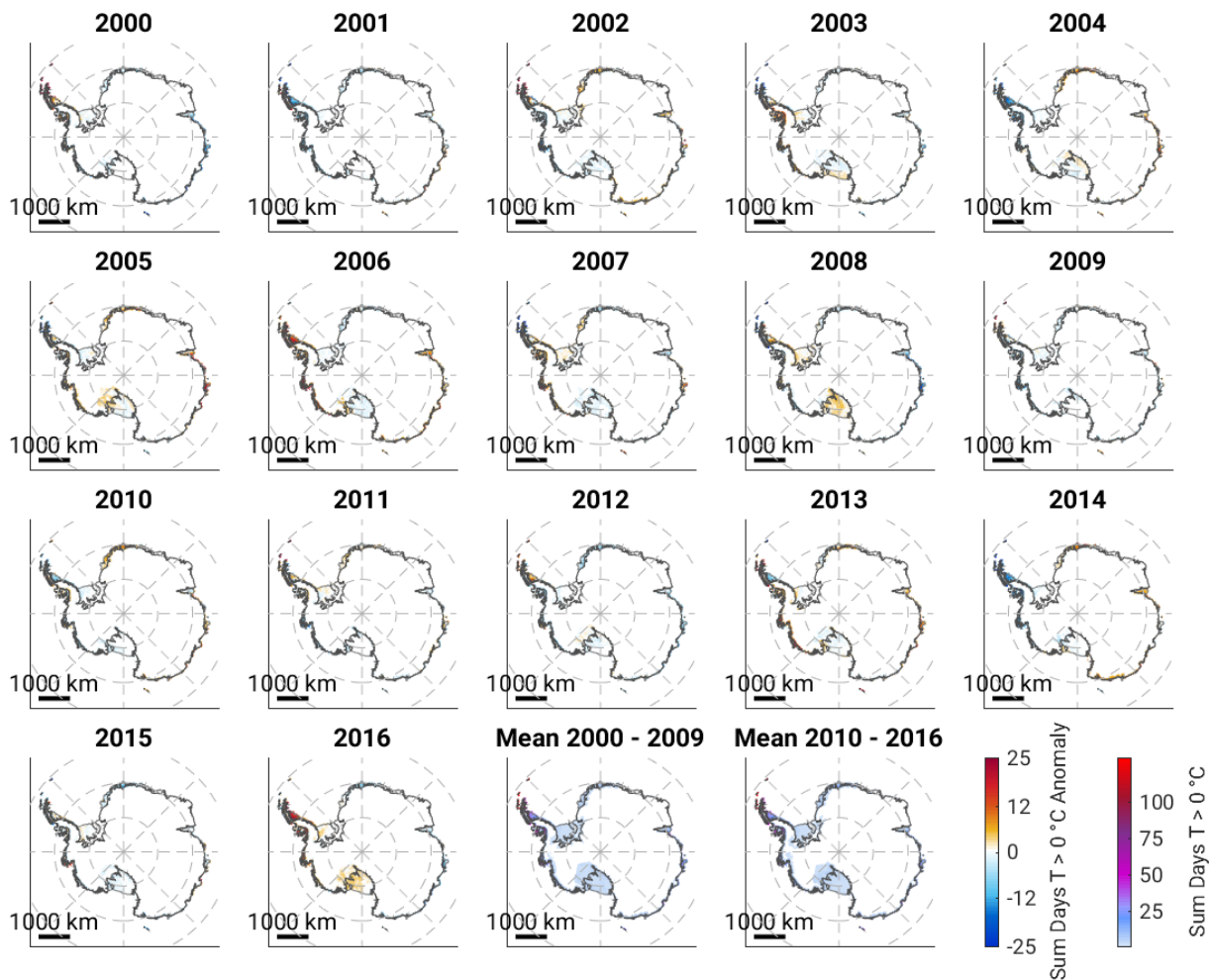


Figure 4.25: Annual maps for annual positive degree days (PDD) anomalies for the period 2000-2016 and the mean of PDD for the period 2000-2009 and 2010-2016. Midday modelled near surface temperature from RACMO2.4 was used.

sures are lower than normal over Antarctica and the westerly winds are stronger over the ocean. In addition, near-surface temperatures over most of mainland Antarctica are lower than normal and higher over regions of Antarctic Peninsula (Thompson and Solomon, 2002). The Southern Oscillation Index (SOI), that is the atmospheric component of the El Niño Southern Oscillation (ENSO), also influences the atmospheric circulation patterns and causes anomalies at sea ice, near-surface temperature and precipitation in West Antarctica (Bromwich et al., 2004).

Antarctic Peninsula has experienced significantly greater warming than the rest of the continent over the past 50 years (van Wessem et al., 2015) and especially central western peninsula near-surface temperatures have shown an increase rate greater than the global average (Marshall et al., 2006). According to QuikSCAT results (2000-2009), strongest melting was observed over the ice shelves of Peninsula at year 2006 and 2003. In 2006 the modelled near surface temperature (Fig. 4.25) is much higher than the 2000-2009 mean temperature, indicating a possible correlation among the high temperature and increased melting. Marshall et al. (2006) demonstrated that the increased temperatures in the region are linked to positive phases of Southern Annular Mode (SAM) that result to the increase in circumpolar westerlies. In addition, recent studies (Tedesco and Monaghan, 2009; Trusel et al., 2012) found that the combination of positive phase anomalies of SAM and SOI are correlated with negative melt indices anomalies.

West Antarctic climate is also influenced by Amundsen Sea Low (ASL) that has deepened likely due to strato-

spheric ozone depletion. ASL is the climatological low pressure center over the extreme southern Pacific Ocean and it leads to anomalies in sea ice, temperature and precipitation from Antarctic Peninsula to Ross Sea coastal and shelf region (Raphael et al., 2016). Sea ice extent is important for melting as a low sea ice cover with cyclonic circulation benefits the advection of oceanic heat and moisture (Trusel et al., 2012). One of the lowest minimum sea ice extent in Ross Sea was recorded in 2005, the year in which Ross Ice Shelf experienced the highest melt duration in the 10 year period 2000-2009. In addition, in 2016 an extensive melting event over Ross Ice Shelf occurred as results from AMSR2 dataset show. According to Nicolas et al. (2017) low-level liquid water clouds were present at that time, that might have intensified the radiative heating of the surface. The same study also concludes that warming over Ross Ice Shelf was caused by the strong El Niño event and positive SAM. Even though less melting tends to occur for positive SOI and SAM phases, it is likely that positive SAM contributed in the mitigation of the magnitude of melt event by counteracting the El-Niño influence.

Overall, West Antarctic climate is influenced by various mechanisms as it is discussed above and yet the mechanisms driving this major melt events are not fully understood. On the other hand, high temperatures and meltwater production in coastal East Antarctica are caused by katabatic winds (Lenaerts et al., 2017). Winds expose large grained snow and blue ice at the surface with lower albedo that enhances the absorption of solar radiation and melt. Amery Ice shelf experienced long melting events in the years 2004, 2005 and 2006 and since then melt duration remains almost constant. However, Lenaerts et al. (2017) reported meltwater features along Roi Baudouin Ice Shelf, Dronning Maud Land, East Antarctica indicating that meltwater production is sometimes underestimated by satellites.

Interannual variability is also present in meltwater volume production (Kuipers Munneke et al., 2012a). Most of the meltwater is produced on the ice shelves and it is more important locally than when it is integrated over the entire ice sheet, as it constitutes a small component of the surface mass balance of the ice sheet (Lenaerts et al., 2012). Besides the long melt seasons observed over the Peninsula, most of the melt is produced there (Kuipers Munneke et al., 2012a). In general, melt over Antarctica is mostly temporary and it refreezes in the snowpack, making the contribution of the runoff in the surface mass balance negligible. However, even though surface drainage in Antarctica is rare, according to recent studies large scale surface drainage systems are responsible for water movement across the ice surface and especially to areas of ice shelves vulnerable to collapse (Lenaerts et al., 2017; Kingslake et al., 2017). These systems can be a result of regionally high temperatures in summer and albedo reduction due to wind erosion and melt (Lenaerts et al., 2017).

Thus, apart from the number of melting days, melt intensity and melt duration throughout the day can give an estimation of the intensity of melting, as days with weak or poor melting are less significant for the ice shelf stability. Specifically, melt duration results from morning QuikSCAT data showed that morning melt duration increase in some years was larger than afternoon melt increase, in regions like the ice shelves at Antarctic Peninsula and Shackleton Ice Shelf. For example at years 2002 and 2003 morning melt over Larsen C Ice Shelf increased more than afternoon melt. This indicates more melting days with longer melt duration during the day. However, only morning melt information can lead to underestimation of melting over ice shelves like Amery, Riisen-Larsen, Ross and Ronne-Filchner.

Trusel et al. (2012) have shown that areas with a large number of melting days per year experience less melt intensity than other areas (e.g. Larsen C Ice Shelf and Wilkins Ice Shelf). This is visible also from the mean maps in Figures 4.24 and 4.26 in these regions. They also noticed that the greatest anticorrelation between melt duration and melt intensity, as discussed in 4.3.2, occurs over locations with high melt duration. Therefore, even though in a continental scale melt index can provide information about relative melt intensity in the periods when melt index was derived using passive microwave instruments (e.g. Torinesi et al., 2003; Liu et al., 2006; Picard and Fily, 2006; Tedesco et al., 2007; Tedesco and Monaghan, 2009), in regional scale melt metrics might not be useful in interpreting as proxies for melt intensity. Moreover, Trusel et al. (2013) have found that melting decibel days (MDD) derived from QuikSCAT can provide an estimation of Antarctic surface meltwater production after they compared the results with independent datasets derived from surface

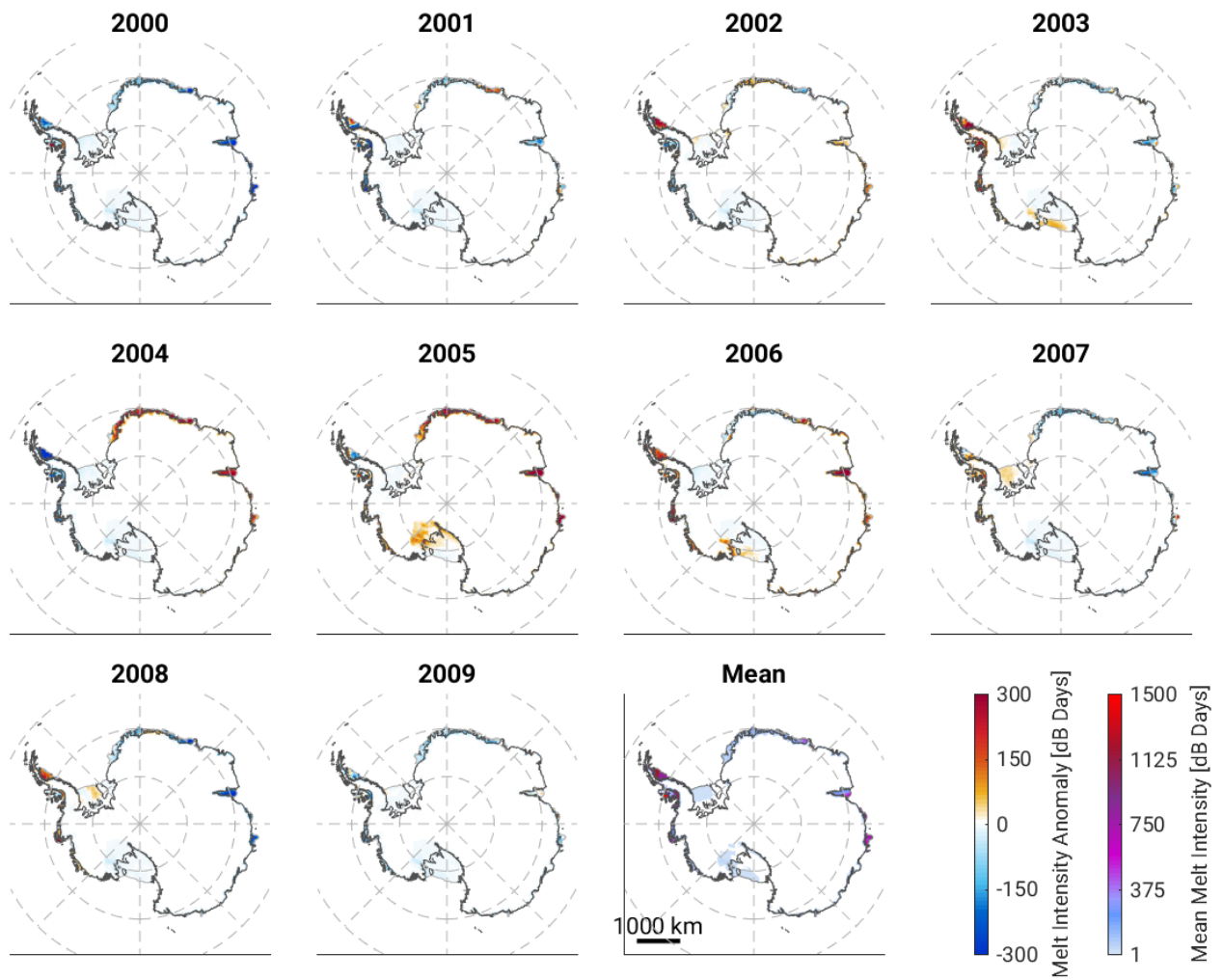


Figure 4.26: Annual maps of melt intensity anomalies for the period 2000-2009 using the Trusel et al. (2012) method for QuikSCAT midday data.

energy balance (SEB) and regional climate modelling.

5

Conclusions

In this thesis the Antarctic surface melting dynamics are presented using radar backscatter data from QuikSCAT and ASCAT. The differences in the melt metrics derived by previous researches necessitated the evaluation of the existing methodologies. Specifically, the Trusel et al. (2012) and Bothale et al. (2015) threshold-based melt detection approaches are applied using QuikSCAT data and their results together with the results of two other melt detection methods that use different thresholds are compared. In addition, an attempt to use ASCAT data to extend the melt time series from 2010 to present is made and the results are compared with melt time series derived from passive microwave instruments.

How does the backscatter coefficient react to different satellites and snowpacks?

It is necessary to determine the dependence of radar backscatter coefficient on snow and satellite parameters, in order to select the threshold for the threshold-based melt detection approach. It is concluded that backscatter sensitivity to liquid water is greater at larger frequencies and it is slightly higher in horizontal than in vertical polarization. In addition, sensitivity increases slightly with incidence angle. This information is important, as it means that QuikSCAT is more sensitive to meltwater than ASCAT, because of the higher frequency and the greater incidence angle. This is confirmed from the second experiment, in which the backscatter change of ASCAT and QuikSCAT for different values of liquid water content is examined and it is shown that the backscatter decreases at a higher rate for QuikSCAT than for ASCAT. Moreover, the sensitivity of QuikSCAT backscatter to liquid water decreases for less rough snow surfaces for values of liquid water content greater than 1%, whereas the sensitivity of ASCAT backscatter remains constant, meaning that QuikSCAT backscatter is more affected by the changes at the top snow layer than ASCAT.

What threshold should be used for the melt detection for QuikSCAT data?

The existing methodologies of Trusel et al. (2012) and Bothale et al. (2015) are evaluated using QuikSCAT morning and midday vertically polarized data. Air temperature data from 10 weather stations are used for the evaluation of the results. A strong correlation exists between melt annual duration and the annual sum of positive degree days for Trusel et al. (2012) results. On the other hand, a weak correlation on the results using the Bothale et al. (2015) method is observed. This is due to the fact that the maximum winter standard deviation used in the latter method for various locations is low, resulting to false melt detection. The decision tree that Trusel et al. (2012) used, in order to determine the yearly threshold for each pixel, takes into account different cases to prevent false melt detection caused by heavy snowfall accumulation that reduces backscatter. In addition, the correlation between the annual melt duration and the annual sum of positive degree days is stronger for midday QuikSCAT data than morning data. The results of the sensitivity test show that a threshold of 3 dB is enough to detect very small liquid water content. Therefore, by taking this into

account two more melt detection methods that combine the approach of the two existing methodologies, M1 and M2, were applied in order to perform a sensitivity analysis and further evaluate the capabilities of the threshold-based melt detection approach. According to the results, the different thresholds affect the melt duration, causing an overestimation of melting days in some cases, and hence a fixed threshold should not be used for the entire Antarctic ice sheet, but the threshold-based melt detection approach should take into account the spatial and temporal variability. Overall, the Trusel et al. (2012) method is the best for melt detection of small amounts of liquid water over the entire Antarctic continent.

How to modify the melt detection method for OSCAT and ASCAT data and produce a consistent melt time series?

QuikSCAT dataset is more complete than OSCAT and ASCAT datasets because of the available midday data, the consistent calibration throughout its mission lifetime and the small number of missing files. On the other hand, OSCAT is omitted from the further processing because of the small time overlap with QuikSCAT, the large number of missing files and the calibration inconsistencies. ASCAT is still operating and has a larger time overlap with QuikSCAT. However, inconsistencies exist between the two datasets, due to the lack of availability of ASCAT midday measurements and their different temporal resolution. In addition, data from 2007 to 2009 are not yet available for processing and thus, the melt detection results could not be compared for the overlapping years. For this reason, annual melt duration was firstly calculated for the period 2010-2016 using morning vertically polarized ASCAT data and three threshold-based melt detection methods (Trusel et al. (2012), M3, M4) and then it was multiplied by a temporal and a diurnal fraction, in order to achieve consistency with QuikSCAT data. As a result, afternoon melt information cannot be retrieved in the regions that do not experience morning melt. In addition, areas that experienced greater morning melt duration in the period 2010-2016 than in the period 2000-2009 (by which the two fractions were computed) resulted in false high melt duration. For this reason, this approach gives reliable results at locations with low interannual variations in melting, like the ice shelves of the Peninsula.

What is the observed temporal and spatial trend of melt dynamics?

Overall, there is not any clear temporal trend in melting. The results from the period 2000-2009 show a peak in melt metrics in 2005, that coincides with more annual positive degree days than the average of the period over the entire ice sheet. This indicates a possible connection among the high temperatures and increased melting. In addition, Antarctic Peninsula experiences the longest melt seasons, and its mean melt index equals the melt index of the rest of the continent, even though its average melt extent is 20% of the total melt extent. In general, West Antarctic climate is influenced by large-scale modes of climate variability, the Southern Annular Mode and the El Niño Southern Oscillation. Positive phases of SAM result to the increase of circumpolar westerlies and they are linked with increased temperatures over the Peninsula. The year 2016 was also a year with high total melt extent according to the surface melting dynamics derived from AMSR2 and it coincides with a strong El Niño event and positive SAM. Further research is needed for the better understanding of the drivers of the surface melting and the prediction of its future occurrence.

What is the temporal and spatial evolution of the Antarctic surface melting dynamics in the period 2000-2016 using scatterometer data?

In conclusion, the surface melting dynamics derived by ASCAT are not consistent with those from QuikSCAT and thus they cannot be compared. Even though results over regions with high melt duration and consistent morning and afternoon melt, like the Antarctic Peninsula, can give some information about melting for the period 2010-2016, afternoon melt information is needed for the assessment of the stability of ice shelves. Although information from AMSR-E and AMSR2 for afternoon melt is available and gives an overview of melt interannual variations, their coarser resolution and the fact that they are less sensitive to melt compared to scatterometers result in the underestimation of melting in terms of melt duration. Overall, a high interannual variability in the Antarctic surface melting dynamics exists and results show that the regions with consistent morning and afternoon melt remain constant through the years. Even though there is not any clear trend in melting for this period, it is clear that spatial variations in surface melting are caused by

the variability of climatic conditions over the Antarctic Ice Sheet. Finally, ice shelves over the regions that experience extensive melt and long and intense melt seasons for many years, like Antarctic Peninsula, are subject to extensive surface ponding and possible hydrofracturing that can lead to their collapse.

Recommendations

The results of the fractional melt detection approach showed that it was not possible to achieve consistency between the results of QuikSCAT and ASCAT. Thus, further research on the capabilities of using ASCAT for the melt time series extension can be done using data from the period 2007-2009. A comparison of the results of this period from ASCAT and QuikSCAT can give more information about the inconsistencies of the sensors, regarding their sensitivities to meltwater, and a better approach for acquiring consistency in melt duration can be implemented. However, the determination of the full extent of melt remains a challenge, since the major drawback of this method is the lack of ASCAT midday observations.

The different climatic and firn conditions and topographic characteristics over the different regions of Antarctic continent result in false melt detection, when a single threshold is used. Additional information for the firn and surface temperatures taken from models, albedo maps, DEM and high spatial resolution optical images can assist in this process. A more detailed investigation of the backscatter spatial variability can be completed by taking into account these differences. As a result, it is possible to employ a dynamic threshold-based melt detection approach that can vary for the different regions of the ice sheet.

Surface melt over Antarctica is temporary and shows a large diurnal variability, and hence the time of observations is important for melt detection. In order to examine whether morning measurements (e.g. ASCAT) are enough for assessing the stability of the ice shelves, a comparison of satellite based morning surface melt fluxes and ground-based melt fluxes can be performed. Based on this information, the underestimation of melt and its importance can be quantified and assessed.

An attempt of comparison of passive and active microwave melt detection algorithms over Antarctica is performed. The differences in sensor characteristics and spatial resolution result in differences in melt duration. A more careful analysis of the calculated melt onset dates (first day of melt) and refreeze dates between the sensors can provide additional information on the origin of the melt duration differences.

Although the main scope of this research is the assessment of the capabilities of the threshold-based melt detection methods using scatterometer data, further research on identifying the snowmelt volume over the ice shelves that are vulnerable to collapse is important. Specifically, the calculation of meltwater volume is possible by using multi-spectral imagery to determine water depth. In addition, high spatial multi-spectral data are useful in the identification of melt features on the ice shelves and the surface of the ice sheet. However, it should be noted that in this case the temporal resolution of these data depends on the presence of cloud cover.

Changes in ice shelf front are also important in assessing ice shelf stability. Observations from visible satellite imagery (e.g. MODIS) can provide this information. Additional information from altimeters shows the elevation change of the ice shelves and the ice sheet, and thus it is possible to identify the regions where the changes are larger. Thinning is the result of both surface and basal melt and relatively thin ice shelves are more sensitive to hydrofracturing. The estimation of volume changes of the ice shelves and the observation of the ice shelf front changes together with the estimation of melt duration and melt intensity offer a more complete assessment of the impact of snowmelt on their overall stability.

Bibliography

- Abdalati, W., Steffen, K., 1997. **Snowmelt on the Greenland ice sheet as derived from passive microwave satellite data.** *Journal of Climate*, 10(2):165–175. [https://doi.org/10.1175/1520-0442\(1997\)010<0165:SOTGIS>2.0.CO;2](https://doi.org/10.1175/1520-0442(1997)010<0165:SOTGIS>2.0.CO;2).
- Ashcraft, I. S., Long, D. G., 2006. **Comparison of methods for melt detection over Greenland using active and passive microwave measurements.** *International Journal of Remote Sensing*, 27(12):2469–2488. <http://dx.doi.org/10.1080/01431160500534465>.
- Barrand, N. E., Vaughan, D. G., Steiner, N., Tedesco, M., Kuipers Munneke, P., van den Broeke, M. R., Hosking, J. S., 2013. **Trends in Antarctic Peninsula surface melting conditions from observations and regional climate modeling.** *Journal of Geophysical Research: Earth Surface*, 118(1):315–330. <http://dx.doi.org/10.1029/2012JF002559>.
- Bartsch, A., Kidd, R. A., Wagner, W., Bartalis, Z., 2007. **Temporal and spatial variability of the beginning and end of daily spring freeze/thaw cycles derived from scatterometer data.** *Remote Sensing of Environment*, 106(3):360–374. <https://doi.org/10.1016/j.rse.2006.09.004>.
- Bentamy, A., Grodsky, S. A., Carton, J. A., Croizé-Fillon, D., Chapron, B., 2012. **Matching ASCAT and QuikSCAT winds.** *Journal of Geophysical Research: Oceans*, 117(C2). <http://dx.doi.org/10.1029/2011JC007479>.
- Bhowmick, S. A., Kumar, R., Kumar, A. K., 2014. **Cross calibration of the OceanSAT-2 scatterometer with QuikSCAT scatterometer using natural terrestrial targets.** *IEEE Transactions on Geoscience and Remote Sensing*, 52(6):3393–3398. <https://doi.org/10.1109/TGRS.2013.2272738>.
- Bothale, R. V., Rao, P. V. N., Dutt, C. B. S., Dadhwal, V. K., Maurya, D., 2015. **Spatio-temporal dynamics of surface melting over Antarctica using OSCAT and QuikSCAT scatterometer data (2001–2014).** *Current Science*, 109(4):733–744.
- Bromwich, D. H., Monaghan, A. J., Guo, Z., 2004. **Modeling the ENSO modulation of Antarctic climate in the late 1990s with the polar MM5.** *Journal of climate*, 17(1):109–132. [https://doi.org/10.1175/1520-0442\(2004\)017<0109:MTEMOA>2.0.CO;2](https://doi.org/10.1175/1520-0442(2004)017<0109:MTEMOA>2.0.CO;2).
- Cassano, J. J. **Climate of extremes.** In *Antarctica: global science from a Frozen Continent*, pages 102–136. Cambridge University Press, 2013.
- Church, J. A., Clark, P. U., Cazenave, A., Gregory, J. M., Jevrejeva, S., Levermann, A., Merrifield, M. A., Milne, G. A., Nerem, R. S., Nunn, P. D. et al., 2013. **Sea level change.** In: *Climate Change 2013: The Physical Science Basis. Contribution of Working Group I to the Fifth Assessment Report of the Intergovernmental Panel on Climate Change*.
- Cook, A. J., Vaughan, D. G., 2010. **Overview of areal changes of the ice shelves on the Antarctic Peninsula over the past 50 years.** *The cryosphere*, 4(1):77–98. <https://doi.org/10.5194/tc-4-77-2010>.
- Cook, Y., Storey, B. **A Continent Under Ice.** In *Exploring the Last Continent*, pages 9–27. Springer, 2015.

- Cuffey, K. M., Paterson, W. S. B., 2010, **The physics of glaciers**. Academic Press.
- Das, S. B., Alley, R. B., 2008. **Rise in frequency of surface melting at Siple Dome through the Holocene: Evidence for increasing marine influence on the climate of West Antarctica**. *Journal of Geophysical Research: Atmospheres*, 113(D2). <http://dx.doi.org/10.1029/2007JD008790>.
- EUMETSAT. **ASCAT Product Guide**, 2015.
- Frey, K. E., Smith, L. C., Alsdorf, D. E., 2003. **Controls on Eurasian coastal sea ice formation, melt onset and decay from ERS scatterometry: regional contrasts and effects of river influx**. *International Journal of Remote Sensing*, 24(24):5283–5315. <http://dx.doi.org/10.1080/0143116031000101684>.
- Fung, A., 1994, **Microwave Scattering and Emission Models and Their Applications**. Artech House.
- Greene, C. A., Gwyther, D. E., Blankenship, D. D., 2017. **Antarctic mapping tools for MATLAB**. *Computers & Geosciences*, 104:151–157. <https://doi.org/10.1016/j.cageo.2016.08.003>.
- Haarpaintner, J., Tonboe, R. T., Long, D. G., Van Woert, M. L., 2004. **Automatic detection and validity of the sea-ice edge: an application of enhanced-resolution QuikScat/SeaWinds data**. *IEEE Transactions on Geoscience and Remote Sensing*, 42(7):1433–1443. <http://dx.doi.org/10.1109/TGRS.2004.828195>.
- Hall, D. K., Martinec, J., 1985, **Remote sensing of ice and snow**. Chapman and Hall.
- Haran, T., Bohlander, J., Scambos, T., Painter, T., Fahnestock, M. **MODIS Mosaic of Antarctica 2003-2004 (MOA2004) Image Map**. National Snow and Ice Data Center, 2005. <http://dx.doi.org/10.7265/N5ZK5DM5>.
- Hillard, U., Sridhar, V., Lettenmaier, D. P., McDonald, K. C., 2003. **Assessing snowmelt dynamics with NASA scatterometer (NSCAT) data and a hydrologic process model**. *Remote Sensing of Environment*, 86(1): 52–69. [http://dx.doi.org/10.1016/S0034-4257\(03\)00068-3](http://dx.doi.org/10.1016/S0034-4257(03)00068-3).
- Hock, R., 2005. **Glacier melt: a review of processes and their modelling**. *Progress in physical geography*, 29 (3):362–391. <http://dx.doi.org/10.1191/0309133305pp453ra>.
- Holland, P. R., Corr, H. F., Pritchard, H. D., Vaughan, D. G., Arthern, R. J., Jenkins, A., Tedesco, M., 2011. **The air content of Larsen ice shelf**. *Geophysical Research Letters*, 38(10). <http://dx.doi.org/10.1029/2011GL047245>.
- Kingslake, J., Ely, J. C., Das, I., Bell, R. E., 2017. **Widespread movement of meltwater onto and across Antarctic ice shelves**. *Nature*, 544(7650):349. <https://doi.org/10.1038/nature22049>.
- Kuipers Munneke, P., Van den Broeke, M. R., Lenaerts, J. T. M., Flanner, M. G., Gardner, A. S., Van de Berg, W. J., 2011. **A new albedo parameterization for use in climate models over the Antarctic ice sheet**. *Journal of Geophysical Research: Atmospheres*, 116(D5). <http://dx.doi.org/10.1029/2010JD015113>.
- Kuipers Munneke, P., Picard, G., den Broeke, M., Lenaerts, J., Meijgaard, E. v., 2012a. **Insignificant change in Antarctic snowmelt volume since 1979**. *Geophysical Research Letters*, 39(1). <https://doi.org/10.1029/2011GL050207>.
- Kuipers Munneke, P., Van den Broeke, M. R., King, J. C., Gray, T., Reijmer, C. H., 2012b. **Near-surface climate and surface energy budget of Larsen C ice shelf, Antarctic Peninsula**. *The Cryosphere*, 6(2):353–363. <http://dx.doi.org/10.5194/tc-6-353-2012>.
- Kunz, L. B., Long, D. G., 2006. **Melt detection in Antarctic ice shelves using scatterometers and microwave radiometers**. *IEEE Transactions on Geoscience and Remote Sensing*, 44(9):2461–2469. <http://dx.doi.org/10.1109/TGRS.2006.874138>.
- Lampkin, D. J., Yool, S. R., 2004. **Monitoring mountain snowpack evolution using near-surface optical and thermal properties**. *Hydrological processes*, 18(18):3527–3542. <http://dx.doi.org/10.1002/hyp.5797>.

- Lenaerts, J. T. M., van Den Broeke, M. R., Berg, W. J., Meijgaard, E. v., Kuipers Munneke, P., 2012. **A new, high-resolution surface mass balance map of Antarctica (1979–2010) based on regional atmospheric climate modeling.** *Geophysical Research Letters*, 39(4). <http://dx.doi.org/10.1029/2011GL050713>.
- Lenaerts, J., Lhermitte, S., Drews, R., Ligtenberg, S., Berger, S., Helm, V., Smeets, C., Van Den Broeke, M., van de Berg, W., van Meijgaard, E. et al., 2017. **Meltwater produced by wind-albedo interaction stored in an East Antarctic ice shelf.** *Nature Climate Change*, 7(1):58–62. <https://doi.org/10.1038/nclimate3180>.
- Lindell, D. B., Long, D. G., 2016. **Multiyear Arctic sea ice classification using OSCAT and QuikSCAT.** *IEEE Transactions on Geoscience and Remote Sensing*, 54(1):167–175. <http://dx.doi.org/10.1109/TGRS.2015.2452215>.
- Lindsley, R. D., Long, D. G. **Standard BYU ASCAT Land/Ice Image Products.** Technical report, BYU Centre for Remote Sensing, Microwave Earth Remote Sensing Lab, Provo, Utah, 2010. Available from <http://http://www.scp.byu.edu/docs/pdf/MERS1002.pdf>.
- Lindsley, R. D., Long, D. G., 2016. **ASCAT and QuikSCAT azimuth modulation of backscatter over East Antarctica.** *IEEE Geoscience and Remote Sensing Letters*, 13(8):1134–1138. <https://doi.org/10.1109/LGRS.2016.2572101>.
- Liu, H., Wang, L., Jezek, K. C., 2006. **Spatiotemporal variations of snowmelt in Antarctica derived from satellite scanning multichannel microwave radiometer and Special Sensor Microwave Imager data (1978–2004).** *Journal of Geophysical Research: Earth Surface*, 111(F1). <http://dx.doi.org/10.1029/2005JF000318>.
- Long, D. G. **Standard BYU QuikSCAT/SeaWinds land/ice image products.** Technical report, BYU Centre for Remote Sensing, Microwave Earth Remote Sensing Lab, Provo, Utah, 2010. Available from <http://www.scp.byu.edu/docs/pdf/QscatReport6.pdf>.
- Long, D. G., Drinkwater, M. R., 2000. **Azimuth variation in microwave scatterometer and radiometer data over Antarctica.** *IEEE Transactions on Geoscience and Remote Sensing*, 38(4):1857–1870. <https://doi.org/10.1109/10.1109/36.851769>.
- Luis, A. J., 2013. **Past, present and future climate of Antarctica.** <http://dx.doi.org/10.4236/ijg.2013.46089>.
- Marshall, G. J., Orr, A., van Lipzig, N. P., King, J. C., 2006. **The impact of a changing Southern Hemisphere Annular Mode on Antarctic Peninsula summer temperatures.** *Journal of Climate*, 19(20):5388–5404. <https://doi.org/10.1175/JCLI3844.1>.
- Masson-Delmotte, V. **Ice with everything.** In *Antarctica: global science from a Frozen Continent*, pages 67–101. Cambridge University Press, 2013.
- Mätzler, C., Wiesmann, A. **Documentation for MEMLS, version 3, Microwave Emission Model of Layered Snowpacks.** Technical report, Microwave Dept., Institute Applied Physics, University of Bern, Bern, Switzerland, 2012.
- Mätzler, C., Wiesmann, A. **Documentation for MEMLS Active, Microwave Emission Model of Layered Snowpacks adapted to include backscattering.** Technical Report 2013-03, Microwave Dept., Institute Applied Physics, University of Bern, Bern, Switzerland, 2014.
- Mätzler, C., 1996. **Notes on microwave radiation from snow samples and emission of layered snowpacks.** Available from http://www.iapmw.unibe.ch/research/projects/snowtools/memls/NOTE_1-14.pdf.
- Matzler, C., Wegmuller, U., 1987. **Dielectric properties of freshwater ice at microwave frequencies.** *Journal of Physics D: Applied Physics*, 20(12):1623.

- Nghiem, S. V., Steffen, K., Neumann, G., Huff, R., 2005. **Mapping of ice layer extent and snow accumulation in the percolation zone of the Greenland ice sheet.** *Journal of Geophysical Research: Earth Surface*, 110 (F2). <http://dx.doi.org/10.1029/2004JF000234>.
- Nghiem, S. V., Steffen, K., Neumann, G., Huff, R. **Snow accumulation and snowmelt monitoring in Greenland and Antarctica.** In *Dynamic Planet*, pages 31–38. Springer, 2007.
- Nicolas, J. P., Vogelmann, A. M., Scott, R. C., Wilson, A. B., Cadeddu, M. P., Bromwich, D. H., Verlinde, J., Lubin, D., Russell, L. M., Jenkinson, C. et al., 2017. **January 2016 extensive summer melt in West Antarctica favoured by strong El Niño.** *Nature Communications*, 8:ncomms15799. <https://doi.org/10.1038/ncomms15799>.
- Oerlemans, J., Van Der Veen, C. J., 1984, **Ice sheets and climate**, volume 21. Springer.
- Ohmura, A., 2001. **Physical basis for the temperature-based melt-index method.** *Journal of applied Meteorology*, 40(4):753–761. [http://dx.doi.org/10.1175/1520-0450\(2001\)040<0753:PBFTTB>2.0.CO;2](http://dx.doi.org/10.1175/1520-0450(2001)040<0753:PBFTTB>2.0.CO;2).
- Panday, P. K., Frey, K. E., Ghimire, B., 2011. **Detection of the timing and duration of snowmelt in the Hindu Kush-Himalaya using QuikSCAT, 2000–2008.** *Environmental Research Letters*, 6(2):024007. <http://dx.doi.org/10.1088/1748-9326/6/2/024007>.
- Perovich, D. K. **The optical properties of sea ice.** Technical report, DTIC Document, 1996.
- Picard, G., Fily, M., 2006. **Surface melting observations in Antarctica by microwave radiometers: Correcting 26-year time series from changes in acquisition hours.** *Remote sensing of environment*, 104(3): 325–336. <https://doi.org/10.1016/j.rse.2006.05.010>.
- Pritchard, H. D., Vaughan, D. G., 2007. **Widespread acceleration of tidewater glaciers on the Antarctic Peninsula.** *Journal of Geophysical Research: Earth Surface*, 112(F3). <http://dx.doi.org/10.1029/2006JF000597>.
- Proksch, M., Mätzler, C., Wiesmann, A., Lemmetyinen, J., Schwank, M., Löwe, H., Schneebeli, M., 2015. **MEMLS3&a: Microwave Emission Model of Layered Snowpacks adapted to include backscattering.** *Geoscientific Model Development*, 8(8):2611–2626.
- Raphael, M., Marshall, G., Turner, J., Fogt, R., Schneider, D., Dixon, D., Hosking, J., Jones, J., Hobbs, W., 2016. **The Amundsen sea low: variability, change, and impact on Antarctic climate.** *Bulletin of the American Meteorological Society*, 97(1):111–121. <https://doi.org/10.1175/BAMS-D-14-00018.1>.
- Rees, W. G., 2005, **Remote sensing of snow and ice.** CRC press.
- Rignot, E., Casassa, G., Gogineni, P., Krabill, W., Rivera, A., Thomas, R., 2004. **Accelerated ice discharge from the Antarctic Peninsula following the collapse of Larsen B ice shelf.** *Geophysical Research Letters*, 31(18). <https://doi.org/10.1029/2004GL020697>.
- Rotschky, G., Schuler, T. V., Haarpaintner, J., Kohler, J., Isaksson, E., 2011. **Spatio-temporal variability of snowmelt across Svalbard during the period 2000-08 derived from QuikSCAT/SeaWinds scatterometry.** *Polar Research*, 30. <http://dx.doi.org/10.3402/polar.v30i0.5963>.
- Scambos, T. A., Hulbe, C., Fahnestock, M., Bohlander, J., 2000. **The link between climate warming and break-up of ice shelves in the Antarctic Peninsula.** *Journal of Glaciology*, 46(154):516–530. <http://dx.doi.org/10.3189/172756500781833043>.
- Sinclair, K. E. **An Ice-Bound Continent.** In *Exploring the Last Continent*, pages 67–89. Springer, 2015.
- Smith, L. C., Sheng, Y., Forster, R. R., Steffen, K., Frey, K. E., Alsdorf, D. E., 2003. **Melting of small Arctic ice caps observed from ERS scatterometer time series.** *Geophysical Research Letters*, 30(20).

- Spencer, M. W., Wu, C., Long, D. G., 2000. **Improved resolution backscatter measurements with the SeaWinds pencil-beam scatterometer.** *IEEE Transactions on Geoscience and remote sensing*, 38(1):89–104. <http://dx.doi.org/10.1109/36.823904>.
- Stiles, W. H., Ulaby, F. T., 1980. **The active and passive microwave response to snow parameters: 1. Wetness.** *Journal of Geophysical Research: Oceans*, 85(C2):1037–1044. <http://dx.doi.org/10.1029/JC085iC02p01037>.
- Stogryn, A., 1986. **A study of the microwave brightness temperature of snow from the point of view of strong fluctuation theory.** *IEEE Transactions on Geoscience and Remote Sensing*, (2):220–231. <http://dx.doi.org/10.1109/TGRS.1986.289641>.
- Tedesco, M., 2009. **Assessment and development of snowmelt retrieval algorithms over Antarctica from K-band spaceborne brightness temperature (1979–2008).** *Remote Sensing of Environment*, 113(5):979–997. <http://dx.doi.org/10.1016/j.rse.2009.01.009>.
- Tedesco, M., 2014, **Remote sensing of the cryosphere.** John Wiley & Sons.
- Tedesco, M., Monaghan, A. J., 2009. **An updated Antarctic melt record through 2009 and its linkages to high-latitude and tropical climate variability.** *Geophysical Research Letters*, 36(18). <https://doi.org/10.1029/2009GL039186>.
- Tedesco, M., Abdalati, W., Zwally, H. J., 2007. **Persistent surface snowmelt over Antarctica (1987–2006) from 19.35 GHz brightness temperatures.** *Geophysical Research Letters*, 34(18). <http://dx.doi.org/10.1029/2007GL031199>.
- Thompson, D. W., Solomon, S., 2002. **Interpretation of recent Southern Hemisphere climate change.** *Science*, 296(5569):895–899. <https://doi.org/10.1126/science.1069270>.
- Torinesi, O., Fily, M., Genthon, C., 2003. **Variability and trends of the summer melt period of Antarctic ice margins since 1980 from microwave sensors.** *Journal of Climate*, 16(7):1047–1060. [http://dx.doi.org/10.1175/1520-0442\(2003\)016<1047:VATOTS>2.0.CO;2](http://dx.doi.org/10.1175/1520-0442(2003)016<1047:VATOTS>2.0.CO;2).
- Trusel, L. D., Frey, K. E., Das, S. B., 2012. **Antarctic surface melting dynamics: Enhanced perspectives from radar scatterometer data.** *Journal of Geophysical Research: Earth Surface*, 117(F2). <http://dx.doi.org/10.1029/2011JF002126>.
- Trusel, L. D., Frey, K. E., Das, S. B., Kuipers Munneke, P., van den Broeke, M. R., 2013. **Satellite-based estimates of Antarctic surface meltwater fluxes.** *Geophysical Research Letters*, 40(23):6148–6153. <http://dx.doi.org/10.1002/2013GL058138>.
- Ulaby, F. T., Stiles, W. H., 1981. **Microwave response of snow.** *Advances in Space Research*, 1(10):131–149. [http://dx.doi.org/10.1016/0273-1177\(81\)90389-6](http://dx.doi.org/10.1016/0273-1177(81)90389-6).
- van den Broeke, M., 2005. **Strong surface melting preceded collapse of Antarctic Peninsula ice shelf.** *Geophysical Research Letters*, 32(12). <https://doi.org/10.1029/2005GL023247>.
- van Wessem, J. M., Reijmer, C. H., van de Berg, W. J., van den Broeke, M. R., Cook, A. J., van Ulft, L. H., van Meijgaard, E., 2015. **Temperature and wind climate of the antarctic Peninsula as Simulated by a high-resolution regional atmospheric climate model.** *Journal of Climate*, 28(18):7306–7326. <https://doi.org/10.1175/JCLI-D-15-0060.1>.
- Vizcaíno, M., Lipscomb, W. H., Sacks, W. J., van den Broeke, M., 2014. **Greenland surface mass balance as simulated by the community earth system model. Part II: twenty-first-century changes.** *Journal of climate*, 27(1):215–226.
- Wang, L., Sharp, M. J., Rivard, B., Marshall, S., Burgess, D., 2005. **Melt season duration on Canadian Arctic ice caps, 2000–2004.** *Geophysical Research Letters*, 32(19). <http://dx.doi.org/10.1029/2005GL023962>.

- Wang, L., Sharp, M., Rivard, B., Steffen, K., 2007. **Melt season duration and ice layer formation on the Greenland ice sheet, 2000–2004.** *Journal of Geophysical Research: Earth Surface*, 112(F4). <http://dx.doi.org/10.1029/2007JF000760>.
- Wang, L., Derksen, C., Brown, R., 2008. **Detection of pan-Arctic terrestrial snowmelt from QuikSCAT, 2000–2005.** *Remote Sensing of Environment*, 112(10):3794–3805. <https://doi.org/10.1016/j.rse.2008.05.017>.
- Wiesmann, A., Mätzler, C., 1999. **Microwave emission model of layered snowpacks.** *Remote Sensing of Environment*, 70(3):307–316. [http://dx.doi.org/10.1016/S0034-4257\(99\)00046-2](http://dx.doi.org/10.1016/S0034-4257(99)00046-2).
- Wismann, V., 2000. **Monitoring of seasonal snowmelt on Greenland with ERS scatterometer data.** *IEEE Transactions on Geoscience and Remote Sensing*, 38(4):1821–1826. <http://dx.doi.org/10.1109/36.851766>.

List of Figures

2.1	(a) Map of Antarctica from (Luis, 2013) and (b) Antarctic ice shelves.	8
2.2	Illustration of the cycle through which glacial ice and water ends up in the oceans (Goddard Space Flight Center NASA).	8
2.3	Range of albedo of different surfaces (Perovich, 1996).	9
2.4	Range of electromagnetic radiation and radar frequency bands (From https://earth.esa.int).	11
2.5	Wet snow (right) causes a decrease in backscattered signal because of the surface scattering and increased absorption (Tedesco, 2014).	12
2.6	A radar pulse is transmitted from the antenna to the ground and is scattered back to the antenna by ground targets (From https://crisp.nus.edu.sg/).	13
2.7	The wet snow layer (right) absorbs the radiation from the bottom layers and emits a stronger signal than that of the dry snow (left) (Tedesco, 2014).	14
3.1	QuikSCAT observation geometry (Long, 2010).	18
3.2	ASCAT observation geometry (EUMETSAT, 2015).	19
3.3	Map of Antarctica showing the location of the weather stations used in this study as blue dots (Ji: Joinville Island, La: Larsen C, Li: Limbert, Br: Brunt, Nu: Neumayer, Hn: Haupt Nunatak, Cs: Casey Skiway, Cp: Cape Poinsett, Pp: Penguin Point, Mn: Manuela).	21
3.4	Geometry of the n-layered snowpack with an electromagnetic wave incident from above at an incidence angle θ_n . Snow-ground reflectivity s_0 , ground temperature T_0 , layer thickness d_j , temperature T_j , transmissivity t_j , volume reflectivity r_j , emissivity e_j , interface reflectivity s_j , refracted angle θ_{j-1} for layer number j from 1 (bottom) to n (top) (Mätzler and Wiesmann, 2014).	22
3.5	Decision tree process for surface melting classification (Trusel et al., 2012).	25
4.1	Angular response of σ^0 to dry and wet snow at different frequencies for vertical and horizontal polarization. The snowpack used is described in Table 3.3.	32
4.2	Change in σ_{vv}^0 with increasing liquid water content [0.2%, 0.5%, 0.7%, 1%, 1.3%, 1.7%, 2%, 2.5%, 3%] for QuikSCAT (frequency 13.4 GHz, incidence angle 54°) and ASCAT (frequency 5.225 GHz and incidence angle 40°) for different values of density (top) and exponential correlation length (bottom) of the top snow layer.	33
4.3	Change in σ_{vv}^0 and T_b with increasing liquid water content for QuikSCAT, ASCAT and AMSR-E / AMSR2.	33
4.4	Time series of QuikSCAT σ_{vv}^0 from morning data (red line), maximum daily temperature (blue line) at the location of weather stations together with varying thresholds of Trusel et al. (2012) (green line) and Bothale et al. (2015) using maximum standard deviation from QuikSCAT data only (black line) and using the maximum standard deviation from QuikSCAT and OSCAT data (brown line). Vertical gray boxes indicate the days with temperature higher than 0 °C.	34

4.5	Dependence of annual QuikSCAT melting days (MD) as computed using the Trusel et al. (2012) method on annual positive days (PD) for (a) vertically polarized morning data (b) horizontally polarized morning data (c) vertically polarized midday data and (d) horizontally polarized midday data.	36
4.6	Annual maps of melt duration and mean melt duration for the period 2000-2009 as calculated using the Trusel et al. (2012) method for the QuikSCAT vertically polarized midday data.	37
4.7	Melt duration maps for 2000 [QuikSCAT midday vertically polarized data] at Amundsen Sea Embayment for (a) Trusel et al. (2012) method, (b) M1 method and (c) M2 method. The black dot in the first figure indicates the location that the time series of Figure 4.8 refers to.	38
4.8	Time series of QuikSCAT σ^0 (blue line) at latitude -73.25° and longitude -98.30° in West Antarctica, together with the threshold of Trusel et al. (2012), M1 and M2 methods. The upwards jumps in σ^0 indicate the formation of ice layers with large ice scatterers, whereas the gradual decrease in σ^0 is caused by snow accumulation.	38
4.9	Time series of ASCAT σ_{vv}^0 from morning data (red line), maximum daily temperature (blue line) at the location of weather stations together with threshold of Trusel et al. (2012) (green line). Vertical gray boxes indicate the melting days.	39
4.10	Annual maps of melt duration for the period 2000-2016 from QuikSCAT (2000 - 2009) and ASCAT (2010-2016) multiplied by the fractions, as calculated using the Trusel et al. (2012).	40
4.11	Annual maps of melt duration for the period 2003-2016 from AMSR-E (2003 - 2011) and AMSR2 (2013-2016) 18.7 GHz horizontally polarized data.	41
4.12	Time series of total melt extent for active and passive microwave data over the Antarctic continent. Melt extent is based on the results using QuikSCAT data for the period 2000 - 2009, ASCAT results from the fractional melt detection method for the period 2010 - 2016, AMSR-E data for the period 2003 - 2011 and AMSR2 data for the period 2013 - 2016.	42
4.13	Time series of total melt index for active and passive microwave data over the Antarctic continent. Melt index is based on the results using QuikSCAT data for the period 2000 - 2009, ASCAT results from the fractional melt detection method for the period 2010 - 2016, AMSR-E data for the period 2003 - 2011 and AMSR2 data for the period 2013 - 2016.	43
4.14	Time series of total melt intensity for QuikSCAT data over the Antarctic continent.	43
4.15	Spatial comparison of melt extent results (a) from Trusel et al. (2012) and M1 methods, (b) from Trusel et al. (2012) and M2 methods and (c) from M1 and M2 methods for year 2002. Blue indicates that both methods detected melt for at least one day of the year, red indicates the regions where only first method (in each case) detected melt, green indicates the regions where both methods did not detect melt and cyan indicates the regions where only the second method (in each case) detected melt.	44
4.16	The amount of pixels that belong to each QuikSCAT class and are classified for AMSR-E as melting (1) and non-melting (0) pixels [x axis]. The box in each year is a zoom in the plot excluding the pixels classified for both QuikSCAT and AMSR-E as non-melting. Classification was performed based on the Trusel et al. (2012) method results.	45
4.17	Maps showing the regions in which melt occurred for at least 1 day for both AMSR-E and QuikSCAT (Trusel et al., 2012) with blue, only for QuikSCAT in red, only for AMSR-E in cyan and the regions where none of the methods detects melt in green for the year 2005.	46
4.18	Annual maps of melt duration difference between AMSR-E melting days and the QuikSCAT (Trusel et al. (2012) method) coarse resolution melting days.	47
4.19	Total annual melt extent for (a) regions with always morning and afternoon melt (top), (b) regions with only afternoon melt (middle) and (c) regions with sometimes morning melt (bottom).	48
4.20	Sections in which Antarctic continent is divided for the calculation of melt metrics in regional scale: (1) Antarctic Peninsula, (2) Ronne-Filchner Ice Shelf, (3) Dronning Maud Land, (4) Amery Ice Shelf, (5) Wilkes Land, (6) Ross Ice Shelf and (7) Marie Byrd Land.	49
4.21	Regional variations in melt extent.	49
4.22	Regional variations in melt index.	50

4.23	Regional variations in melt intensity.	50
4.24	Annual maps of melt duration anomalies for the period 2000-2009 using the Trusel et al. (2012) method.	51
4.25	Annual maps for annual positive degree days (PDD) anomalies for the period 2000-2016 and the mean of PDD for the period 2000-2009 and 2010-2016. Midday modelled near surface temperature from RACMO2.4 was used.	52
4.26	Annual maps of melt intensity anomalies for the period 2000-2009 using the Trusel et al. (2012) method for QuikSCAT midday data.	54
A.1	Time series of QuikSCAT σ_{hh}^0 from morning data (red line), maximum daily temperature (blue line) at the location of weather stations together with varying thresholds of Trusel et al. (2012) (green line) and Bothale et al. (2015) using maximum standard deviation from QuikSCAT data only (black line) and using the maximum standard deviation from QuikSCAT and OSCAT data (brown line). Vertical gray boxes indicate the days with temperature higher than 0 °C.	74
A.2	Comparison between QuikSCAT and OSCAT data for horizontal and vertical polarization and the winter backscatter standard deviation for each year at Brunt (Br). Horizontal lines indicate the thresholds for Trusel et al. (2012) methodology (pink line), Bothale et al. (2015) using QuikSCAT data only (red line) and using QuikSCAT and OSCAT data (cyan line).	75
A.3	Comparison between QuikSCAT horizontally and vertically polarized backscatter from morning and midday/afternoon data and the winter backscatter standard deviation for each year at Neumayer (Nu).	75
A.4	Dependence of annual QuikSCAT melting days (MD) as computed using the Bothale et al. (2015) methodology only for QuikSCAT data on annual positive days (PD) for (a) vertically polarized morning data (b) horizontally polarized morning data (c) vertically polarized midday data and (d) horizontally polarized midday data.	76
A.5	Dependence of annual QuikSCAT melting days (MD) as computed using the Bothale et al. (2015) methodology using QuikSCAT and OSCAT data on annual positive days (PD) for (a) vertically polarized morning data (b) horizontally polarized morning data.	77
A.6	Dependence of annual QuikSCAT melting days (MD) as computed using the M1 methodology (4.2.2) on annual positive days (PD) for (a) vertically polarized morning data (b) horizontally polarized morning data (c) vertically polarized midday data and (d) horizontally polarized midday data.	78
A.7	Dependence of annual QuikSCAT melting days (MD) as computed using the M2 methodology (4.2.2) on annual positive days (PD) for (a) vertically polarized morning data (b) horizontally polarized morning data (c) vertically polarized midday data and (d) horizontally polarized midday data.	79
A.8	Annual maps of melt duration and mean melt duration for the period 2000-2009 as calculated using the M1 method for the QuikSCAT vertically polarized midday data.	80
A.9	Annual maps of melt duration and mean melt duration for the period 2000-2009 as calculated using the M2 method for the QuikSCAT vertically polarized midday data.	81
A.10	Mean melt duration difference between the Trusel et al. (2012) and M1 method for the period 2000-2009 [QuikSCAT vertically polarized midday data].	82
A.11	Mean melt duration difference between the Trusel et al. (2012) and M2 method for the period 2000-2009 [QuikSCAT vertically polarized midday data].	83
A.12	Mean melt duration difference between the M1 and M2 method for the period 2000-2009 [QuikSCAT vertically polarized midday data].	84
A.13	Time series of QuikSCAT σ^0 (blue line) at latitude -67.42° and longitude -66.75° in Peninsula (location shown at Fig. A.10a), together with the threshold of Trusel et al. (2012), M1 and M2 methods.	85
A.14	Mean melt duration difference between the Trusel et al. (2012) and the M3 method for the period 2010-2016 [ASCAT vertically polarized morning data].	86

A.15 Mean melt duration difference between the Trusel et al. (2012) and the M4 method for the period 2010-2016 [ASCAT vertically polarized morning data].	87
A.16 Mean melt duration difference between the M3 and the M4 method for the period 2010-2016 [ASCAT vertically polarized morning data].	88
A.17 Time series of ASCAT σ^0 (blue line) at latitude -73.54° and longitude -97.02° in West Antarctica (location in Fig. A.14d), together with the threshold of Trusel et al. (2012), M3 and M4 methods.	89
A.18 Time series of ASCAT σ^0 (blue line) at latitude -68.03° and longitude 81.10° in East Antarctica (location in Fig. A.14e), together with the threshold of Trusel et al. (2012), M3 and M4 methods.	90
A.19 Annual maps of melt duration for the period 2000-2016 from QuikSCAT (2000 - 2009) and ASCAT (2010-2016) multiplied by the fractions, as calculated using the M1 and M3 methods respectively.	91
A.20 Annual maps of melt duration for the period 2000-2016 from QuikSCAT (2000 - 2009) and ASCAT (2010-2016) multiplied by the fractions, as calculated using the M2 and M4 methods respectively.	92
A.21 Annual maps of melt duration uncertainty for the period 2010-2016 from ASCAT (2010-2016) multiplied by the fractions, as calculated using the Trusel et al. (2012) method.	93
A.22 Annual maps of melt duration uncertainty for the period 2010-2016 from ASCAT (2010-2016) multiplied by the fractions, as calculated using M3 method.	94
A.23 Annual maps of melt duration uncertainty for the period 2010-2016 from ASCAT (2010-2016) multiplied by the fractions, as calculated using M4 method.	95
A.24 The amount of pixels that belong to each QuikSCAT class and are classified for AMSR-E as melting (1) and non-melting (0) pixels [x axis]. The box in each year is a zoom in the plot excluding the pixels classified for both QuikSCAT and AMSR-E as non-melting. Classification was performed based on the M1 method results.	96
A.25 Maps showing the regions in which melt occurred for at least 1 day for both AMSR-E and QuikSCAT (M1) with blue, only for QuikSCAT (M1) in red, only for AMSR-E in cyan and the regions where none of the methods detects melt in green for the year 2005.	97
A.26 Annual maps showing the regions in which melt occurred for at least 1 day for both AMSR-E and QuikSCAT (Trusel et al., 2012) with blue, only for QuikSCAT (Trusel et al., 2012) in red, only for AMSR-E in cyan and the regions where none of the methods detects melt in green.	98
A.27 Annual maps showing the regions in which melt occurred for at least 1 day for both AMSR-E and QuikSCAT (M1) with blue, only for QuikSCAT (M1) in red, only for AMSR-E in cyan and the regions where none of the methods detects melt in green.	99
A.28 Annual maps of melt duration difference between AMSR-E melting days and the QuikSCAT (M1) coarse resolution melting days.	100
A.29 Maps of Antarctica showing the regions which experience always morning and afternoon melt (blue), only afternoon melt (red) and sometimes morning and afternoon melt (green) and the mean values of overlapping morning and afternoon melt for the period 2000-2009, where 1 is morning and afternoon melt for all the years and 0 is only afternoon melt for all the years. (a) and (b) represent the results using the Trusel et al. (2012) method, (c) and (d) with M1 and (e) and (f) with M2.	101
A.30 Annual maps of melt duration anomalies for the period 2000-2009 using the M1 method.	102
A.31 Annual maps of melt duration anomalies for the period 2000-2009 using the M2 method.	103
A.32 Annual maps of melt duration anomalies for the period 2003-2016 from AMSR-E (2003-2011) and AMSR2 (2013-2016).	104
A.33 Annual maps of melt duration anomalies for the period 2000-2009 using the (Trusel et al., 2012) method for morning QuikSCAT data.	105
A.34 Annual maps of melt duration anomalies for the period 2000-2009 using the M1 method for morning QuikSCAT data.	106
A.35 Annual maps of melt duration anomalies for the period 2000-2009 using the M2 method for morning QuikSCAT data.	107

A.36 Annual maps of melt intensity anomalies for the period 2000-2009 using the M1 method for QuikSCAT midday data.	108
A.37 Annual maps of melt intensity anomalies for the period 2000-2009 using the M2 method for QuikSCAT midday data.	109

List of Tables

3.1	Characteristics of the sensors used in the study	20
3.2	List of dataset from the National Climatic Data Center (NCDC) Global Surface Summary of the Day (GSOD)	21
3.3	Simulation parameters	23
3.4	Overview of threshold based melt detection methods	27
4.1	Comparison of the kappa coefficient of the different melt detection methods applied on the different datasets of vertically polarized morning and midday data from QuikSCAT and ASCAT with AWS maximum temperature data	35
4.2	Correlation coefficient between three methods used for QuikSCAT data and AMSR-E data for melt extent	42
4.3	Correlation coefficient between three methods used for QuikSCAT data and AMSR-E data for melt index	43

A

Appendix

A.1 Additional Figures

A.1.1 Backscatter Time Series

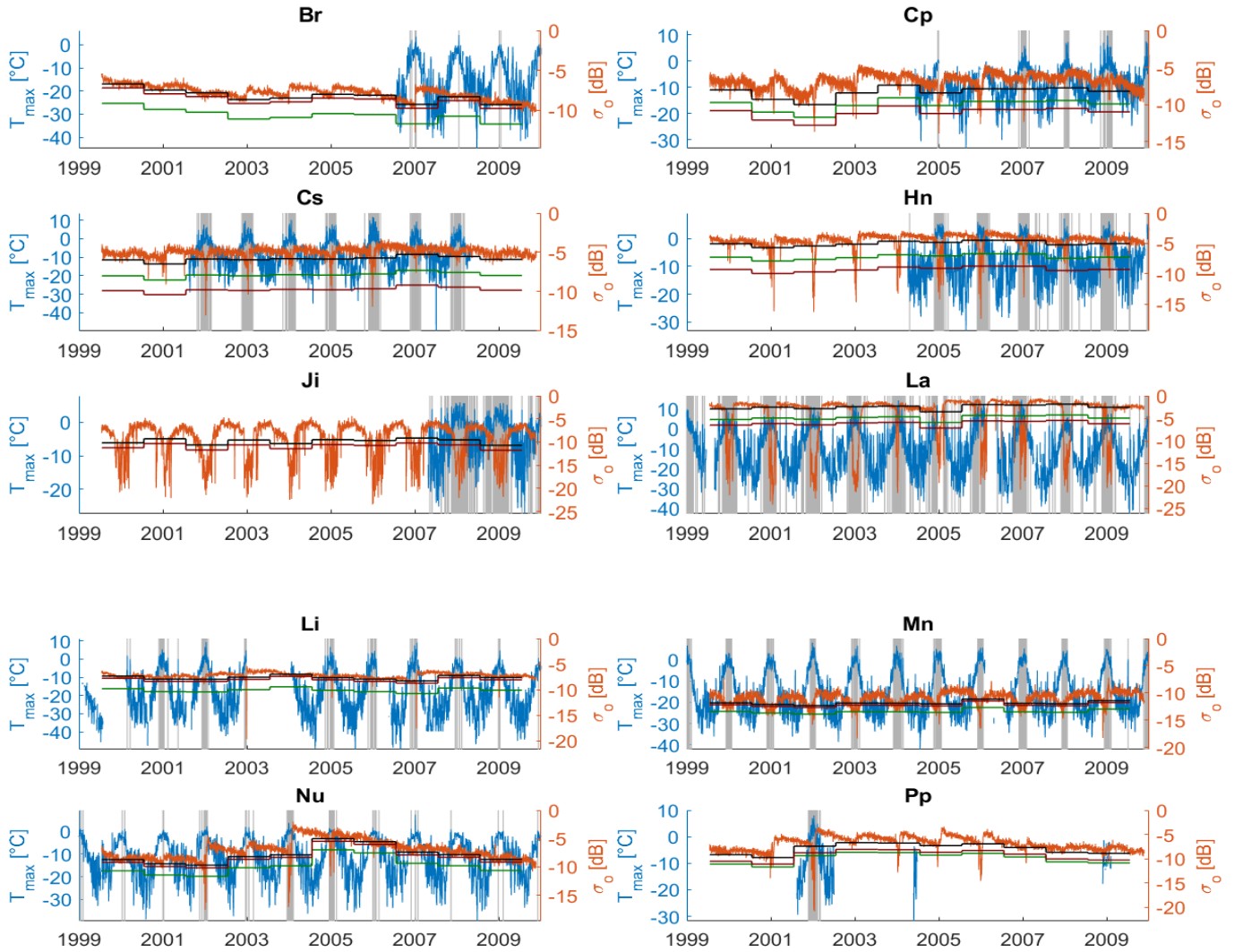


Figure A.1: Time series of QuikSCAT σ_{hh}^0 from morning data (red line), maximum daily temperature (blue line) at the location of weather stations together with varying thresholds of Trusel et al. (2012) (green line) and Bothale et al. (2015) using maximum standard deviation from QuikSCAT data only (black line) and using the maximum standard deviation from QuikSCAT and OSCAT data (brown line). Vertical gray boxes indicate the days with temperature higher than 0°C .

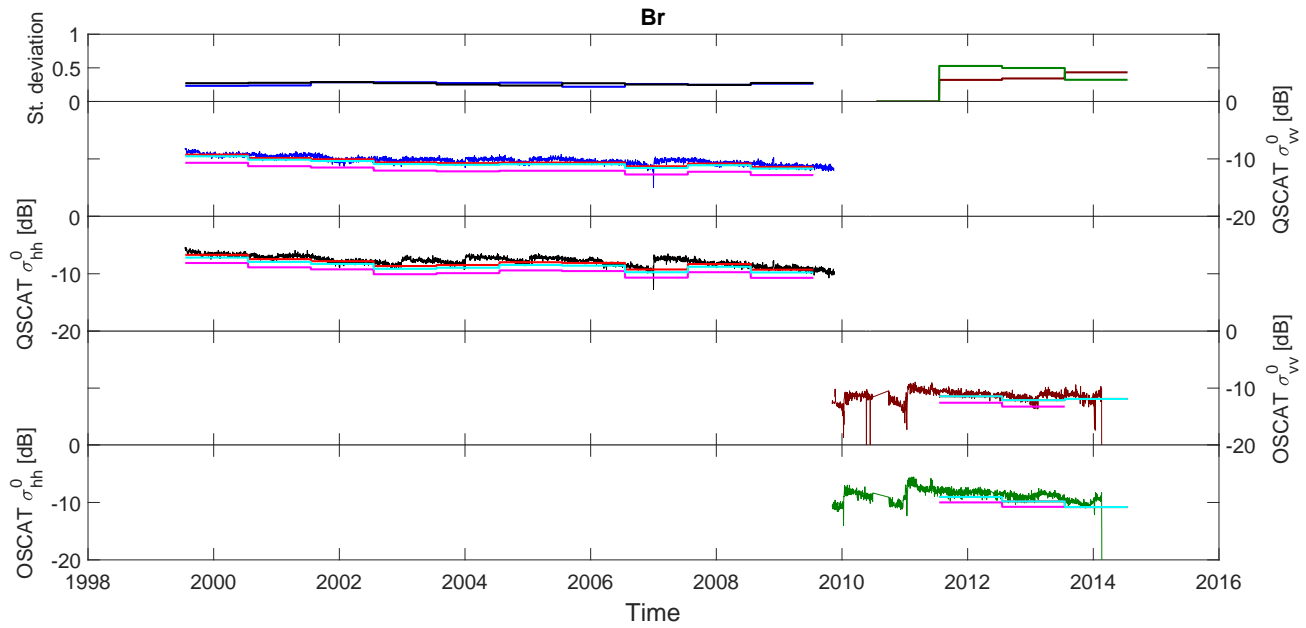


Figure A.2: Comparison between QuikSCAT and OSCAT data for horizontal and vertical polarization and the winter backscatter standard deviation for each year at Brunt (Br). Horizontal lines indicate the thresholds for Trusel et al. (2012) methodology (pink line), Bothale et al. (2015) using QuikSCAT data only (red line) and using QuikSCAT and OSCAT data (cyan line).

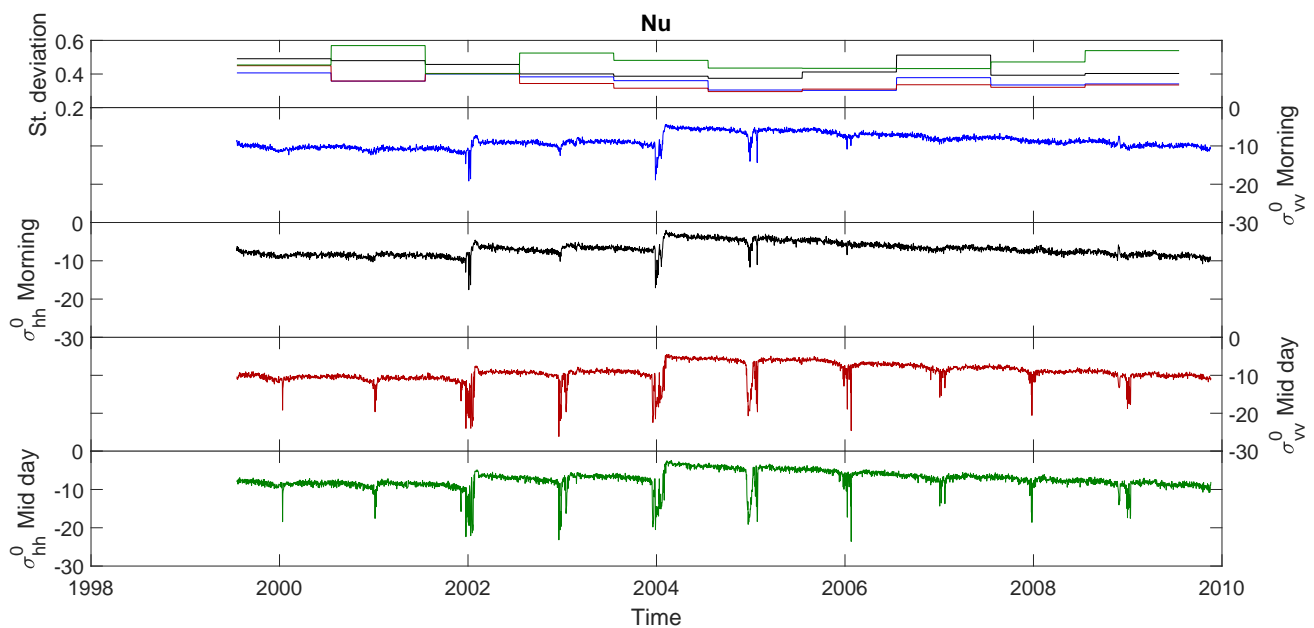


Figure A.3: Comparison between QuikSCAT horizontally and vertically polarized backscatter from morning and midday/afternoon data and the winter backscatter standard deviation for each year at Neumayer (Nu).

A.1.2 Melt Detection Validation

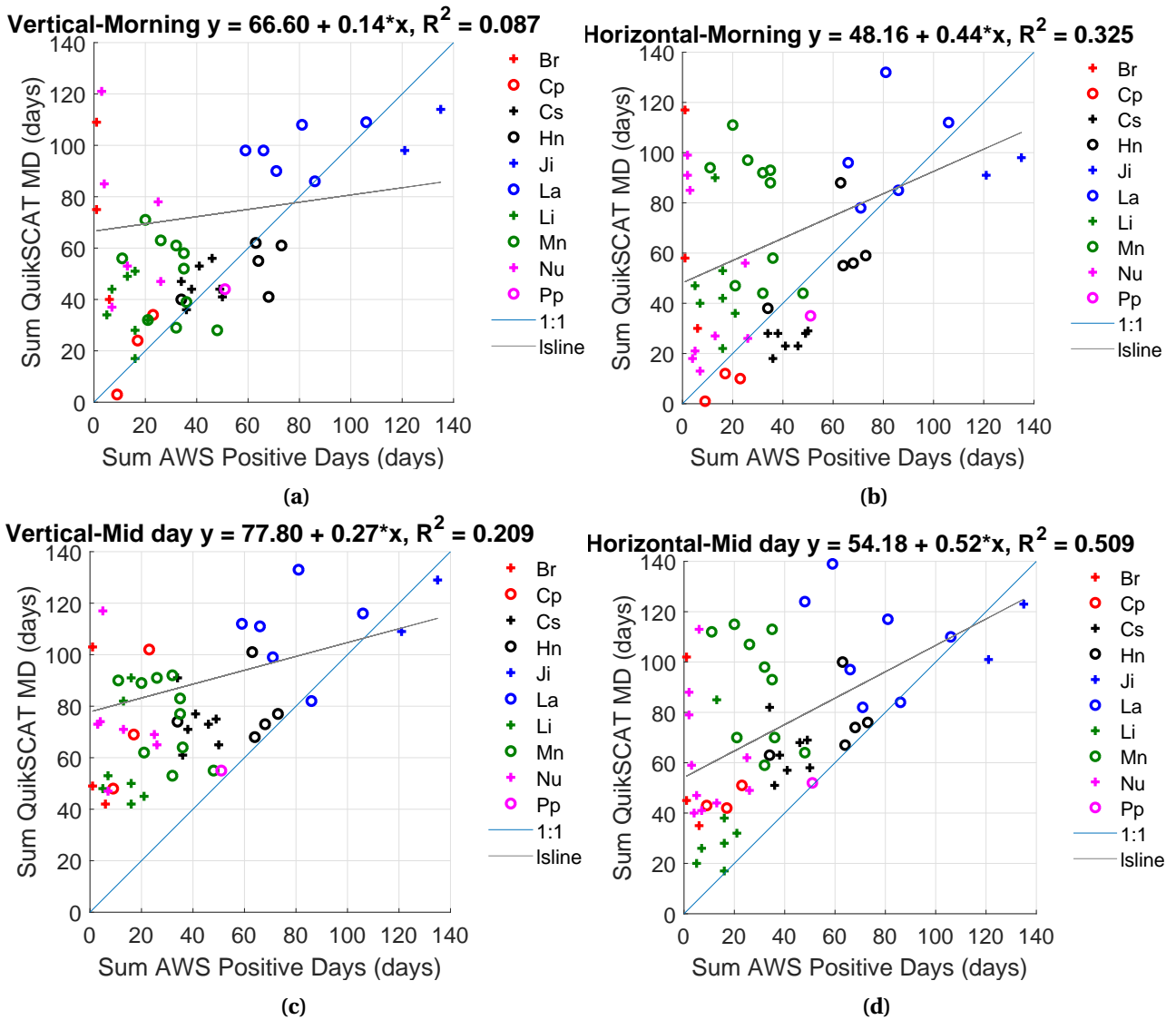


Figure A.4: Dependence of annual QuikSCAT melting days (MD) as computed using the Bothale et al. (2015) methodology only for QuikSCAT data on annual positive days (PD) for (a) vertically polarized morning data (b) horizontally polarized morning data (c) vertically polarized midday data and (d) horizontally polarized midday data.

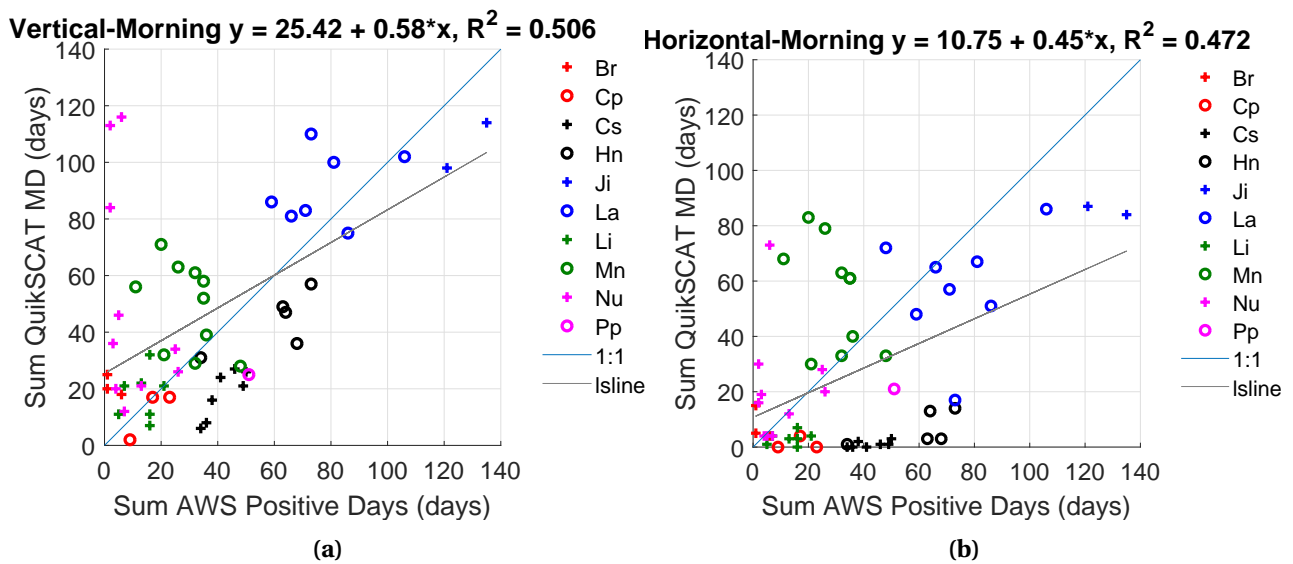


Figure A.5: Dependence of annual QuikSCAT melting days (MD) as computed using the Bothale et al. (2015) methodology using QuikSCAT and OSCAT data on annual positive days (PD) for (a) vertically polarized morning data (b) horizontally polarized morning data.

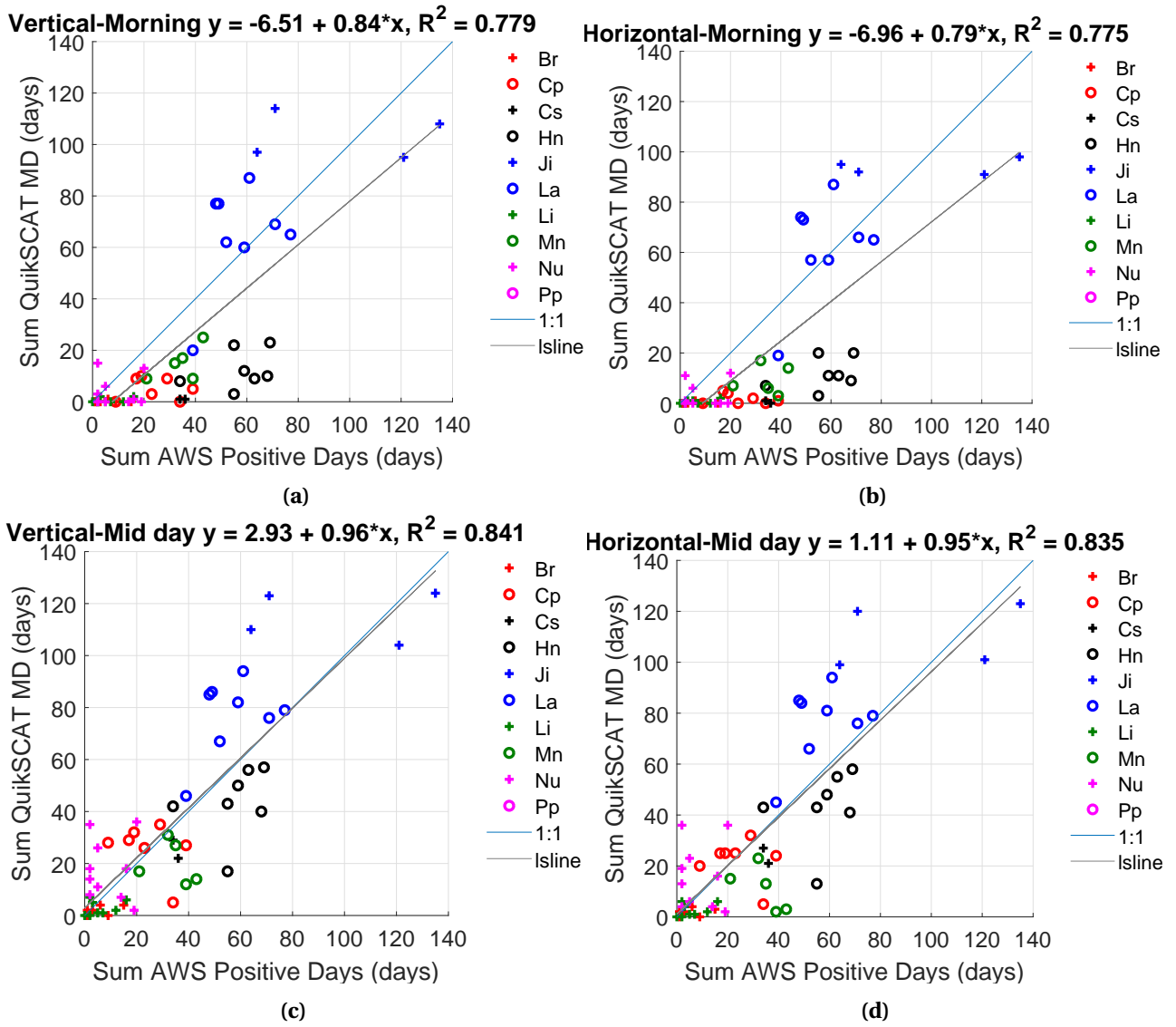


Figure A.6: Dependence of annual QuikSCAT melting days (MD) as computed using the M1 methodology (4.2.2) on annual positive days (PD) for (a) vertically polarized morning data (b) horizontally polarized morning data (c) vertically polarized midday data and (d) horizontally polarized midday data.

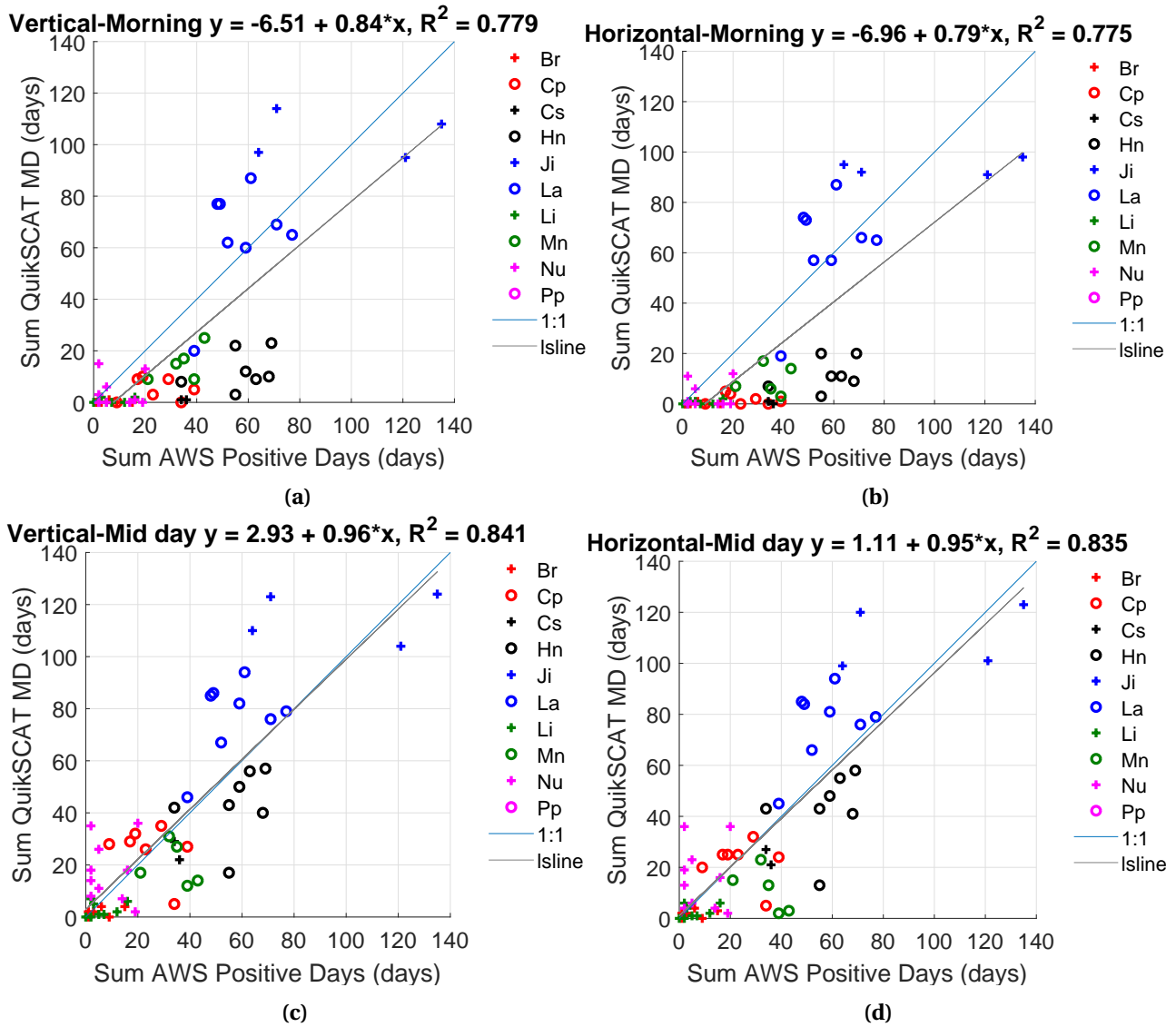


Figure A.7: Dependence of annual QuikSCAT melting days (MD) as computed using the M2 methodology (4.2.2) on annual positive days (PD) for (a) vertically polarized morning data (b) horizontally polarized morning data (c) vertically polarized midday data and (d) horizontally polarized midday data.

A.1.3 Melt duration maps

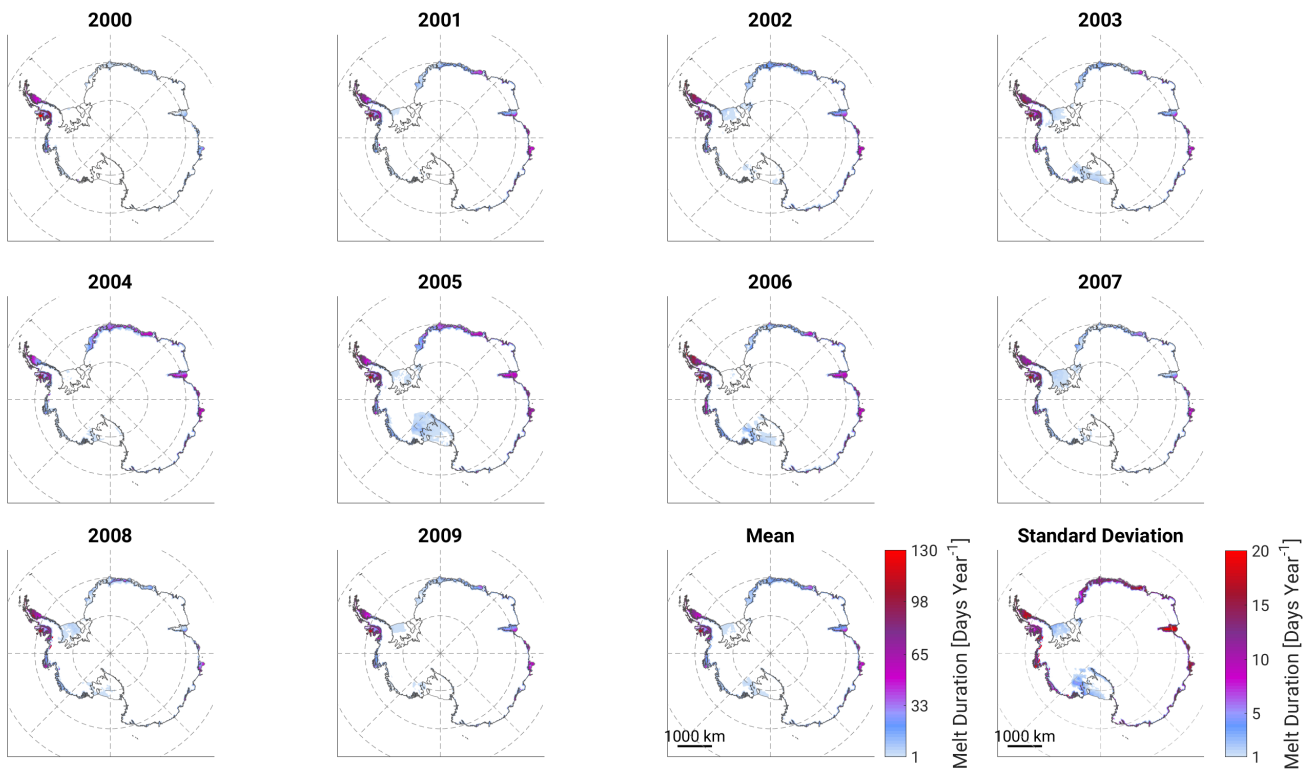


Figure A.8: Annual maps of melt duration and mean melt duration for the period 2000-2009 as calculated using the M1 method for the QuikSCAT vertically polarized midday data.

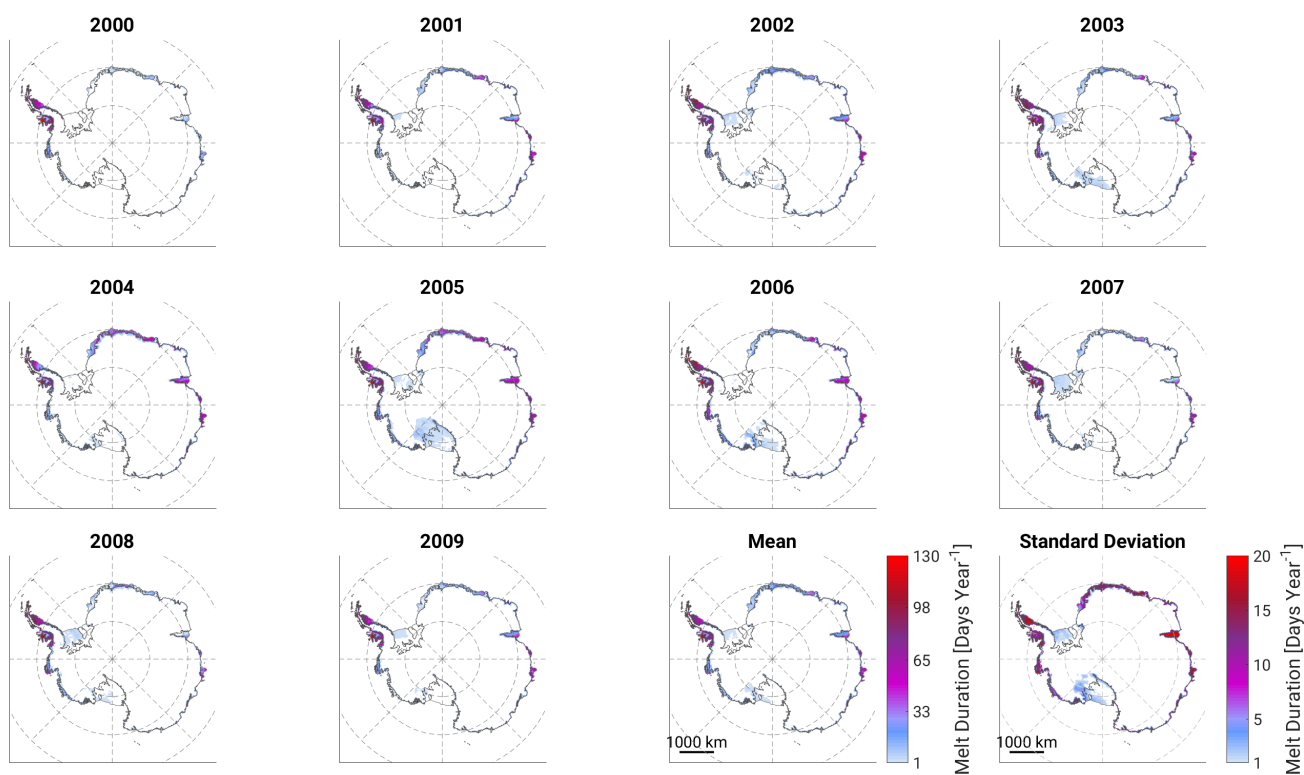


Figure A.9: Annual maps of melt duration and mean melt duration for the period 2000-2009 as calculated using the M2 method for the QuikSCAT vertically polarized midday data.

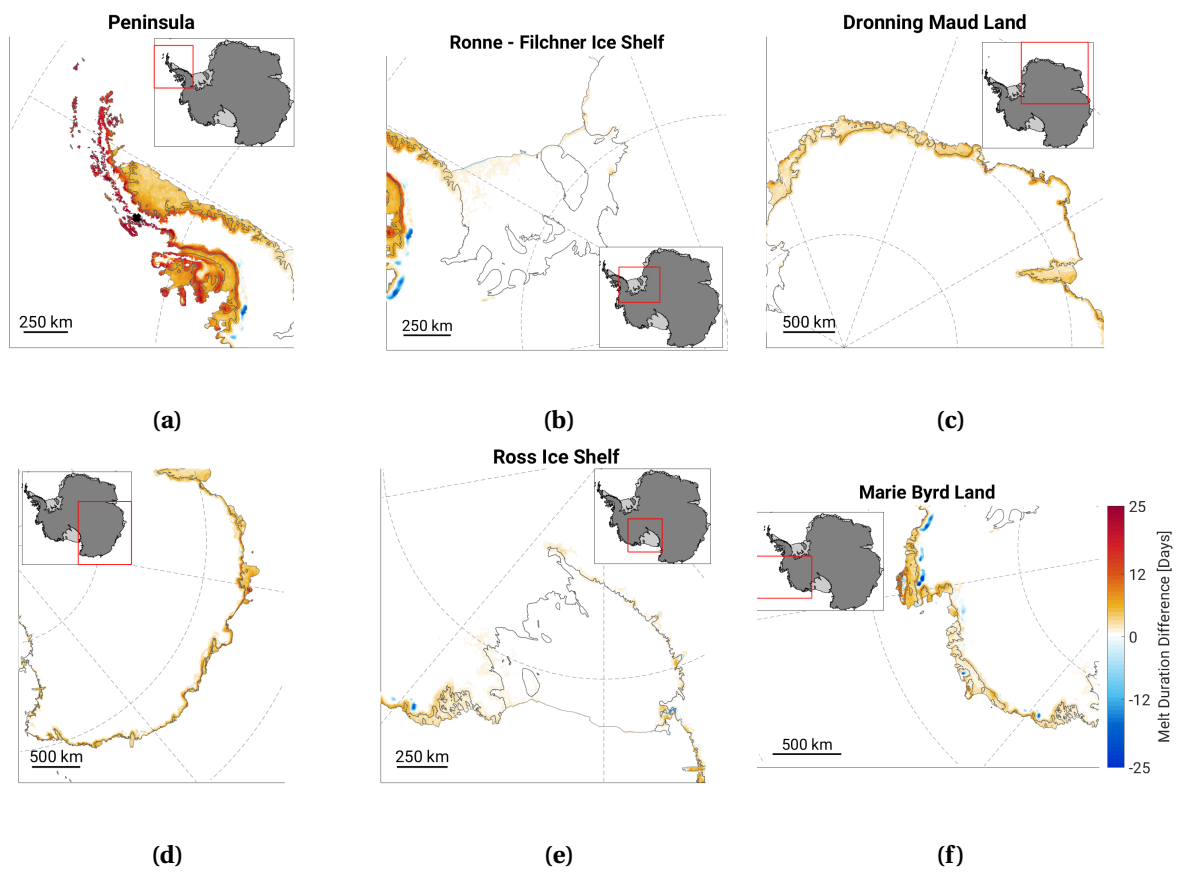


Figure A.10: Mean melt duration difference between the Trusel et al. (2012) and M1 method for the period 2000-2009 [QuikSCAT vertically polarized midday data].

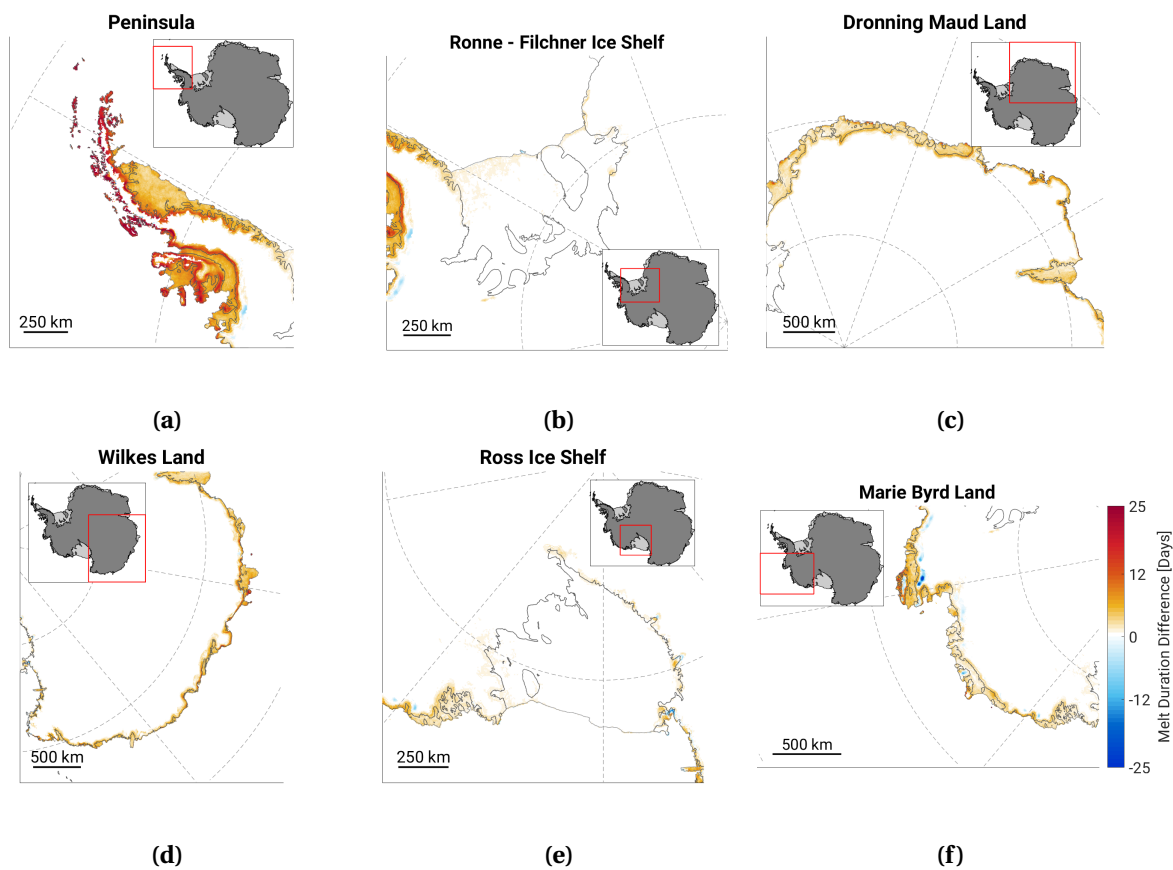


Figure A.11: Mean melt duration difference between the Trusel et al. (2012) and M2 method for the period 2000-2009 [QuikSCAT vertically polarized midday data].

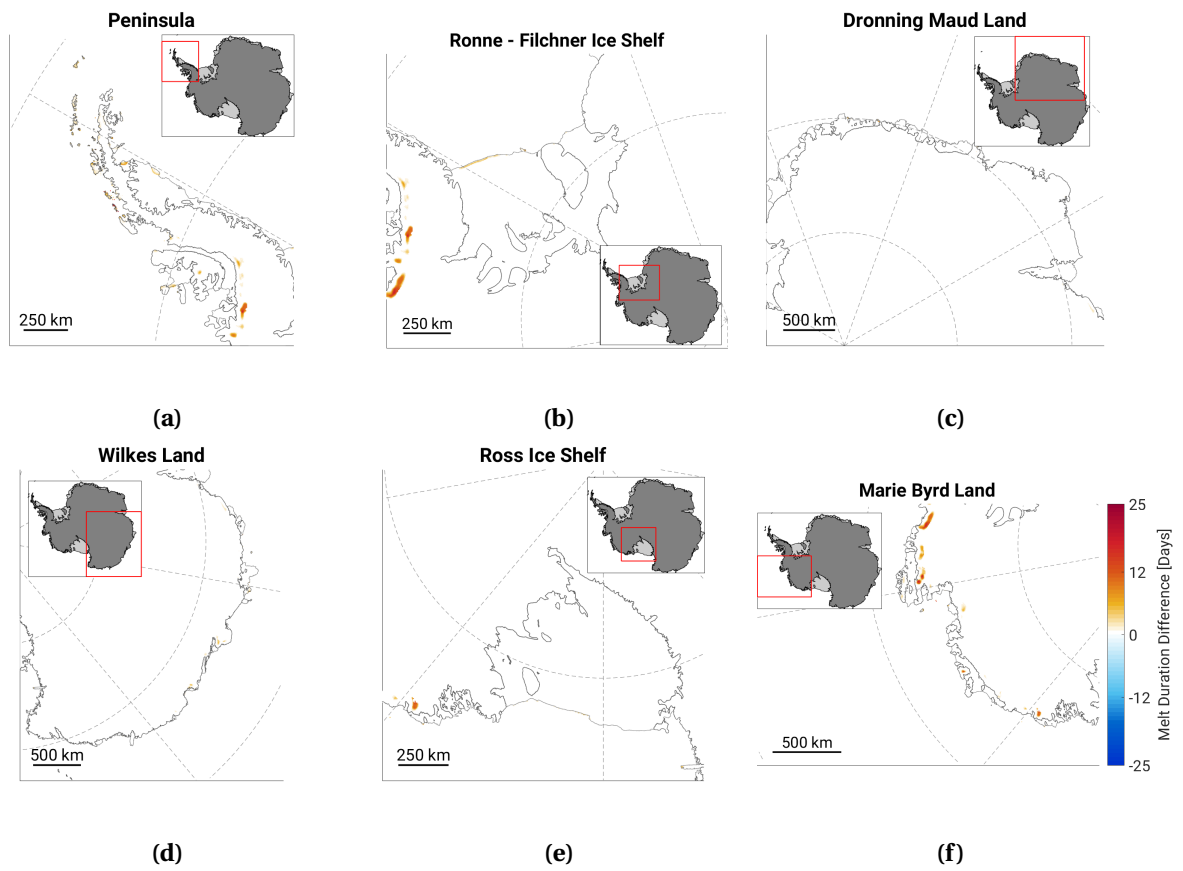


Figure A.12: Mean melt duration difference between the M1 and M2 method for the period 2000-2009 [QuikSCAT vertically polarized midday data].

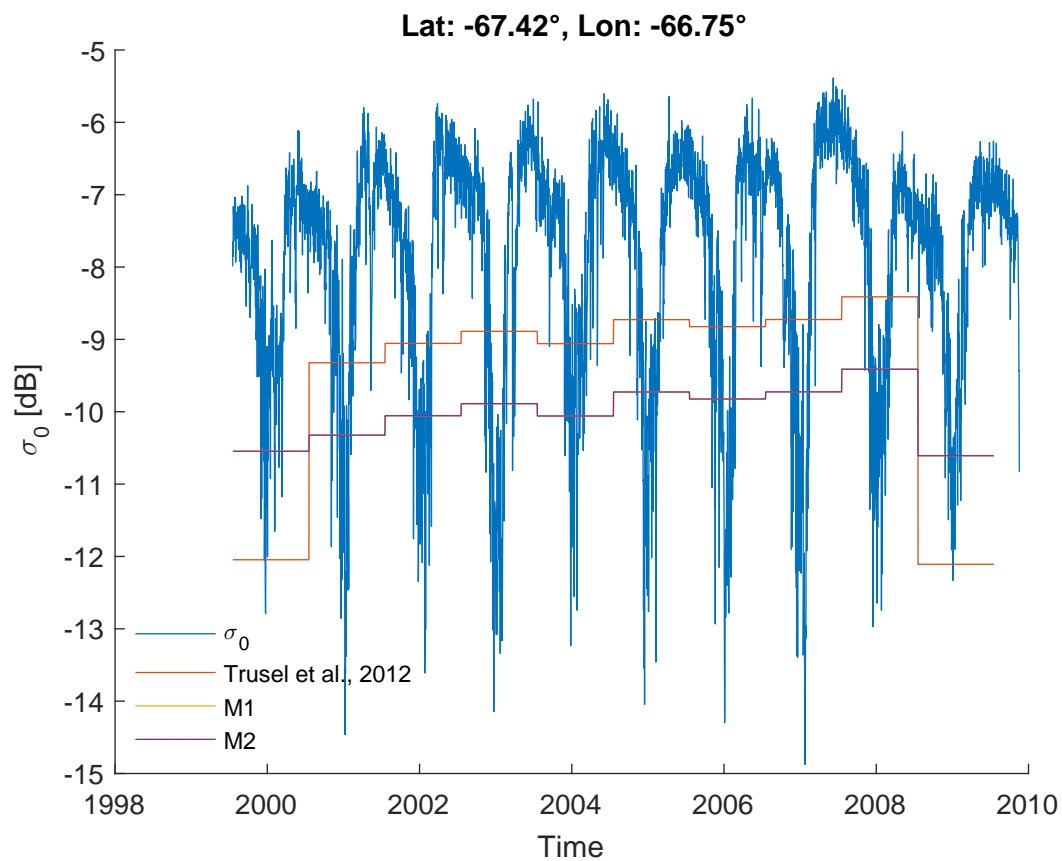


Figure A.13: Time series of QuikSCAT σ^0 (blue line) at latitude -67.42° and longitude -66.75° in Peninsula (location shown at Fig. A.10a), together with the threshold of Trusel et al. (2012), M1 and M2 methods.

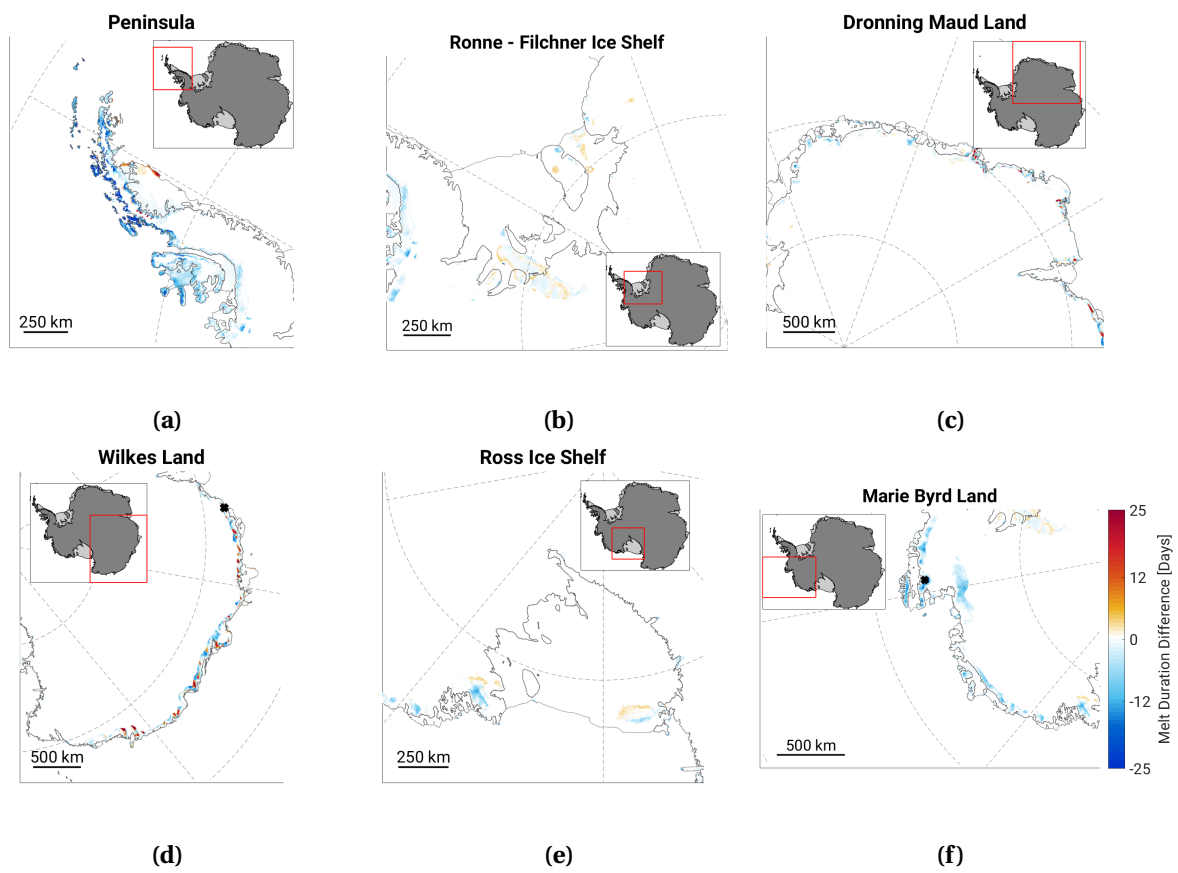


Figure A.14: Mean melt duration difference between the Trusel et al. (2012) and the M3 method for the period 2010-2016 [ASCAT vertically polarized morning data].

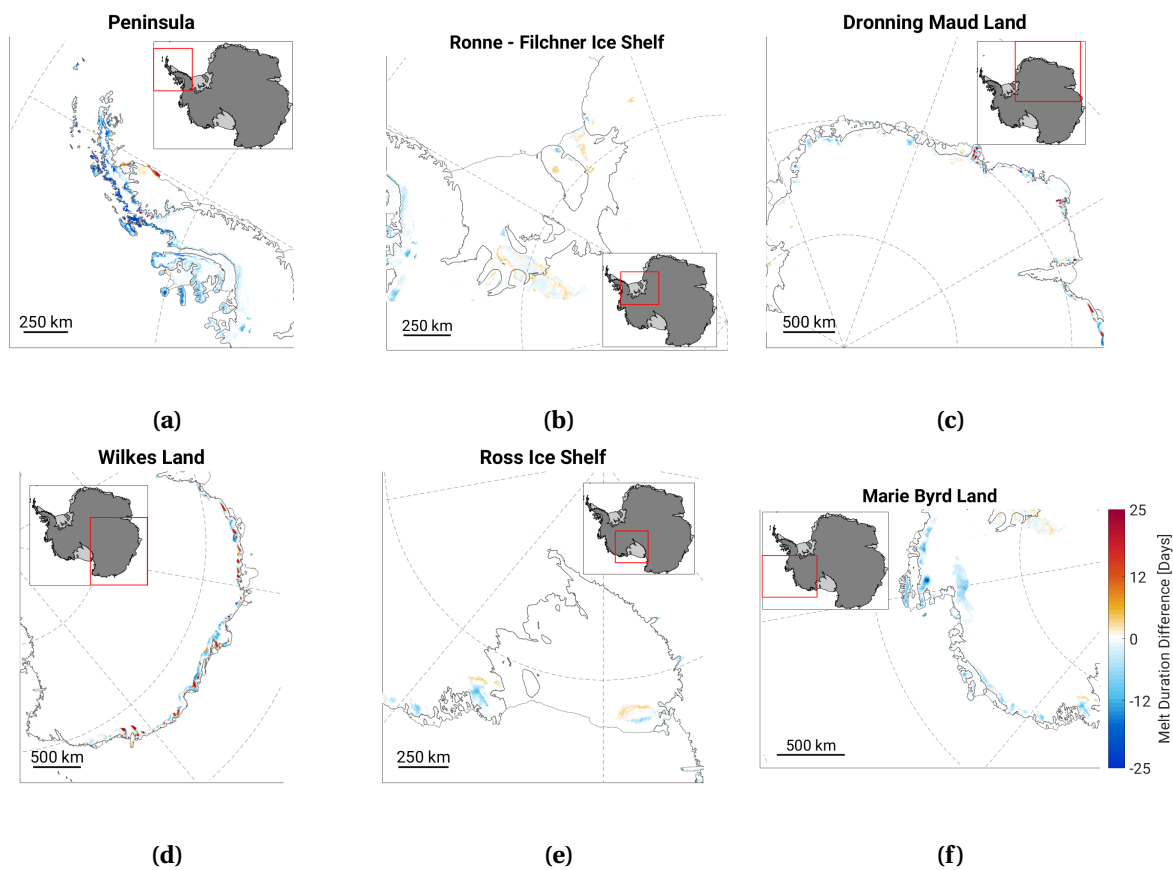


Figure A.15: Mean melt duration difference between the Trusel et al. (2012) and the M4 method for the period 2010-2016 [ASCAT vertically polarized morning data].

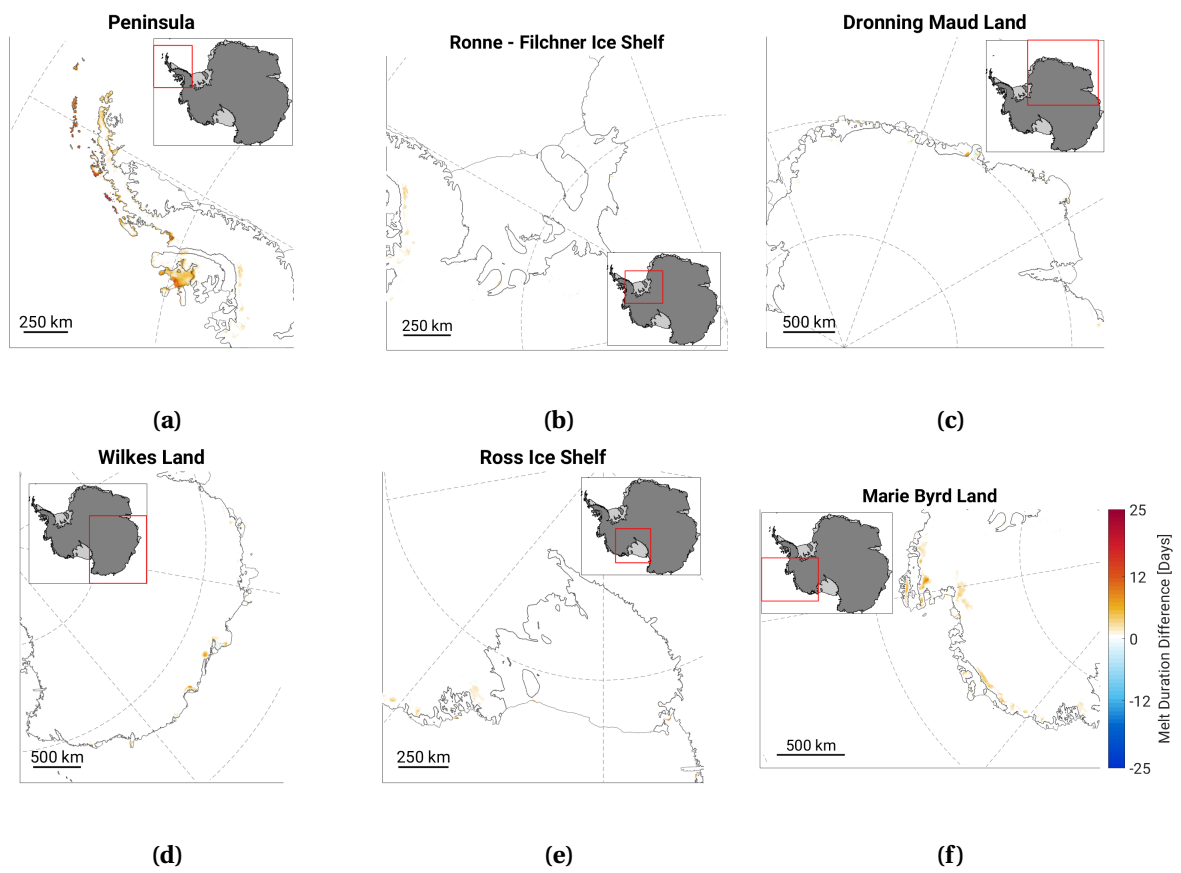


Figure A.16: Mean melt duration difference between the M3 and the M4 method for the period 2010-2016 [ASCAT vertically polarized morning data].

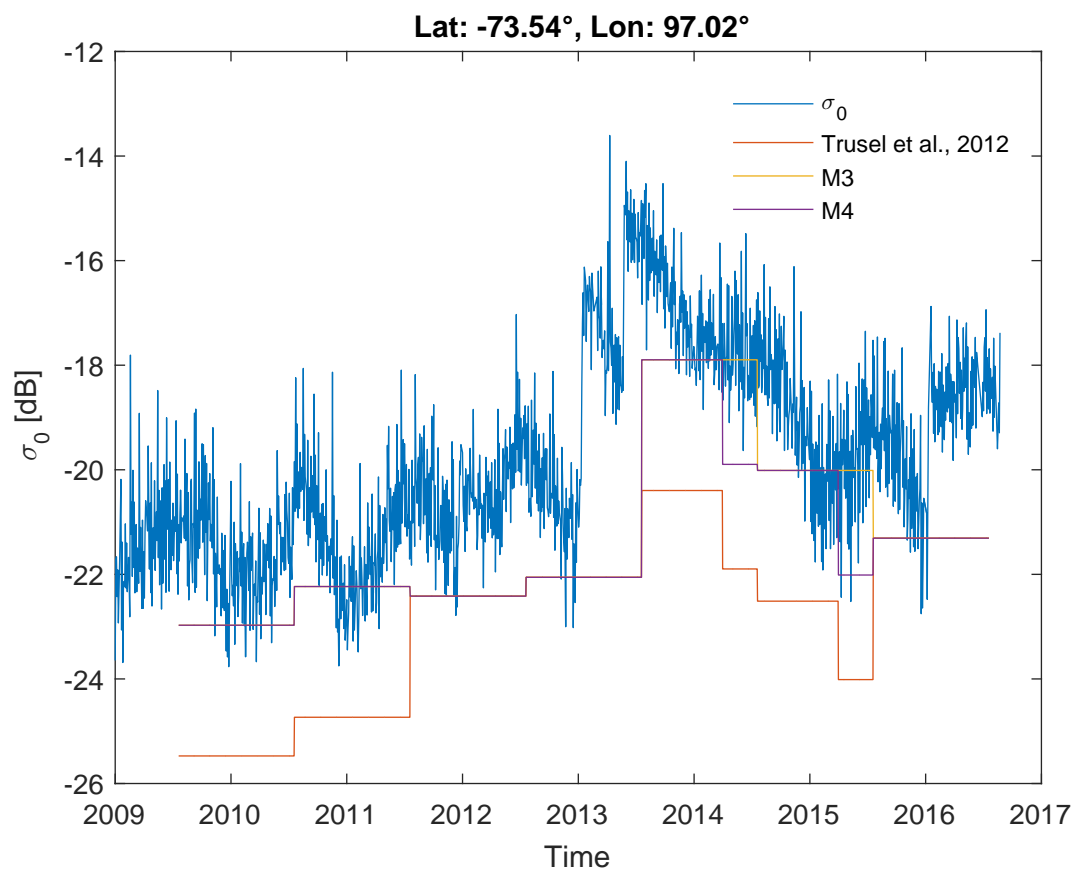


Figure A.17: Time series of ASCAT σ_0 (blue line) at latitude -73.54° and longitude -97.02° in West Antarctica (location in Fig. A.14d), together with the threshold of Trusel et al. (2012), M3 and M4 methods.

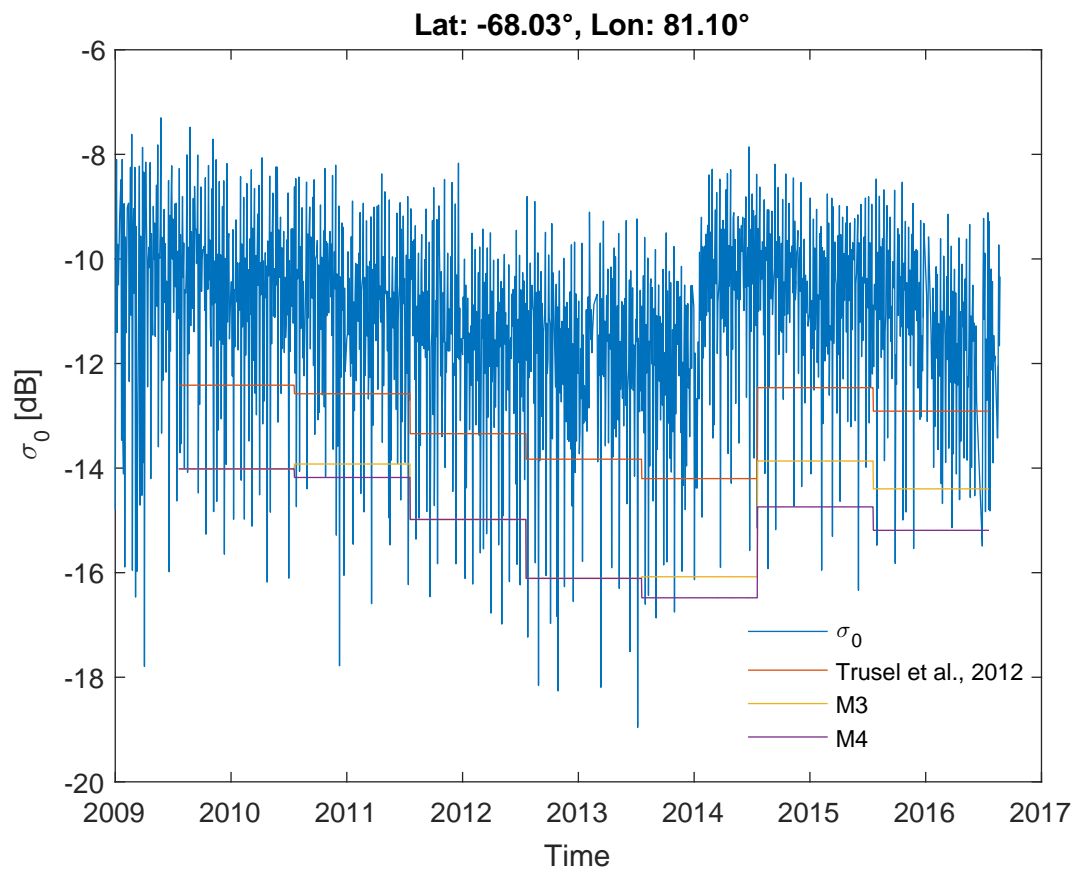


Figure A.18: Time series of ASCAT σ_0 (blue line) at latitude -68.03° and longitude 81.10° in East Antarctica (location in Fig. A.14e), together with the threshold of Trusel et al. (2012), M3 and M4 methods.

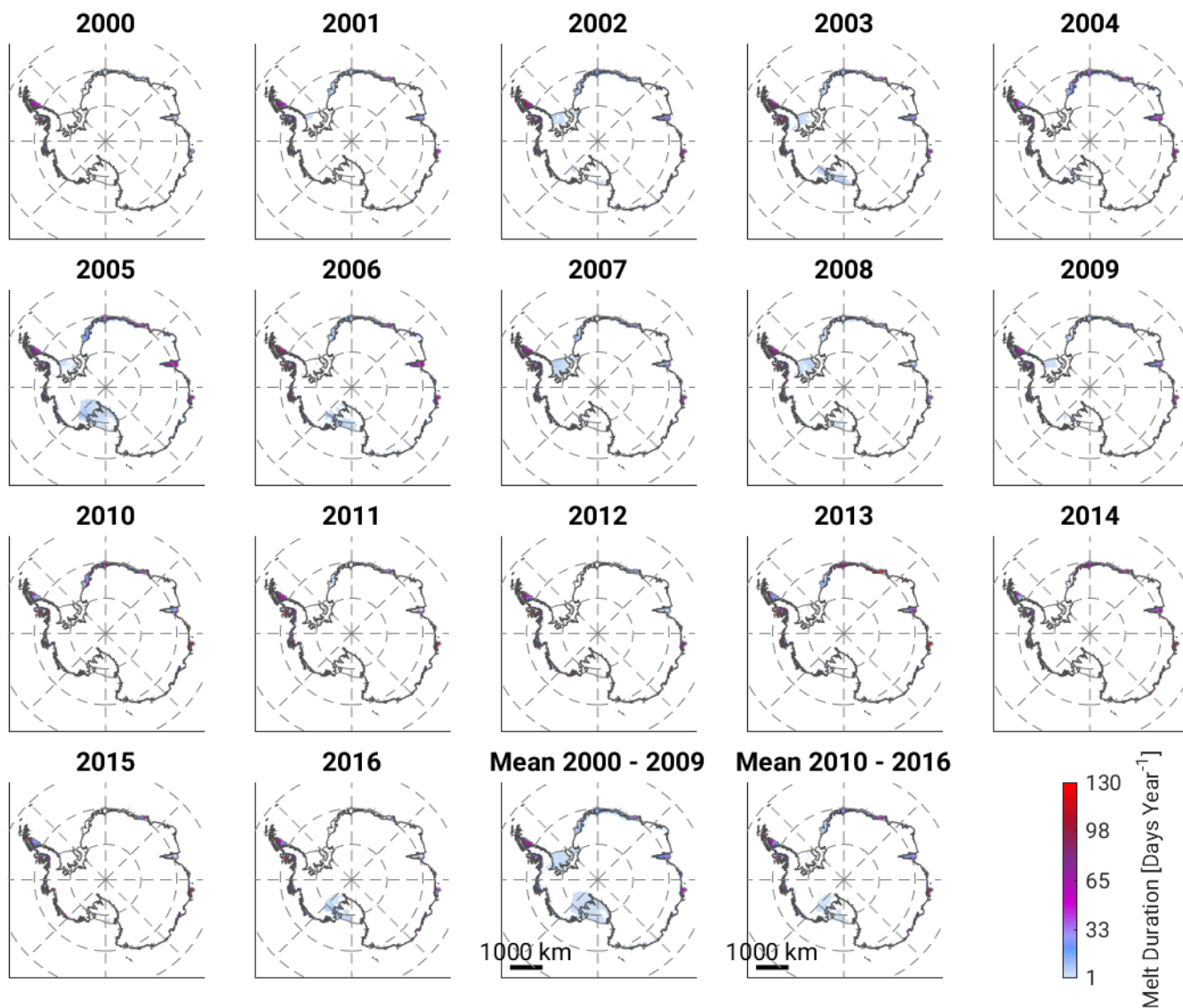


Figure A.19: Annual maps of melt duration for the period 2000-2016 from QuikSCAT (2000 - 2009) and ASCAT (2010-2016) multiplied by the fractions, as calculated using the M1 and M3 methods respectively.

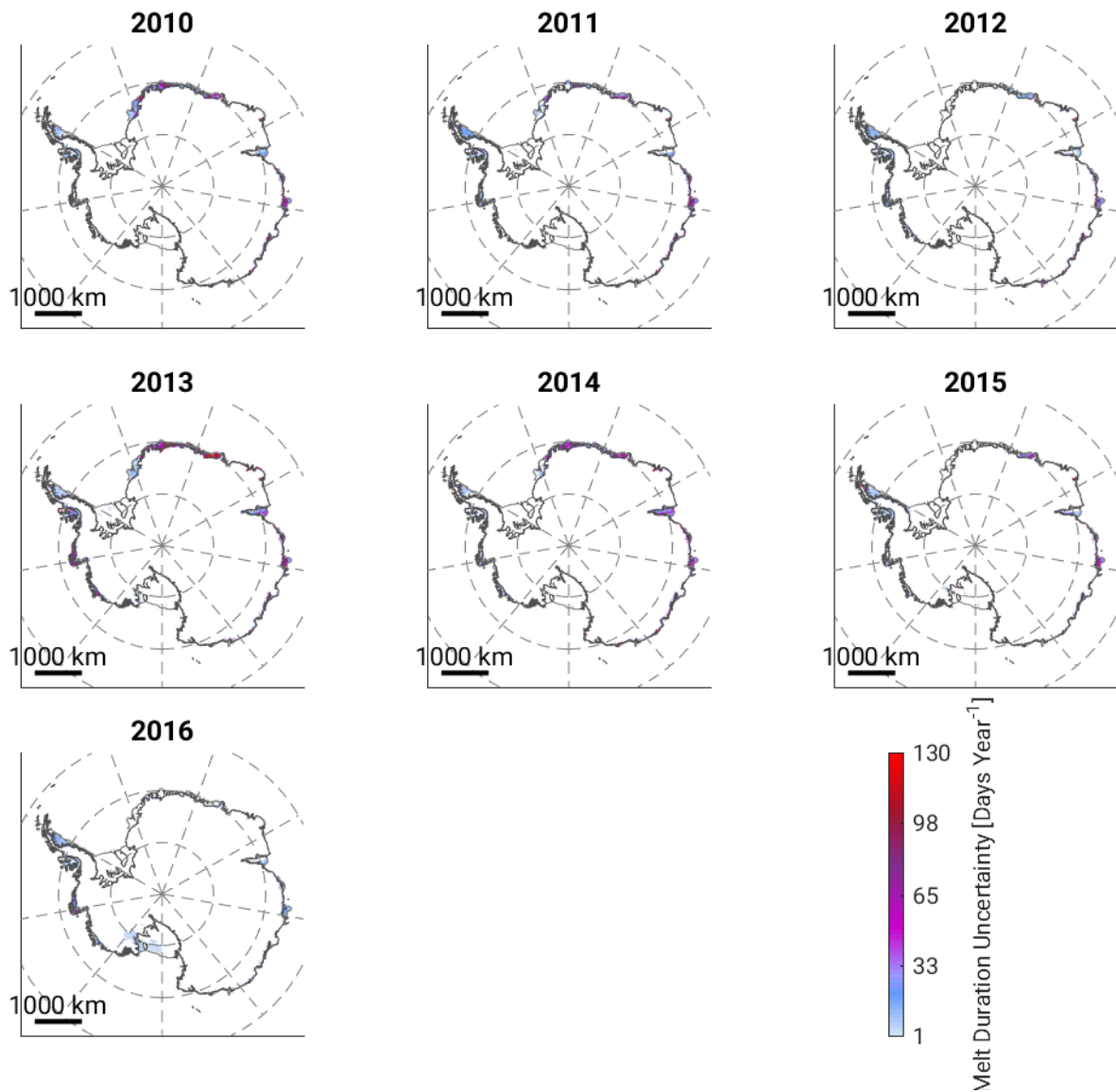


Figure A.21: Annual maps of melt duration uncertainty for the period 2010-2016 from ASCAT (2010-2016) multiplied by the fractions, as calculated using the Trusel et al. (2012) method.

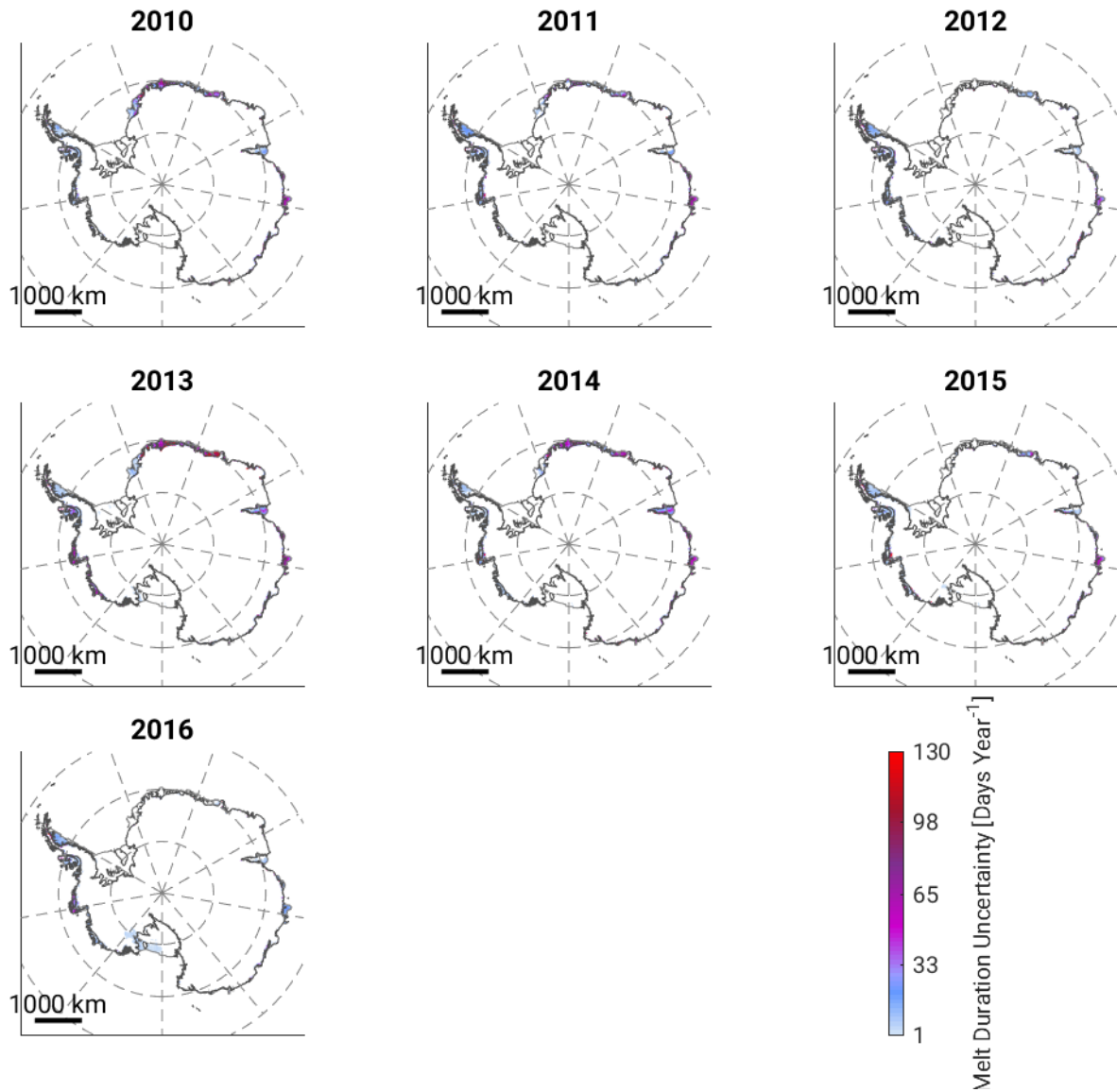


Figure A.22: Annual maps of melt duration uncertainty for the period 2010-2016 from ASCAT (2010-2016) multiplied by the fractions, as calculated using M3 method.

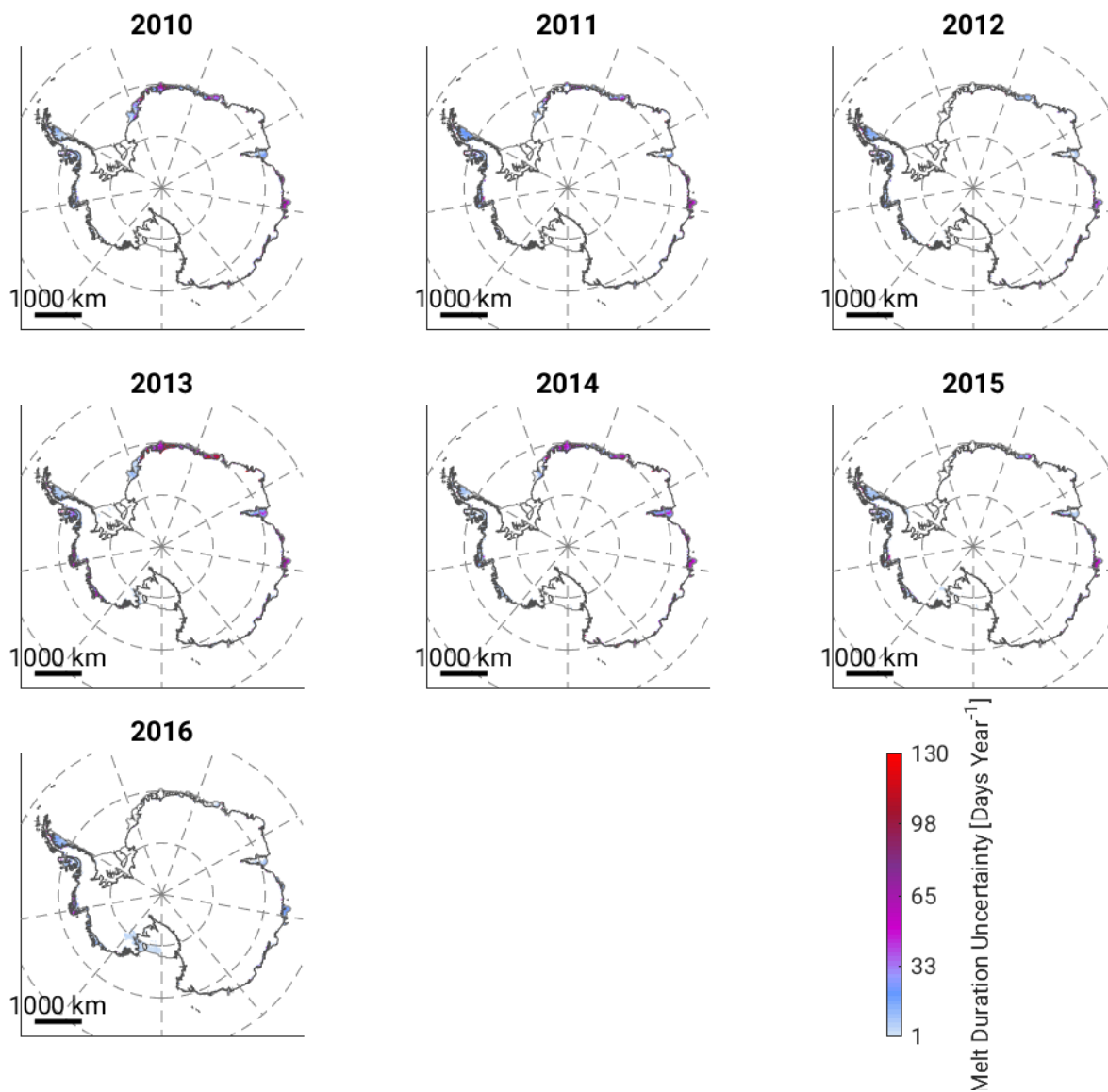


Figure A.23: Annual maps of melt duration uncertainty for the period 2010-2016 from ASCAT (2010-2016) multiplied by the fractions, as calculated using M4 method.

A.1.4 Comparison QuikSCAT - AMSR-E

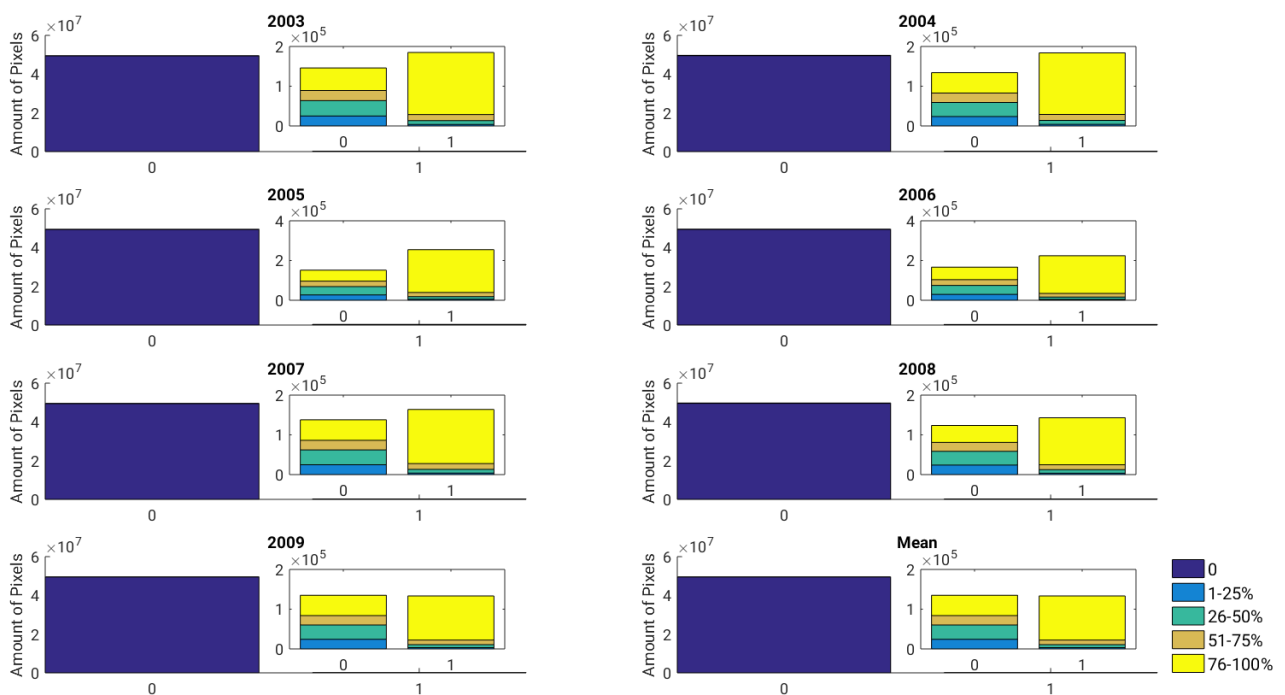


Figure A.24: The amount of pixels that belong to each QuikSCAT class and are classified for AMSR-E as melting (1) and non-melting (0) pixels [x axis]. The box in each year is a zoom in the plot excluding the pixels classified for both QuikSCAT and AMSR-E as non-melting. Classification was performed based on the M1 method results.

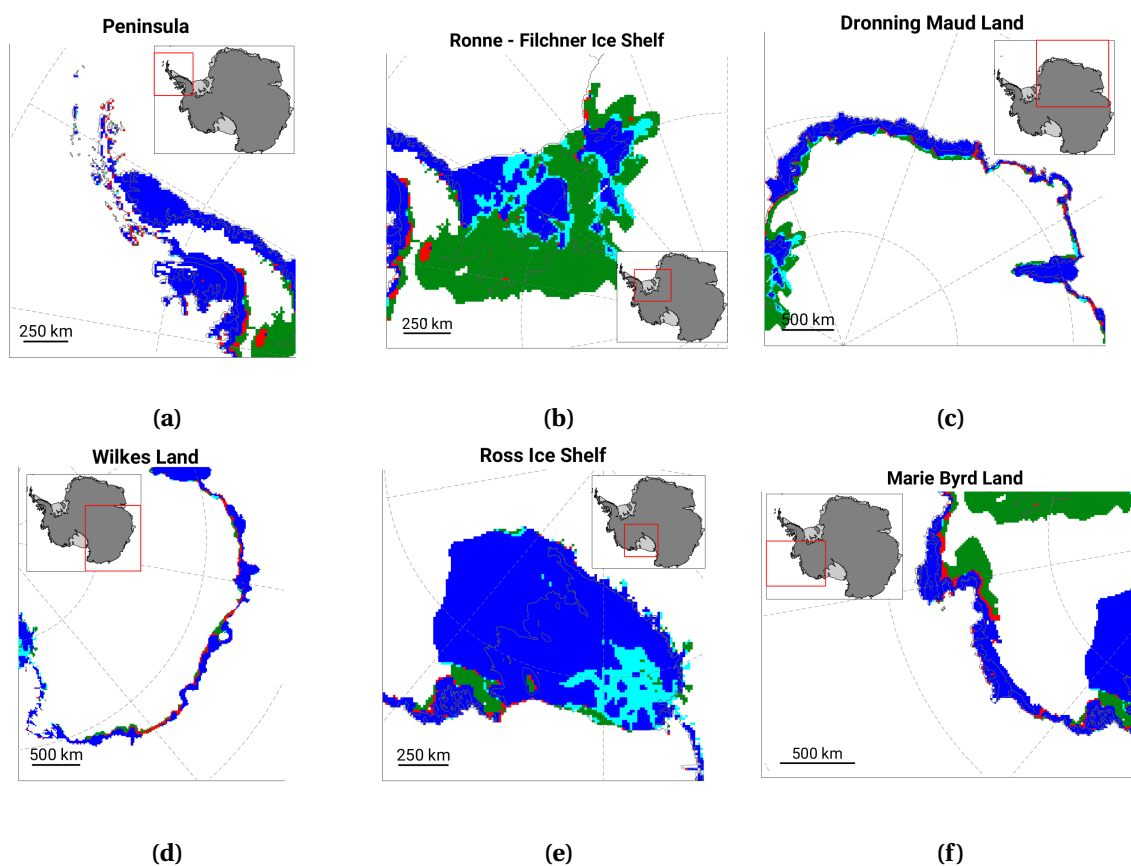


Figure A.25: Maps showing the regions in which melt occurred for at least 1 day for both AMSR-E and QuikSCAT (M1) with blue, only for QuikSCAT (M1) in red, only for AMSR-E in cyan and the regions where none of the methods detects melt in green for the year 2005.

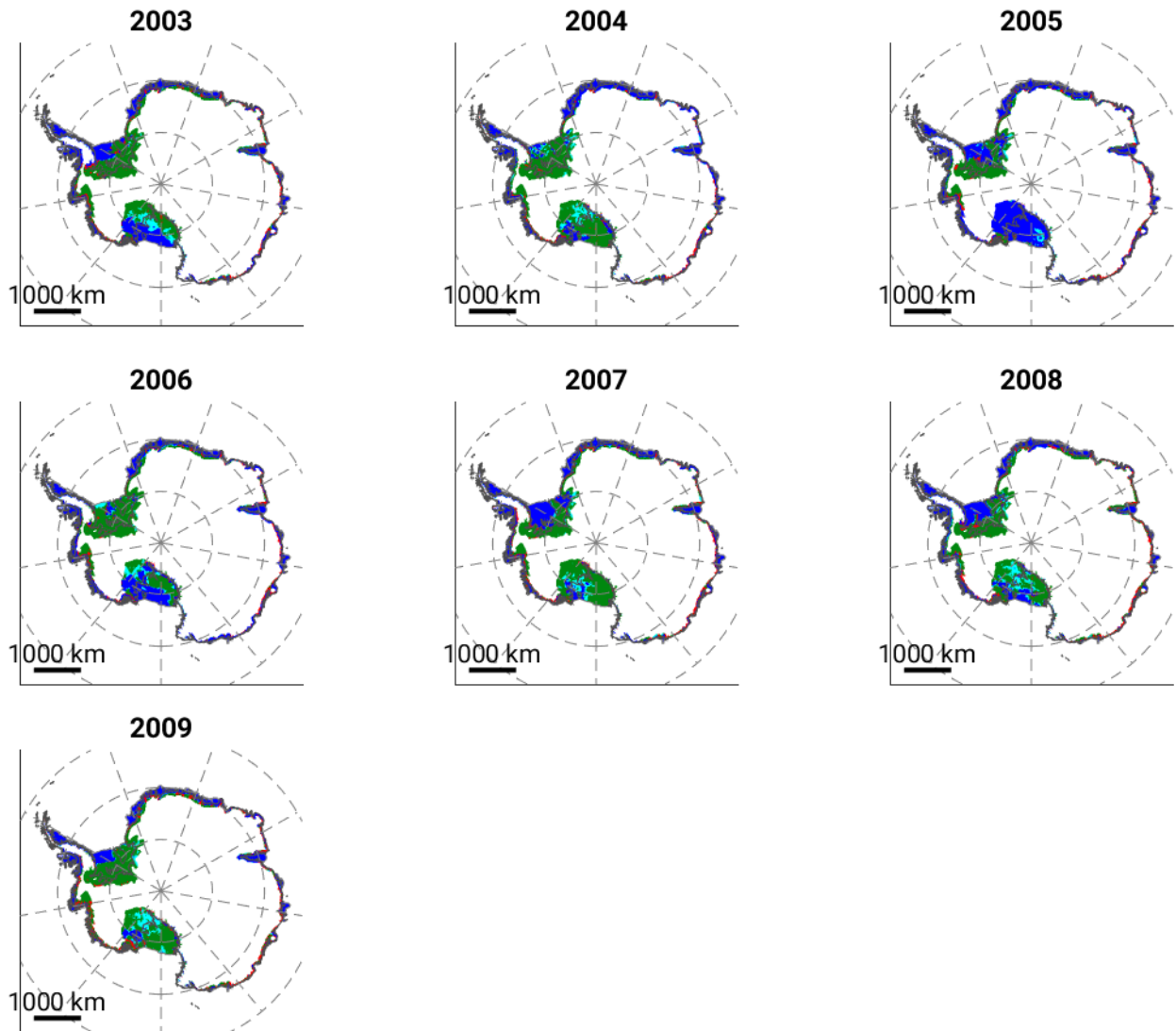


Figure A.26: Annual maps showing the regions in which melt occurred for at least 1 day for both AMSR-E and QuikSCAT (Trusel et al., 2012) with blue, only for QuikSCAT (Trusel et al., 2012) in red, only for AMSR-E in cyan and the regions where none of the methods detects melt in green.

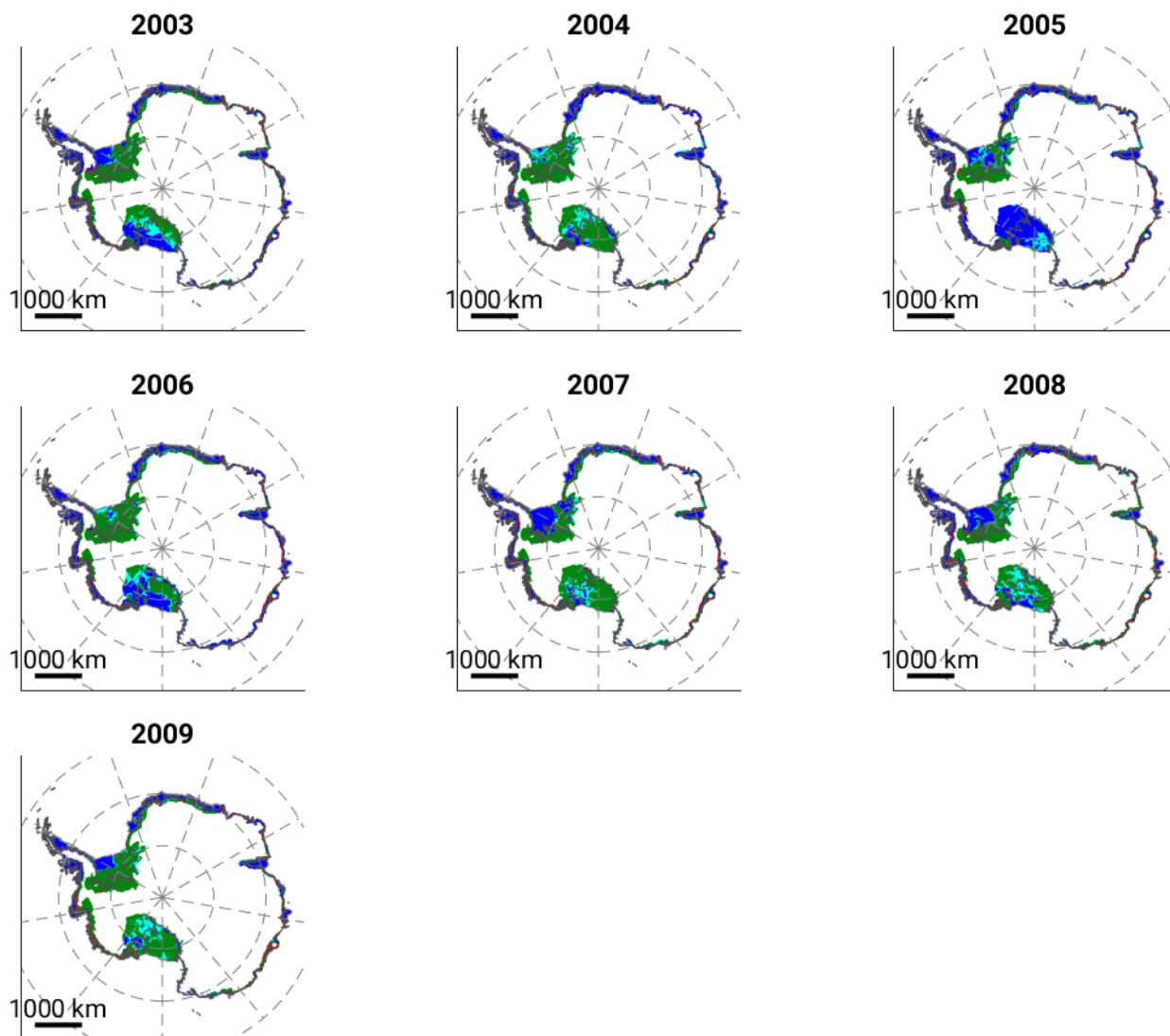


Figure A.27: Annual maps showing the regions in which melt occurred for at least 1 day for both AMSR-E and QuikSCAT (M1) with blue, only for QuikSCAT (M1) in red, only for AMSR-E in cyan and the regions where none of the methods detects melt in green.

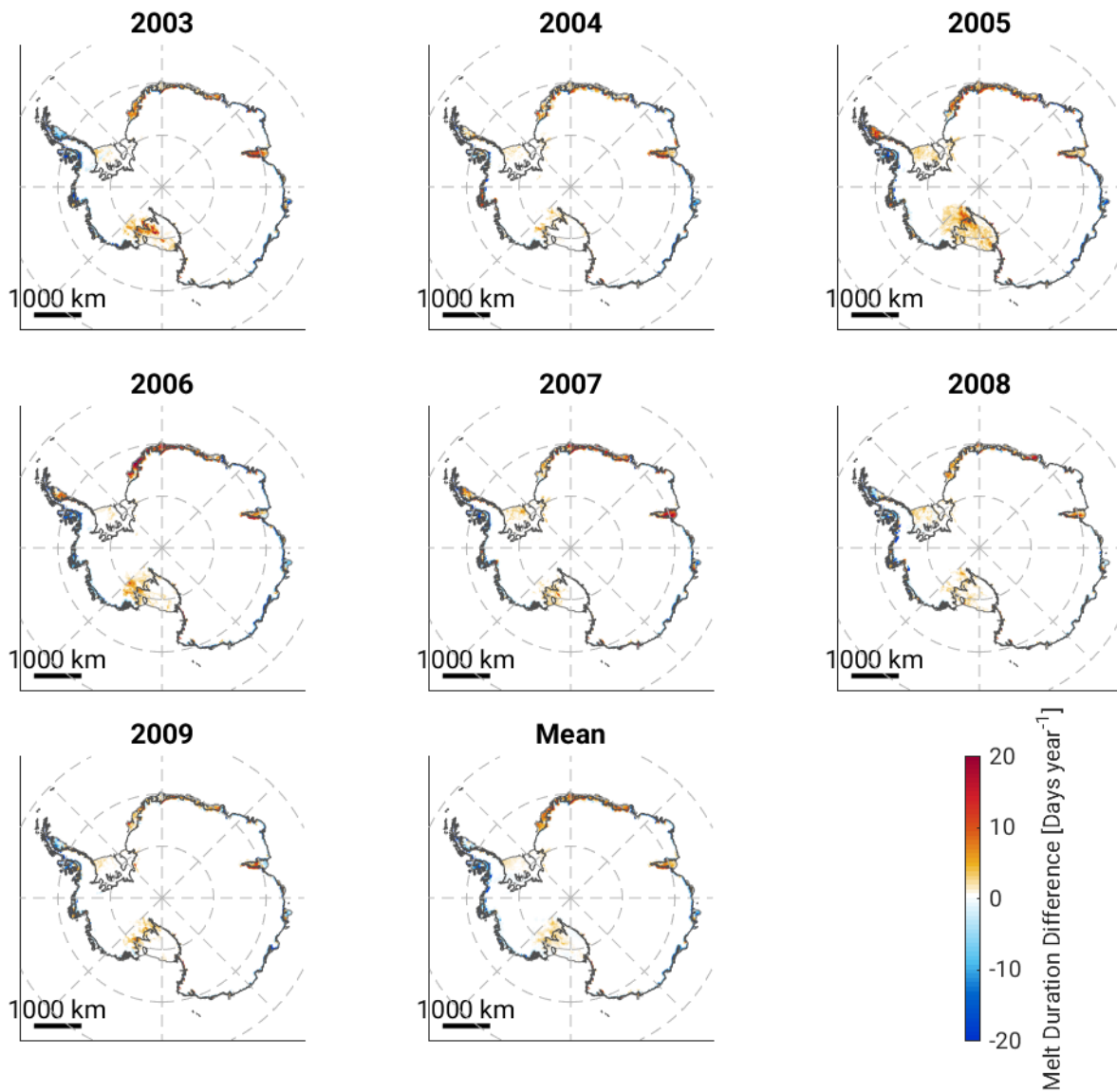


Figure A.28: Annual maps of melt duration difference between AMSR-E melting days and the QuikSCAT (M1) coarse resolution melting days.

A.1.5 Comparison Morning and Afternoon Melt

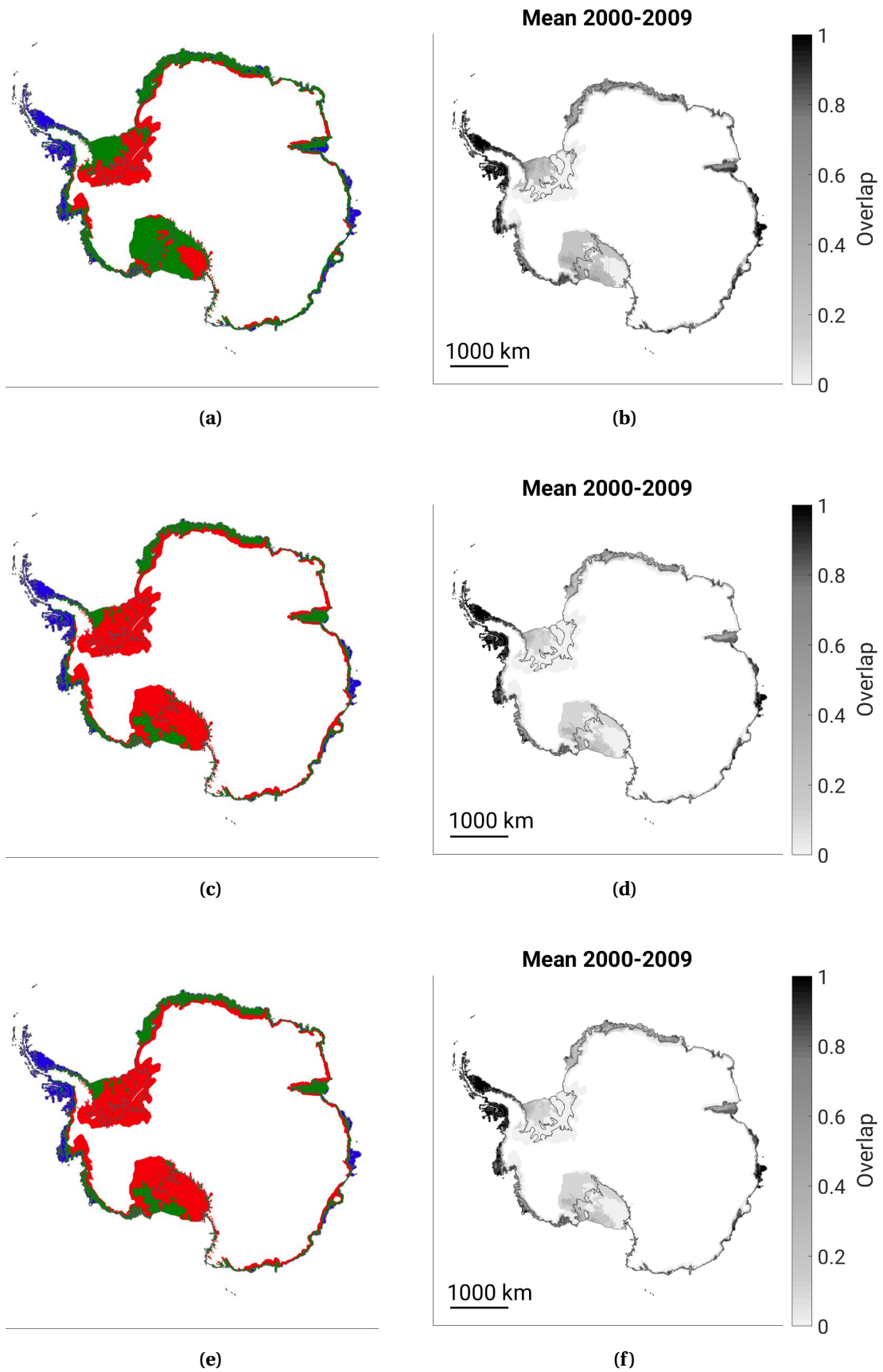


Figure A.29: Maps of Antarctica showing the regions which experience always morning and afternoon melt (blue), only afternoon melt (red) and sometimes morning and afternoon melt (green) and the mean values of overlapping morning and afternoon melt for the period 2000-2009, where 1 is morning and afternoon melt for all the years and 0 is only afternoon melt for all the years. (a) and (b) represent the results using the Trusel et al. (2012) method, (c) and (d) with M1 and (e) and (f) with M2.

A.1.6 Melt Duration Anomaly Maps

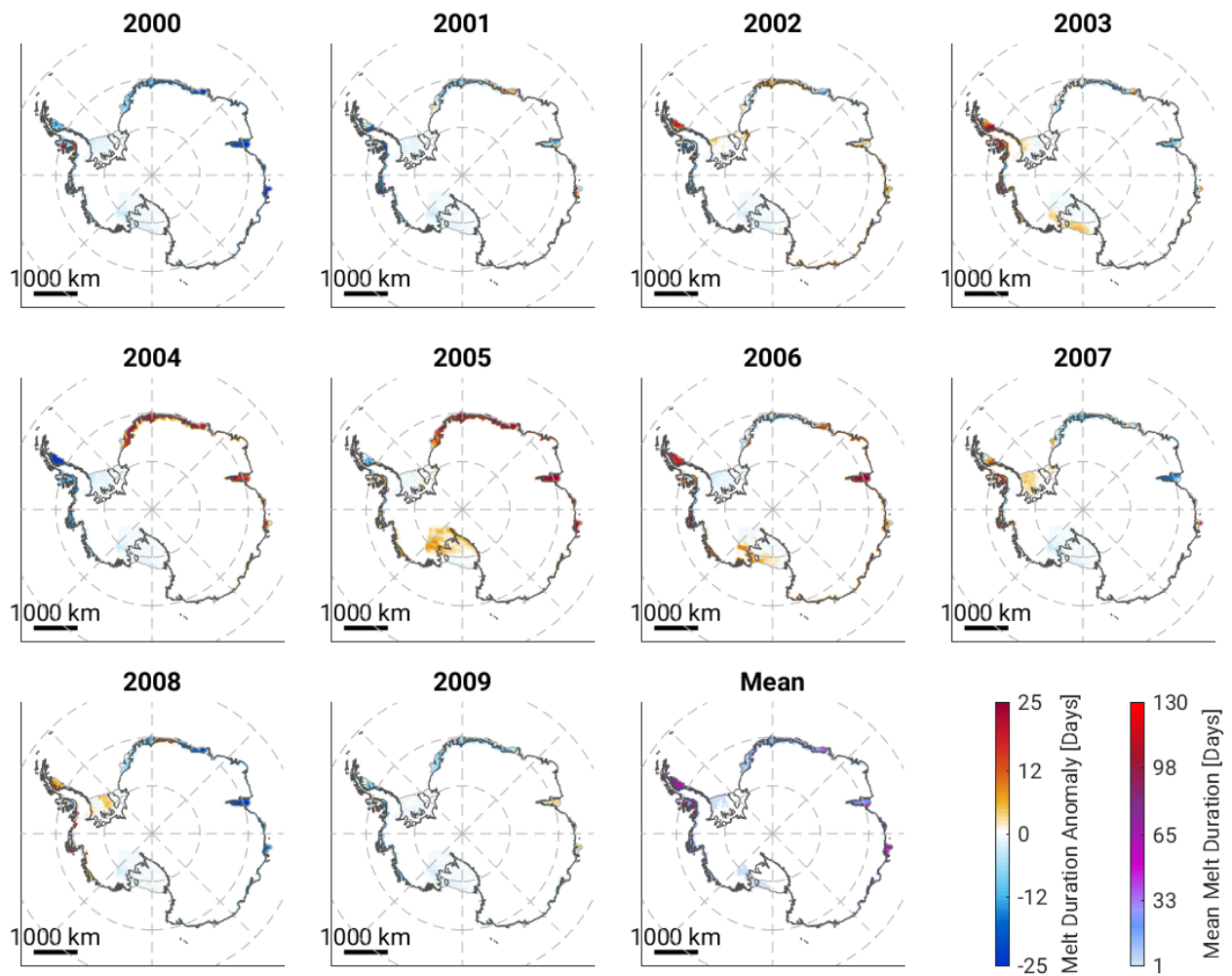


Figure A.30: Annual maps of melt duration anomalies for the period 2000-2009 using the M1 method.

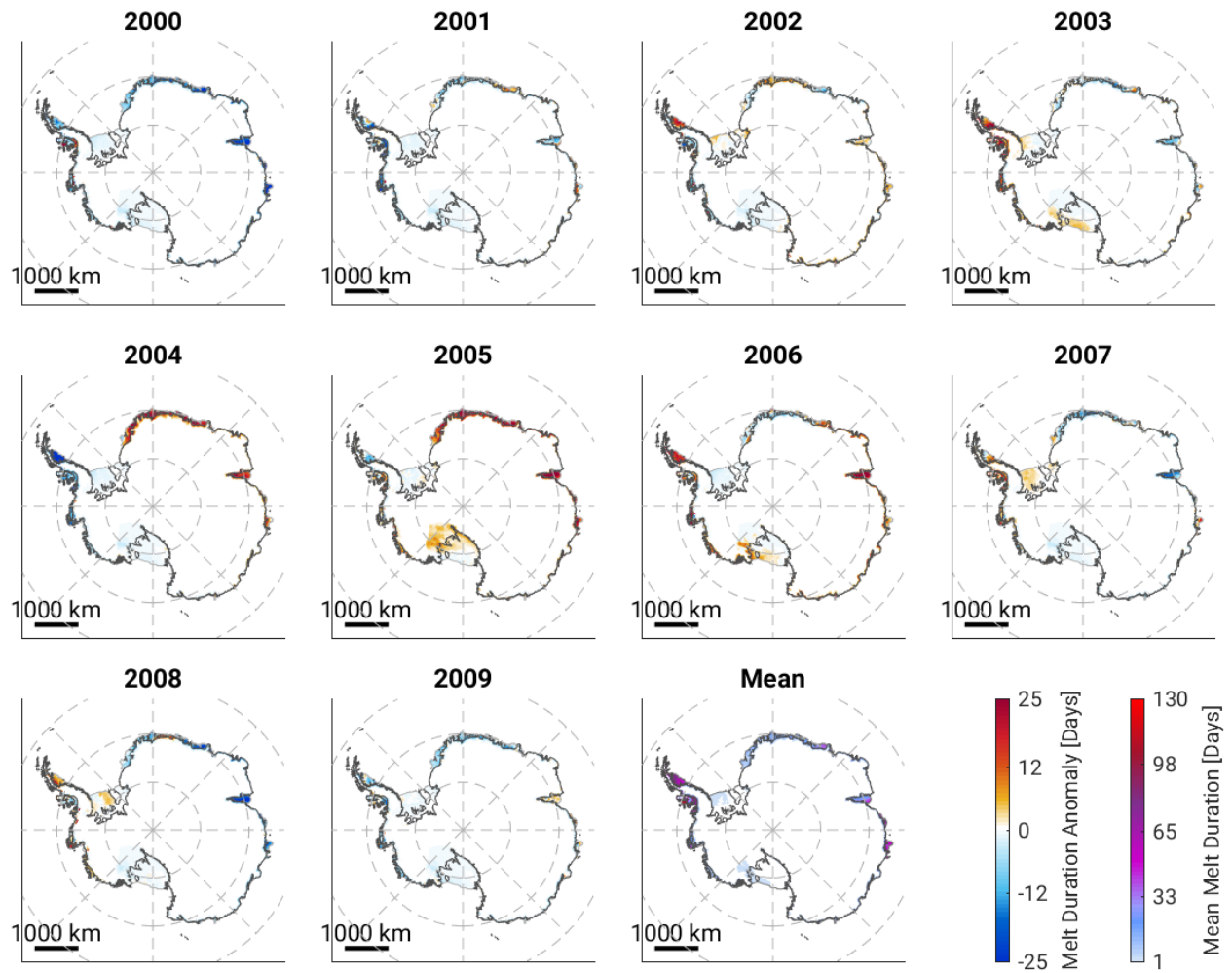


Figure A.31: Annual maps of melt duration anomalies for the period 2000-2009 using the M2 method.

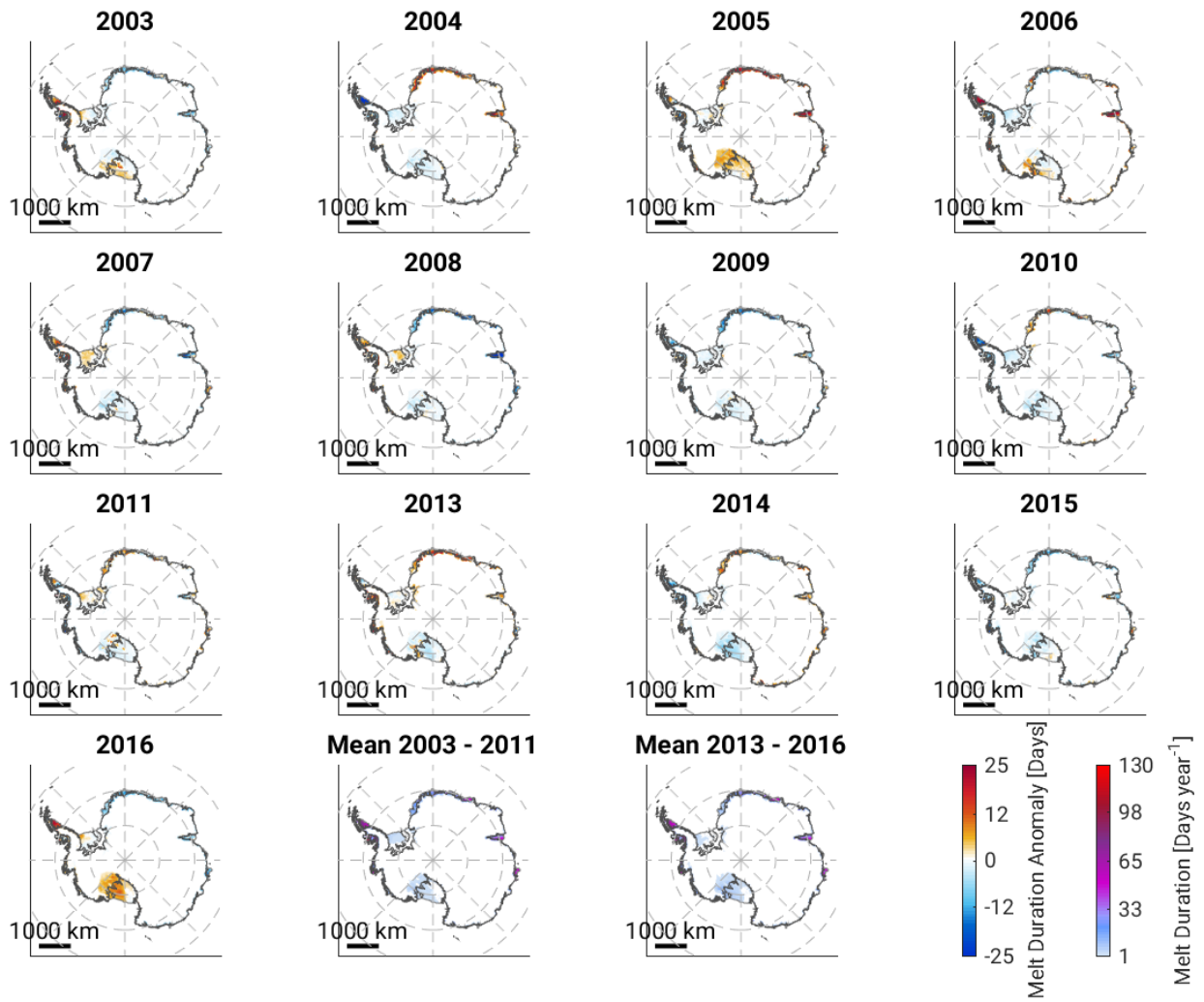


Figure A.32: Annual maps of melt duration anomalies for the period 2003-2016 from AMSR-E (2003-2011) and AMSR2 (2013-2016).

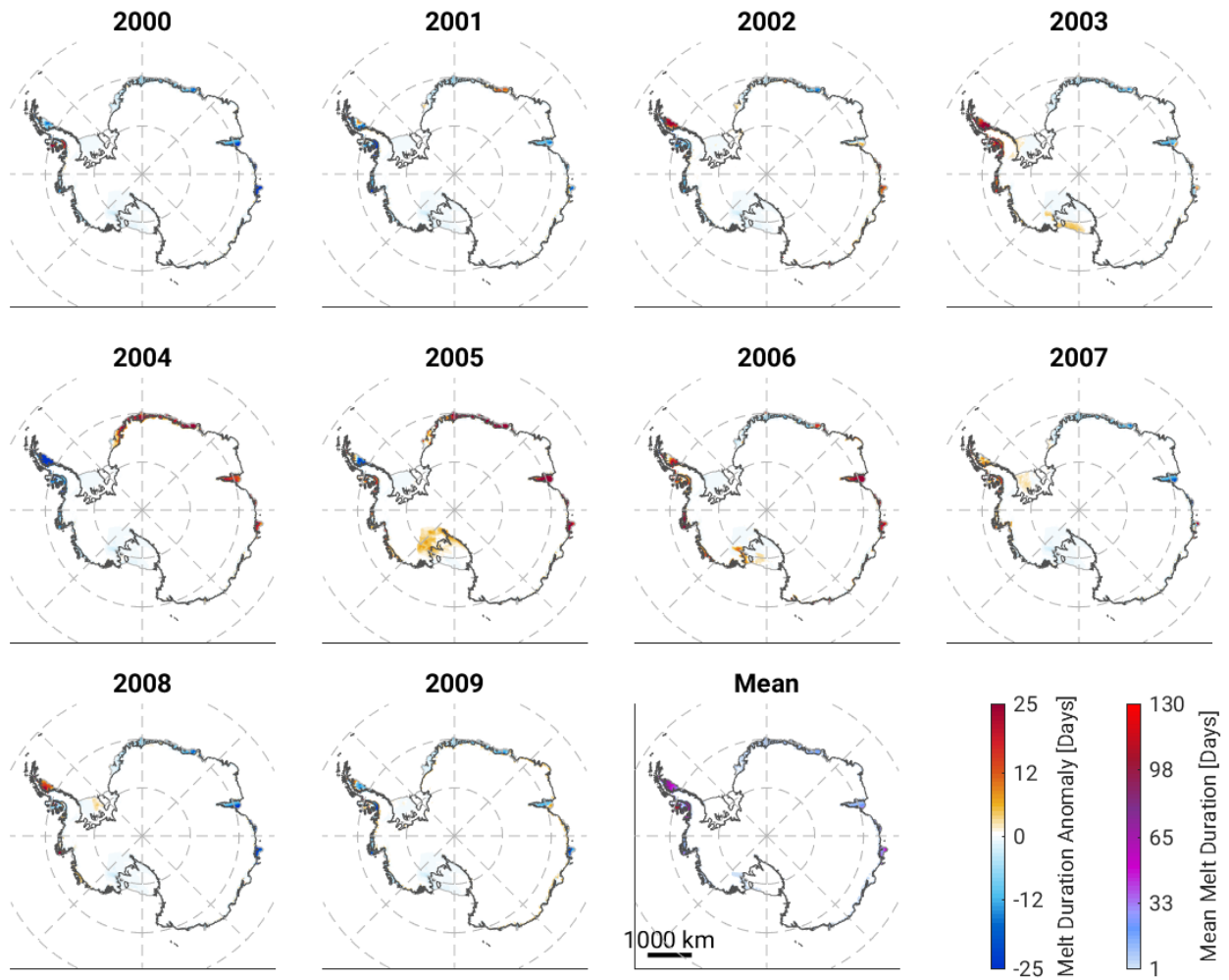


Figure A.33: Annual maps of melt duration anomalies for the period 2000-2009 using the (Trusel et al., 2012) method for morning QuikSCAT data.

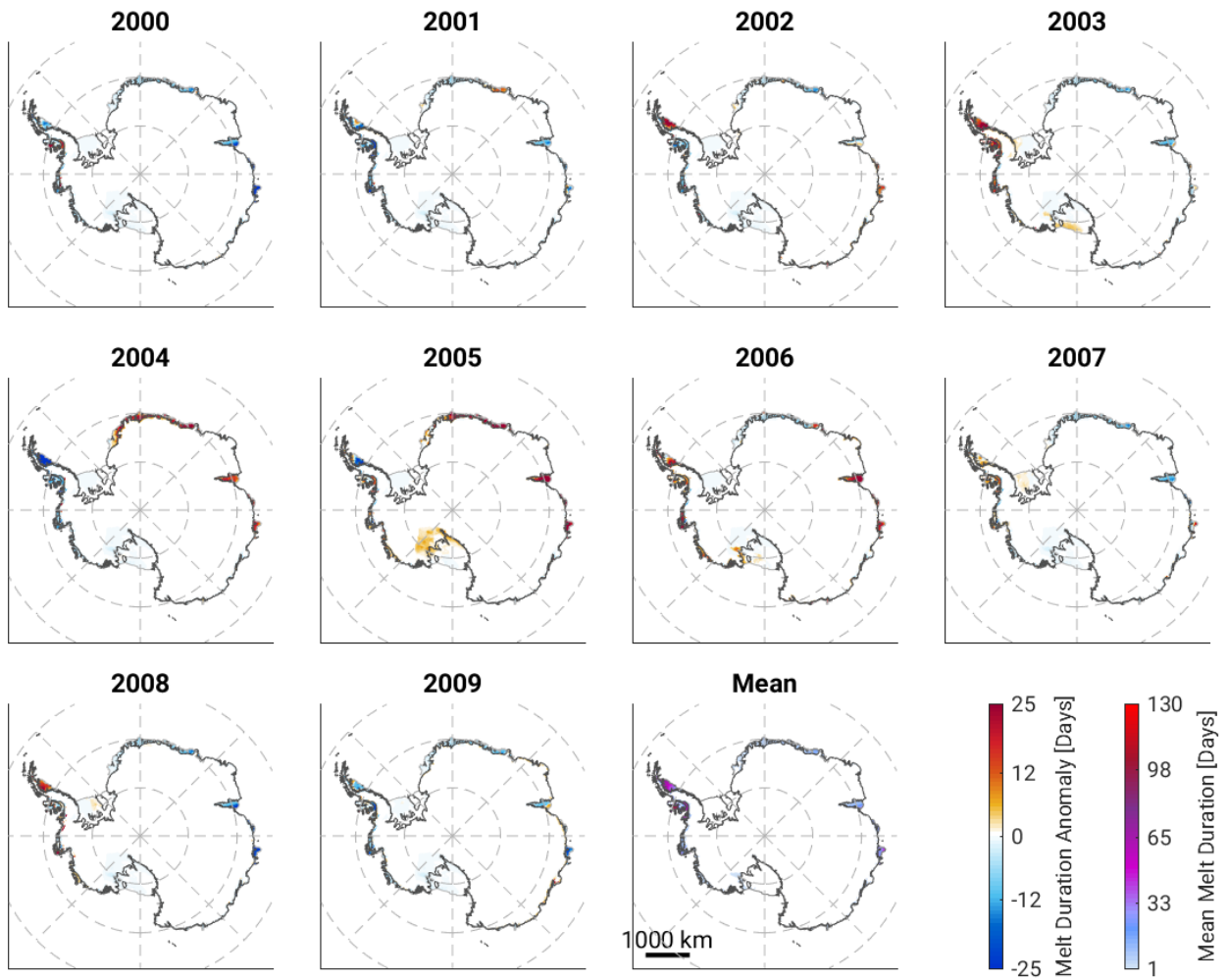


Figure A.34: Annual maps of melt duration anomalies for the period 2000-2009 using the M1 method for morning QuikSCAT data.

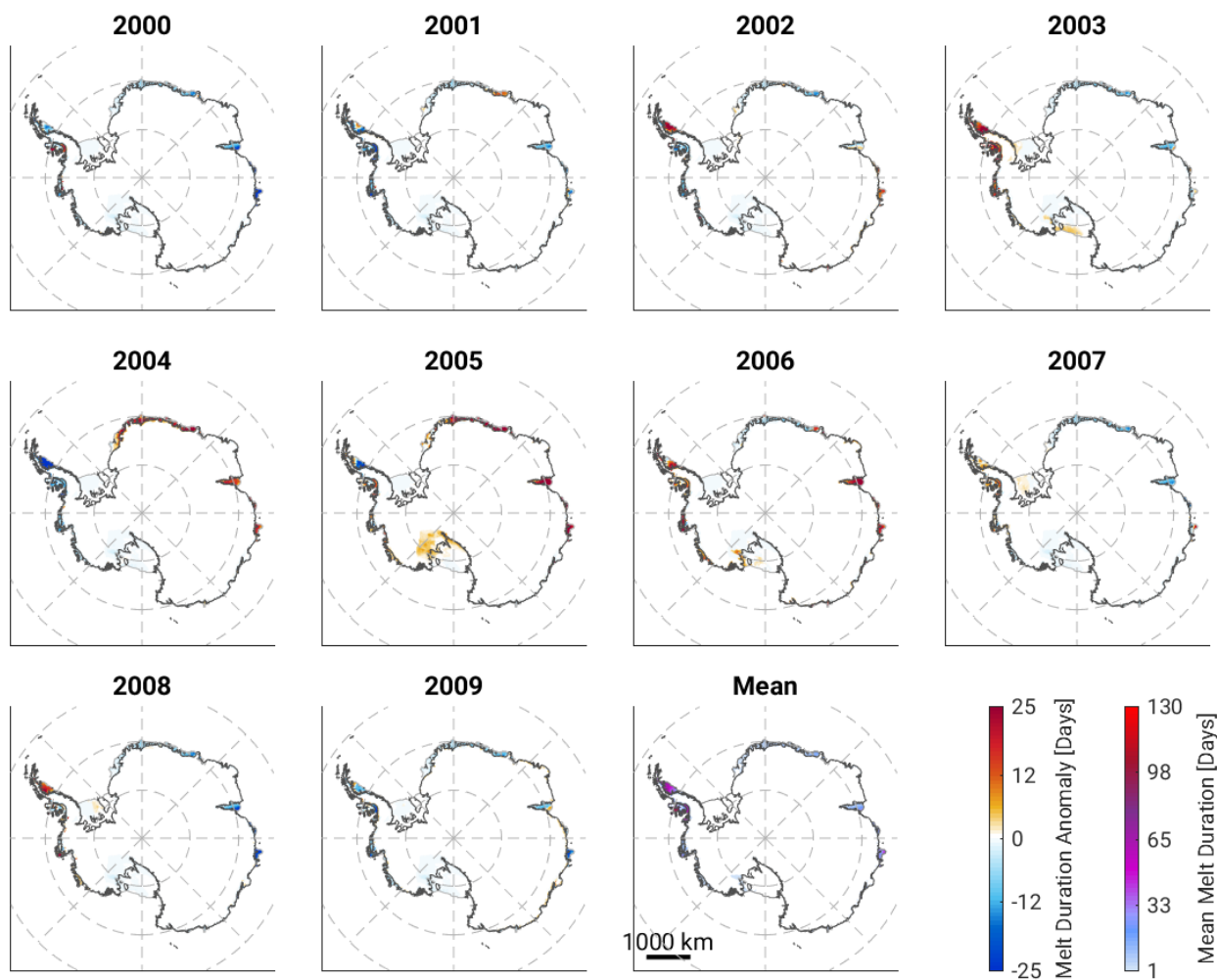


Figure A.35: Annual maps of melt duration anomalies for the period 2000-2009 using the M2 method for morning QuikSCAT data.

A.1.7 Melt Intensity Anomaly Maps

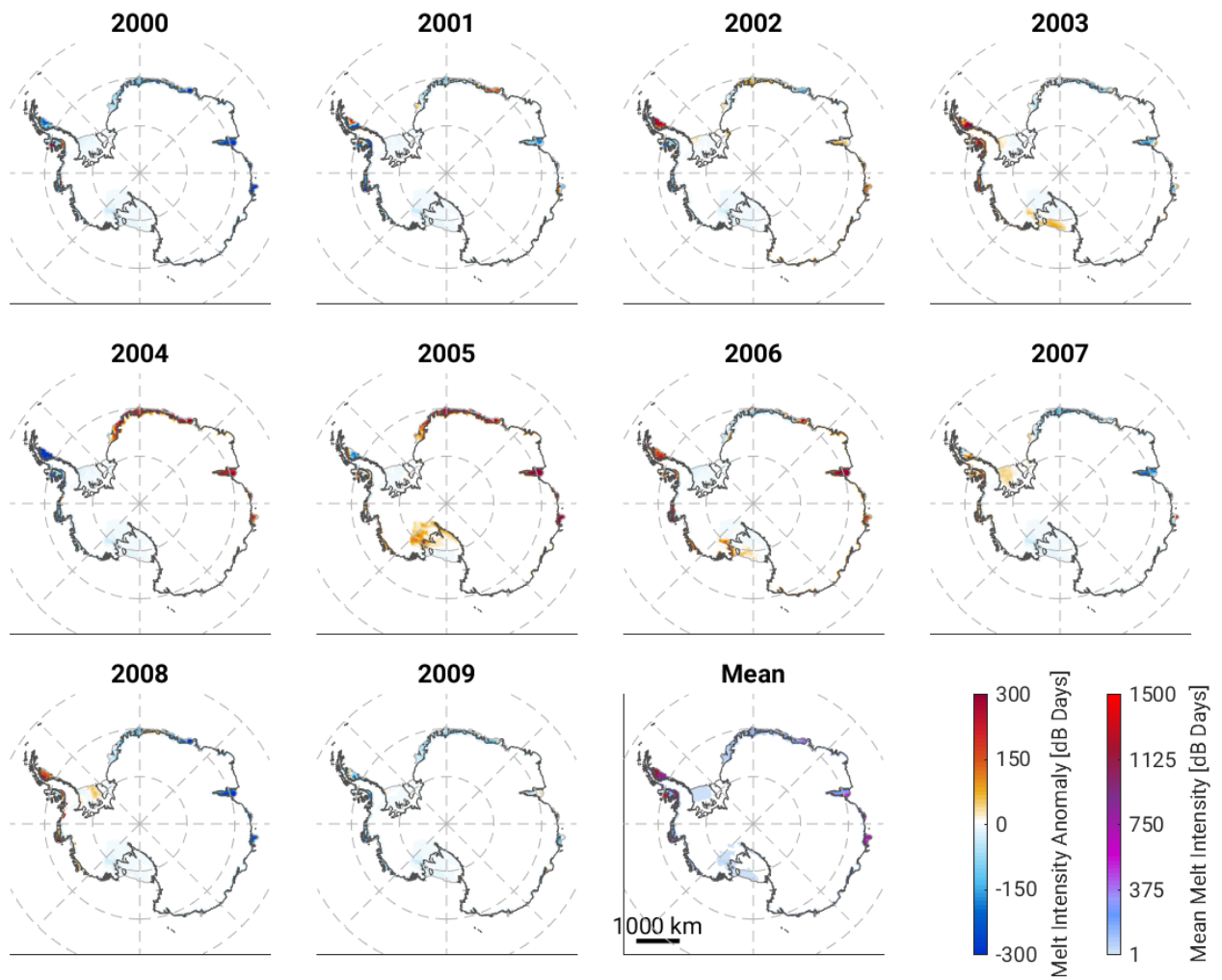


Figure A.36: Annual maps of melt intensity anomalies for the period 2000-2009 using the M1 method for QuikSCAT midday data.

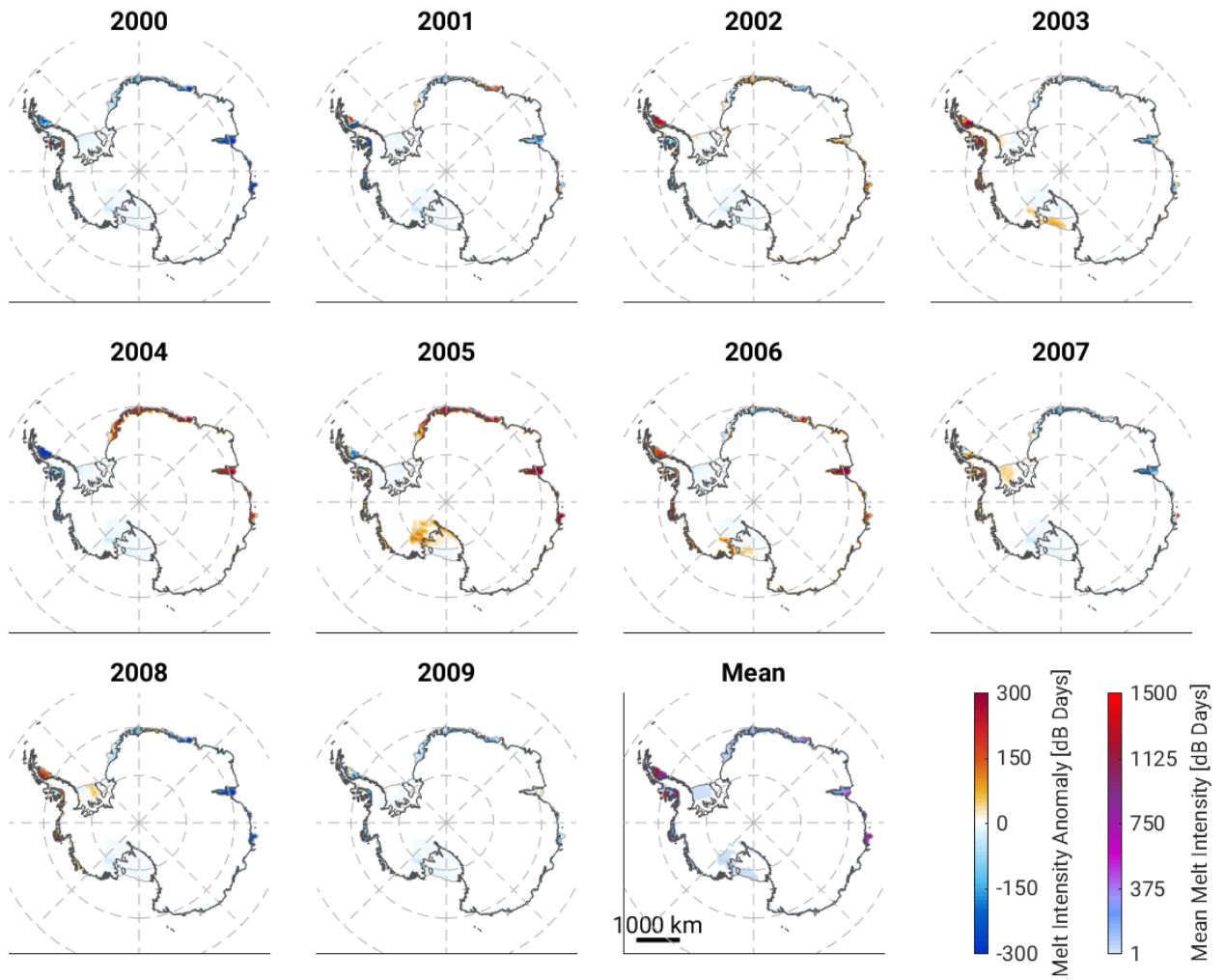


Figure A.37: Annual maps of melt intensity anomalies for the period 2000-2009 using the M2 method for QuikSCAT midday data.